

# Propagation of single and multi-photon states in integrated laser-written waveguide networks

vorgelegt von

Diego Guzmán Silva, M. Sc.

geboren am 16. Juni 1987 in Santiago, Chile

Betreuer: Prof. Dr. Alexander Szameit

Dissertation  
zur Erlangung des akademischen Grades

*doctor rerum naturalium (Dr. rer. nat.)*

der Mathematisch-Naturwissenschaftlichen Fakultät  
der Universität Rostock.

eingereicht Rostock, 9. Februar 2018

verteidigt Rostock, 6. Juli 2018



## Gutachter

Prof. Dr. Alexander Szameit

Universität Rostock

Institut für Physik

Rostock, Germany

Prof. Dr. Stefan Nolte

Friedrich-Schiller-Universität Jena

Institut für Angewandte Physik

Jena, Germany

# Propagation of single and multi-photon states in integrated laser-written waveguide networks

Diego Guzmán Silva

Februar 2018

---

# Abstract

The aim of this thesis is to analyze both theoretically and experimentally the propagation of single and multi-photon states in integrated waveguides arrays, which can be applied in quantum computation and simulation. As a first part, the impact of decoherence on the dynamics of a system is studied, analyzing the cases of distinguishable and indistinguishable photons. The next part covers the study of quantum suppressions, where conditions necessary for suppression of certain output distributions is investigated. Finally the implementation of a photonic quantum SWAP gate is presented. All experimental realizations were performed through integrated photonic quantum circuits, fabricated with the femtosecond laser writing technique.

---

# Zusammenfassung

Das Ziel dieser Arbeit ist es sowohl theoretisch wie auch praktisch, die Propagation von einzel- und viel-Photonen Zuständen in integrierten Wellenleitersystemen zu untersuchen, mit Anwendung auf die Bereiche Quantum Computation und Quanten Simulationen. Zu Beginn wird der Einfluss von Dekohärenz auf die Dynamik unterscheidbarer und ununterscheidbare Photonen studiert. Weiterführend wird die Unterdrückung bestimmter Quantenzustände, "Quantum Suppression", analysiert. Der letzte Teil der Arbeit befasst sich mit der Implementierung eines photonischen Quanten-SWAP-Gates. In all diesen Arbeiten geschieht die experimentelle Umsetzung mittels passiver, integrierter, photonischer Quanten Schaltkreise, welche mittels Femtosekundenlaser hergestellt werden.



---

# Acknowledgements

Firstly, I thank God for taking care of me and guiding me all this time abroad.

I want to thank also, and show my gratitude to all the people that were involved in my PhD during these years. Starting with my advisor Prof. Dr Alexander Szameit, who trusted in a person who came from very far away, giving me not only the opportunity to join his group but also for teaching me and showing me all his scientific knowledge at any time (and also thanks for show me how a German highway is).

I thank also the working group, for providing a stimulating and comfortable environment for research. Of invaluable help were all the comments and advices received from the postdoc guys of our group: Armando Perez Leija, Marco Ornigotti, Matthias Heinrich and Maxime Lebugle, who with their help both theoretical and experimental made me move forward. I cannot forget to mention to Robert Keil (postdoc in Innsbruck) for all his ideas and comments in the short time we spent together.

I want to say thanks to all my colleagues during the PhD: Markus Gräfe, Christian Vetter, Simon Stützer, Rene Heilmann, Toni Eichelkraut, Steffen Weimann, Julia Zeuner, Mark Kremer, Kai Wang, Lukas Maczewsky and Erick Meyer, who helped me in some way or another during this time. Special mention to Markus and Steffen for showing me and teaching me how to use the different labs and also for helping me to get a nice flats to live (including the devolution of the infamous *kaution*). And also thanks to the new people I met here in Rostock, specially to my office mates Rike and Eric, and Jelena Boldt for being the nicest secretary ever.

Quisiera finalizar agradeciendo a mi familia quienes siempre estuvieron preocupados por mi y motivándome. Dejando para el final a la persona que más estoy agradecido durante este doctorado, hablo de mi esposa Valeria, quien ha sido mi gran soporte durante este tiempo, acompañándome en esta travesía en los buenos y en los malos tiempos. Para ti mi amor, muchas pero muchas gracias.



# Contents

<b>Abstract</b>	<b>v</b>
<b>Acknowledgements</b>	<b>vii</b>
<b>Contents</b>	<b>ix</b>
<b>1 Introduction</b>	<b>1</b>
<b>2 Fundamentals</b>	<b>5</b>
2.1 Propagation of (quantum) light in waveguides . . . . .	5
2.2 Two photon quantum interference . . . . .	9
2.3 Direct laser inscription . . . . .	13
2.4 Generation and detection of indistinguishable photon pairs . . . . .	18
<b>3 Prevalence of quantum coherence in open quantum systems</b>	<b>21</b>
3.1 Closed and open quantum systems . . . . .	22
3.2 Master equation for single photon states . . . . .	24
3.3 Experiment and results . . . . .	27
3.4 Master equation for two-photon states . . . . .	30
3.5 Experiment and results . . . . .	32
3.6 Conclusions . . . . .	36
<b>4 Quantum suppression law in <math>J_x</math> lattices</b>	<b>39</b>
4.1 Multi-photon interference . . . . .	40
4.2 Suppression law for Bell multiport beam splitter . . . . .	43
4.3 Suppression law for parity-symmetric input states in a $J_x$ lattice . . . . .	44

4.3.1	Even photon number states . . . . .	46
4.3.2	Odd photon number states . . . . .	48
4.4	Experiment and results . . . . .	49
4.5	Conclusions . . . . .	52
<b>5</b>	<b>Experimental realization of a photonic quantum SWAP gate</b>	<b>55</b>
5.1	The SWAP operation . . . . .	56
5.2	Implementation of a photonic SWAP gate . . . . .	57
5.3	Experiment and results . . . . .	58
5.4	Conclusions . . . . .	63
<b>6</b>	<b>Conclusions and Outlook</b>	<b>65</b>
<b>A</b>	<b>Derivation of the dynamical equation for <math>\rho</math> in OQS</b>	<b>69</b>
	<b>Bibliography</b>	<b>71</b>
	<b>List of publications and conference contributions</b>	<b>83</b>

---

# Introduction

Understanding how light propagates in a guided structure, such as an optical waveguide, and how its properties can be manipulated is crucial for development of new light-based technologies, both in the classical and quantum regime. In the last decades, areas like quantum information [1], quantum cryptography [2], quantum metrology [3] and quantum simulation [4] have had a great impact due to development of quantum sources, integrated circuits and detection systems, making these areas more realistic from experimental point of view. Ultimately, all these advances in quantum technologies could be determinant in the fabrication of a possible quantum computer [5], which promises to outperform a classical computer in several tasks like, for example searching databases [1] and quantum simulations.

To this date, however, none of the available quantum technologies have proven to be a complete and purely quantum platform, as they execute small and simple tasks which can be performed by a classical computer in a more (or comparable) efficient way. Nevertheless, such technologies could be the building blocks of a future genuine quantum platform. In a view of that, work done by Knill, Laflamme and Milburn [6] attracted a lot of attention showing theoretical possibility to create an efficient quantum computation with linear optics, namely using only beam splitters, phase shifters, single photon sources and photo-detectors. Several physical platforms have been used for the development of quantum technologies such as ultracold atoms [7], trapped ions [8], spin chains [9], nuclear magnetic resonance [10] and photons [11].

Photons, in particular, offer significant advantages, such as low decoherence, high mobility, easy manipulation and individual addressing, by employing simple optical components, high speed transmission and the possibility to encode information in several degrees of freedom, such as polarization, path, time or orbital angular momentum [12]. One drawback is the lack of interaction between photons, which prevents nonlinear effect used for the implementation of some deterministic quantum operations [13]. The generation of multi-photon states is still an open challenge. Due to the scalability of the photon sources, generation of 8- and 10-photon entangled states represents actual milestone [14, 15].

Photons on chip integrated photonic waveguides [11] can be viewed as a very good platform since it provides high stability, low noise and small size. This is opposite with the situation in bulk optics where the increase of the components' dimensions and the size of the setup enhance problems related to stability and noise, making integrated arrays of waveguides to be ideal candidate for photonic platform. All these features make the integrated photonic waveguides a very controllable platform, allowing to study not only photons but it opens also the possibility to study other quantum systems as well, through quantum simulations with photons [12].

Arrays of waveguides have interesting properties such as formation of bands and gaps, analogous to the formation of band-gap energy spectra in crystal lattices studied by Bloch [16]. The study of propagation of light in these periodic media can be traced back to the time of Lord Rayleigh [17] until today, where optical analogues of many quantum effects have been observed like the Bloch oscillations [18, 19], quantum Zeno effect [20] and Anderson localization [21]. All these achievements are largely due to the plasticity of waveguides, where the manipulation of the flow of light is very versatile [22], adding another advantage to waveguides as a quantum platform. Interestingly, the propagation of light in these arrays manifests through discrete diffraction or ballistic spreading, which can be modelled by using the discrete Schrödinger equation [23]. These properties make waveguides ideal for the observation of genuine quantum effects like quantum walk [24], the quantum analog of the classical random walk, as it is pointed out in [25]. This marks the starting point where integrated waveguides and photons start to work in a more solid fashion. Moreover, few time after Bromberg *et al.* described quantum correlations in waveguides [26], needed to study quantum properties of the propagation

of photons in these arrays.

In summary, quantum integrated optics has proven to be a fertile ground for research with a constant progress in diverse areas like quantum computation [27, 28], quantum simulation [12, 29] and quantum effects [30]. The purpose of this thesis, therefore, is to use integrated photonic circuits, fabricated using the femtosecond laser writing technique in order to implement several quantum gates and quantum simulation devices.

The thesis is organized as follows: in Chapter 2 the theoretical background for the evolution of light in waveguide lattices is explained. In the same chapter, the experimental part is reviewed including the femtosecond laser writing technique and generation of photons. In Chapter 3 the quantum simulations of an open quantum system using waveguides with dynamical noise are presented, analyzing the role of indistinguishability for single and two-photon states. In Chapter 4 a quantum law for zero transmission in waveguides is discussed due to quantum properties of photons. Chapter 5 deals with the problem of engineering a quantum gate performing a SWAP operation, where a photonic integrated chip is proved experimentally. Final conclusions and outlook are presented in Chapter 6.



## Fundamentals

### 2.1 Propagation of (quantum) light in waveguides

The starting point are Maxwell's equations [31]:

$$\begin{aligned}
 \vec{\nabla} \cdot \vec{\mathcal{D}} &= \rho \quad , \\
 \vec{\nabla} \cdot \vec{\mathcal{B}} &= 0 \quad , \\
 \vec{\nabla} \times \vec{\mathcal{E}} &= -\frac{\partial \vec{\mathcal{B}}}{\partial t} \quad , \\
 \vec{\nabla} \times \vec{\mathcal{H}} &= \frac{\partial \vec{\mathcal{D}}}{\partial t} + \vec{J} \quad ,
 \end{aligned} \tag{2.1}$$

where  $\vec{\mathcal{D}}$  is the electric displacement,  $\vec{\mathcal{B}}$  is the magnetic induction,  $\vec{\mathcal{E}}$  is the electrical field,  $\vec{\mathcal{H}}$  is the magnetic field,  $\vec{J}$  is the current density and  $\rho$  is the charge density. If one assumes to consider a non-magnetic (for which  $\vec{\mathcal{B}} = \mu_0 \vec{\mathcal{H}}$  holds, being  $\mu_0$  the vacuum magnetic permeability), isotropic dielectric medium, characterized by the permittivity  $\epsilon = \epsilon(r)$ , and also assuming that in this medium there are no free charges ( $\rho = 0$ ) or current ( $\vec{J} = 0$ ), one can, from the above equations, derive the following wave equation:

$$\nabla^2 \vec{\mathcal{E}}(r, t) = \frac{n^2(r)}{c^2} \frac{\partial^2}{\partial t^2} \vec{\mathcal{E}}(r, t) \quad , \tag{2.2}$$

where  $c = 1/\sqrt{\epsilon_0 \mu_0}$  standing for the speed of light,  $n$  being the refractive index of the medium  $n(r) = \sqrt{\epsilon(r)}$  and the approximation  $\vec{\nabla} \cdot \vec{\mathcal{E}} \approx 0$  has been used due to a slow and small change of  $\epsilon$  in waveguides. Considering the propagation of monochromatic electromagnetic waves in the form  $\vec{\mathcal{E}} = \text{Re}\{\vec{E}(r)e^{-i\omega t}\}$  where  $\vec{E}$  representing the electric complex amplitude, the Helmholtz equation is obtained:

$$\nabla^2 \vec{E}(r) + k^2 \vec{E}(r) = 0 \quad , \tag{2.3}$$

where  $k = k_0 n(r) = \sqrt{\epsilon(r)}\omega/c$ . For simplicity, assume that the waveguides form a 1D array (higher dimensions can be easily derived from this approach), where  $x$  is the transversal coordinate  $n(r) \rightarrow n(x)$  and  $z$  stands for the propagation direction. The waveguide supports propagation of at least one mode (the fundamental) and the amplitude of observed mode slowly changes in  $z$  direction (changes of refractive index along  $z$  direction can be neglected). The mode is characterized with a propagation constant  $\beta = k_0 n_0$ , where  $n_0$  denotes the unperturbed refractive index. Presuming only linear polarization in  $x$  direction ( $\vec{E} \rightarrow E(x, z)e^{i\beta z}\vec{e}_x$ ) and replacing it in Eq. (2.3)

$$\frac{\partial}{\partial x^2}E(x, z) + \frac{\partial^2}{\partial z^2}E(x, z) + 2i\beta\frac{\partial}{\partial z}E(x, z) - \beta^2E(x, z) + \frac{\omega^2}{c^2}n^2(x)E(x, z) = 0 \quad .$$

Since  $E$  changes slowly in  $z$  direction, the paraxial approximation is used  $|\partial^2 E/\partial z^2| \ll |k\partial E/\partial z|$ . Moreover, changes of the refractive index modulation are very small,  $n(x) = n_0 + \Delta n(x)$  with  $\Delta n$  in the order of  $10^{-4}$  to  $10^{-3}$ , so  $-\beta^2 + \omega^2 n^2(x)/c^2 \approx 2\beta^2 \Delta n(x)/n_0$ , getting finally:

$$i\frac{\partial}{\partial z}E(x, z) + \frac{1}{2\beta}\frac{\partial^2}{\partial x^2}E(x, z) + \frac{\beta\Delta n(x)}{n_0}E(x, z) = 0 \quad . \quad (2.4)$$

Having in mind that  $\omega = 2\pi c/\lambda$  and  $\lambda = \lambda/2\pi$ , previous equation can be transformed into:

$$i\lambda\frac{\partial}{\partial z}E(x, z) + \frac{\lambda^2}{2n_0}\frac{\partial^2}{\partial x^2}E(x, z) + \Delta nE(x, z) = 0 \quad . \quad (2.5)$$

Comparing it to the Schrödinger equation:

$$i\hbar\frac{\partial}{\partial t}\psi(x, t) + \frac{\hbar^2}{2M}\frac{\partial^2}{\partial x^2}\psi(x, t) - V(x)\psi(x, t) = 0 \quad , \quad (2.6)$$

one can see that although they describe different entities, the mathematical structure is identical, and the following correspondences can be made:

$$\begin{aligned} E &\Longleftrightarrow \psi \\ z &\Longleftrightarrow t \\ \Delta n &\Longleftrightarrow -V \\ \lambda &\Longleftrightarrow \hbar \\ n_0 &\Longleftrightarrow M \end{aligned} \quad (2.7)$$

Notice that now it is possible to study the dynamics of the wave-function, observing directly the dynamics of light in waveguides arrays along the propagation distance

$z$  (instead of time  $t$ ) which is one of the main advantages of optical systems. Application of such platform led to the big achievements in the field of photonics such as: observing for the first time optical Bloch oscillations [18, 19], optical discrete solitons [32] and Anderson localization [21].

Although the propagation of light can be described using Eq. (2.4), it is sometimes useful to make a discretization in the transverse direction since the observed system consists of waveguides which fundamental eigenmode is mostly localized inside the waveguides, while the interaction between channels can be approximated to the first neighbors via evanescent fields. This approximation is used within the scope of the coupled mode theory [33] and is analogous to the tight binding model in solid state physics [34]. Starting by writing the electrical field as a superposition of eigenmodes  $E(x, z) = \sum_j a_j(z) f_j(x) e^{-i\beta_j z}$ , where  $a$  is the amplitude along  $z$  direction,  $f$  is the amplitude of transverse component of the mode and the sum runs over  $j$ , with  $j$  being the number of the waveguide, it is possible to derive a discrete equation for the amplitude of the envelope of the electric field at lattice site  $n$ :

$$i \frac{d}{dz} a_n(z) + \beta_n a_n(z) + C_{n,n-1} a_{n-1}(z) + C_{n,n+1} a_{n+1}(z) = 0 \quad , \quad (2.8)$$

where  $\beta_n$  is the propagation constant of the mode in the waveguide  $n$  and  $C_{n,n\pm 1}$  stand for the coupling constants between two adjacent waveguides  $n$  and  $n \pm 1$ , and is related to the overlap integral of the transversal modes  $\int f_n f_{n\pm 1}^* (n^2(x) - n_{j\pm 1}^2(x)) dx$ . Along this thesis only equal coupling will be considered ( $C_{n,n+1} = C_{n,n-1} \equiv C$ ), getting finally:

$$i \frac{d}{dz} a_n(z) + \beta_n a_n(z) + C[a_{n-1}(z) + a_{n+1}(z)] = 0 \quad . \quad (2.9)$$

This equation is important not only because it describes the dynamics of light in waveguides array but also the dynamics of single photons [26]. It is also used to make characterization of the array, allowing quantification of the coupling constant  $C$  and detuning ( $\Delta\beta = \beta_n - \beta_m$ ) via experiment.

Notice that the Hamiltonian of the system is given by:

$$H = - \sum_j^N [\beta_j a_j^* a_j + C a_{j-1}^* a_j + C a_{j+1}^* a_j] \quad . \quad (2.10)$$

where the canonical variables  $q, p$  can be identified as  $q \rightarrow a$  and  $p \rightarrow i a^*$  [35]. Then using the Hamilton equation  $\frac{dq}{dz} = \frac{\partial H}{\partial p}$  one can derive the equation of motion in Eq. (2.9).

In order to describe the propagation of quantum light (photons) in waveguide arrays, one proceeds to quantize the field in each waveguide using the operators  $\hat{a}$  and  $\hat{a}^\dagger$  [36], obeying the commutation relations:

$$[\hat{a}_j, \hat{a}_k^\dagger] = \delta_{j,k} \quad , \quad [\hat{a}_j, \hat{a}_k] = 0 \quad , \quad [\hat{a}_j^\dagger, \hat{a}_k^\dagger] = 0 \quad , \quad (2.11)$$

where  $\hat{a}_j^\dagger$  is the bosonic creation operator and  $\hat{a}_j$  is the bosonic annihilation operator which creates or destroys a photon in waveguide  $j$ , respectively. Now the Hamiltonian is (setting  $\hbar = 1$ ):

$$\hat{H} = - \sum_j^N \left[ \beta_j \hat{a}_j^\dagger \hat{a}_j + C \hat{a}_{j-1}^\dagger \hat{a}_j + C \hat{a}_{j+1}^\dagger \hat{a}_j \right] \quad . \quad (2.12)$$

It is worth noticing that since it was assumed that all couplings in systems are equal, this Hamiltonian is hermitian. It is possible to calculate the evolution of the system in the Heisenberg picture, where the operators  $\hat{a}_j^{(\dagger)}$  evolve. This evolution is given by the Heisenberg equation:

$$i \frac{d}{dz} \hat{a}_n^\dagger = [\hat{a}_n^\dagger, \hat{H}] \quad . \quad (2.13)$$

Evaluating this commutator and using the commutators in Eq. (2.11), one arrives to the equation for the evolution of the creation operator  $\hat{a}^\dagger$  [26]:

$$-i \frac{d}{dz} \hat{a}_n^\dagger(z) + \beta_n \hat{a}_n^\dagger(z) + C[\hat{a}_{n-1}^\dagger(z) + \hat{a}_{n+1}^\dagger(z)] = 0 \quad . \quad (2.14)$$

The general solution of Eq. (2.14) is derived by direct integration:

$$\hat{a}_n^\dagger(z) = e^{i\beta_n z} \sum_k U_{n,k}(z) \hat{a}_k^\dagger(0) \quad , \quad U_{n,k}(z) = \left( e^{iz\tilde{C}} \right)_{n,k} \quad , \quad (2.15)$$

where  $U_{n,k}(z)$  is a unitary transformation corresponding to the exponent of the matrix  $iz\tilde{C}_{n,k}$ , which describes the amplitude for the transition of a single photon from waveguide  $n$  to waveguide  $k$ . Notice that the solution given by the matrix exponential  $U$  is the same for the classical case in Eq. (2.9). The elements of the matrix  $\tilde{C}$  will correspond to the couplings and propagation constants, forming a tri-diagonal matrix

$$\tilde{C} = \begin{pmatrix} \beta_1 & C & 0 & \dots & 0 \\ C & \beta_2 & C & 0 & \dots \\ 0 & C & \beta_3 & C & 0 \\ \vdots & & \ddots & & \vdots \\ 0 & \dots & 0 & C & \beta_N \end{pmatrix} \quad .$$

## 2.2 Two photon quantum interference

In each experiment it will be important to determine the average photon number  $n_i$  within each waveguide  $i$ , calculating the expectation value of the photon number distribution (also called probability distribution):

$$n_i(z) = \langle \hat{a}_i^\dagger(z) \hat{a}_i(z) \rangle = \langle \psi | \hat{a}_i^\dagger(z) \hat{a}_i(z) | \psi \rangle \quad . \quad (2.16)$$

Here  $\langle \rangle$  denotes the expectation value of an operator with respect to the state of the system  $|\psi\rangle$ . If now, there are two identical photons in the system, the photon number correlation function  $\Gamma$  [26] can be calculated as follows:

$$\Gamma_{p,q}(z) = \langle \hat{a}_p^\dagger(z) \hat{a}_q^\dagger(z) \hat{a}_q(z) \hat{a}_p(z) \rangle \quad . \quad (2.17)$$

This correlation function describes the probability to detect one photon in waveguide  $p$  and  $q$ , that is, a coincidence measurement. As it will be clarified in the following lines, this correlation function can give a truly view of the quantum properties of the traveling light in the system. To prove this, consider the most simple waveguide array, i.e., the directional coupler, which consists of two identical waveguides, fulfilling the condition:  $\beta_1 = \beta_2 = \beta$ . Writing Eq. (2.14) in a matrix notation

$$i \frac{d}{dz} \begin{pmatrix} \hat{a}_1^\dagger(z) \\ \hat{a}_2^\dagger(z) \end{pmatrix} = \begin{pmatrix} \beta & C \\ C & \beta \end{pmatrix} \begin{pmatrix} \hat{a}_1^\dagger(0) \\ \hat{a}_2^\dagger(0) \end{pmatrix} \quad ,$$

and using Eq. (2.15):

$$\begin{pmatrix} \hat{a}_1^\dagger(z) \\ \hat{a}_2^\dagger(z) \end{pmatrix} = \begin{pmatrix} \cos(Cz) & i \sin(Cz) \\ i \sin(Cz) & \cos(Cz) \end{pmatrix} \begin{pmatrix} \hat{a}_1^\dagger(0) \\ \hat{a}_2^\dagger(0) \end{pmatrix} \quad , \quad (2.18)$$

where the global phase factor  $e^{i\beta z}$  has been omitted. From now on (for convenience) the initial condition  $\hat{a}_i^\dagger(0)$  will be written as  $\hat{a}_i^\dagger$ . For a single photon input in channel 1

$$|\psi\rangle = \hat{a}_1^\dagger |0, 0\rangle = |1, 0\rangle \quad ,$$

where the creation operator is acting in the waveguide 1, given by the first position of the ket  $|0, 0\rangle$ . The average photon number  $n_1$  is calculated to be:

$$\begin{aligned} n_1(z) &= \langle \hat{a}_1^\dagger(z) \hat{a}_1(z) \rangle = \langle \psi | \hat{a}_1^\dagger(z) \hat{a}_1(z) | \psi \rangle \\ &= \langle 1, 0 | [U_{1,1} \hat{a}_1^\dagger + U_{1,2} \hat{a}_2^\dagger] [U_{1,1}^* \hat{a}_1 + U_{1,2}^* \hat{a}_2] | 1, 0 \rangle \\ &= \langle 1, 0 | |U_{1,1}|^2 \hat{a}_1^\dagger \hat{a}_1 + U_{1,1} U_{1,2}^* \hat{a}_1^\dagger \hat{a}_2 + U_{1,2} U_{1,1}^* \hat{a}_2^\dagger \hat{a}_1 + |U_{1,2}|^2 \hat{a}_2^\dagger \hat{a}_2 | 1, 0 \rangle \\ &= |U_{1,1}|^2 \langle 1, 0 | \hat{a}_1^\dagger \hat{a}_1 | 1, 0 \rangle + U_{1,1} U_{1,2}^* \langle 1, 0 | \hat{a}_1^\dagger \hat{a}_2 | 1, 0 \rangle \\ &\quad + U_{1,2} U_{1,1}^* \langle 1, 0 | \hat{a}_2^\dagger \hat{a}_1 | 1, 0 \rangle + |U_{1,2}|^2 \langle 1, 0 | \hat{a}_2^\dagger \hat{a}_2 | 1, 0 \rangle \\ n_1(z) &= |U_{1,1}|^2 = \cos^2(Cz) \quad . \end{aligned} \quad (2.19)$$

Doing the same procedure for channel 2, one obtains  $n_2(z) = \sin^2(Cz)$ . So, the one photon probability oscillates between the two waveguides (see Fig. 2.1). Notice that the same result is obtained for the light amplitude of a classical wave using Eq. (2.9). Conversely, measurements of the probability distribution of single photons do not reveal the quantum properties of light, in the sense that the same dynamics can be observed with classical light [25].

An interesting case is when the directional coupler terminates at  $z = \pi/4C$ . This is known as 50:50 coupler and the probability to find a single photon in each waveguide is equal to  $1/2$ . If now two identical photons are launched into this 50:50 coupler, one in each waveguide (a separable state)

$$|\psi_{sep}\rangle = \hat{a}_1^\dagger \hat{a}_2^\dagger |0, 0\rangle = |1, 1\rangle \quad ,$$

the average photon number is now constant

$$n_{1(2)}\left(\frac{\pi}{4C}\right) = \langle \hat{a}_{1(2)}^\dagger \hat{a}_{1(2)} \rangle = |U_{1,1}|^2 + |U_{1,2}|^2 = 1 \quad .$$

In order to see nonclassical properties of light, the correlation function  $\Gamma$  will be considered, using Eq. (2.17):

$$\begin{aligned} \Gamma_{1,2}\left(\frac{\pi}{4C}\right) &= \langle \hat{a}_1^\dagger \hat{a}_2^\dagger \hat{a}_2 \hat{a}_1 \rangle = \langle 1, 1 | \hat{a}_1^\dagger \hat{a}_2^\dagger \hat{a}_2 \hat{a}_1 | 1, 1 \rangle \\ &= \langle 1, 1 | [U_{1,1}U_{2,1}\hat{a}_1^\dagger \hat{a}_1^\dagger + U_{1,1}U_{2,2}\hat{a}_1^\dagger \hat{a}_2^\dagger + U_{1,2}U_{2,1}\hat{a}_2^\dagger \hat{a}_1^\dagger + U_{1,2}U_{2,2}\hat{a}_2^\dagger \hat{a}_2^\dagger] \\ &\quad \times [U_{2,1}^*U_{1,1}^*\hat{a}_1 \hat{a}_1 + U_{2,1}^*U_{1,2}^*\hat{a}_1 \hat{a}_2 + U_{2,2}^*U_{1,1}^*\hat{a}_2 \hat{a}_1 + U_{2,2}^*U_{1,2}^*\hat{a}_2 \hat{a}_2] | 1, 1 \rangle \quad . \end{aligned} \quad (2.20)$$

Notice that terms  $\langle 1, 1 | \hat{a}_i^\dagger \hat{a}_i^\dagger \hat{a}_i \hat{a}_i | 1, 1 \rangle$  and  $\langle 1, 1 | \hat{a}_i^\dagger \hat{a}_i^\dagger \hat{a}_j \hat{a}_j | 1, 1 \rangle$  are zero, while term  $\langle 1, 1 | \hat{a}_i^\dagger \hat{a}_j^\dagger \hat{a}_i \hat{a}_j | 1, 1 \rangle$  equals to one. Therefore, the corresponding photon number correlation functions are obtained to be:

$$\begin{aligned} \Gamma_{1,2}\left(\frac{\pi}{4C}\right) &= (U_{1,1}U_{2,2} + U_{1,2}U_{2,1})(U_{1,1}^*U_{2,2}^* + U_{1,2}^*U_{2,1}^*) \\ \Gamma_{1,2}\left(\frac{\pi}{4C}\right) &= |U_{1,1}U_{2,2} + U_{1,2}U_{2,1}|^2 = \cos^2\left(2C\frac{\pi}{4C}\right) = 0 \quad , \end{aligned} \quad (2.21)$$

and

$$\Gamma_{1,1}\left(\frac{\pi}{4C}\right) = \Gamma_{2,2}\left(\frac{\pi}{4C}\right) = 1 \quad . \quad (2.22)$$

This means, that after a distance of  $z = \pi/4C$  the two photons are found together in the same waveguide (photon bunching), and never in different waveguides. This

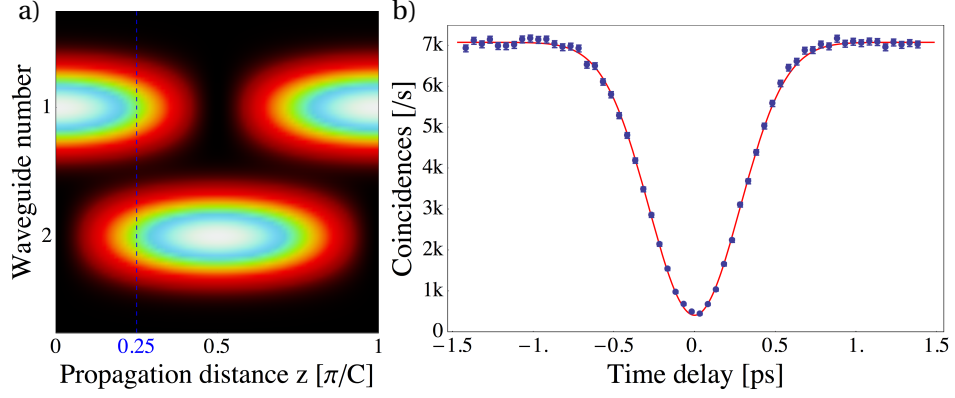


Figure 2.1: Light dynamics in a directional coupler and Hong-Ou-Mandel effect. a) Average photon number in a directional coupler for a single photon input (equivalent to the intensity of classical light). Indicated with a blue dashed line is the length needed to have a 50:50 coupler, where the output is equal for both waveguides and used to see the HOM effect. b) By tuning the delay time of arrival photons to a 50:50 coupler, a typical “HOM-dip” is observed. The uncertainty corresponds to the standard deviation following a Poissonian distribution of the measured counts and it is smaller than the point size.

is completely different to the behavior of classical light or distinguishable photons, where the probability to find photons in both exit ports of the coupler is equal to the one of finding them in a single exit port. This phenomenon is a clear signature of quantum path interference and it was first observed by Hong, Ou and Mandel in 1987 using bulk beam splitter [37] and has been known as the Hong-Ou-Mandel (HOM) effect. Another interesting result of the 50:50 coupler is that when the HOM effect is observed, the output state is a path-entangled state [38]:

$$\hat{a}_1^\dagger \hat{a}_2^\dagger \xrightarrow{\text{DC}} \frac{i}{2} (|2, 0\rangle + |0, 2\rangle) \quad , \quad (2.23)$$

which is one case ( $N=2$ ) of the general entangled N00N states [39].

The observation of the HOM effect can be performed by launching single photons with different arrival time (delay time) to a directional coupler, where at the output coincidence measurements between two detectors are done. In that way, photons arriving at different time are distinguishable and therefore coincidences measurements between two detectors are different from zero. On the other hand, when the time delay between photons approaches to zero, the coincidences start decrease until no coincidences for zero delay. An experimental picture is shown in Fig. 2.1 where the time delay between photons was tuned via a translational stage.

Although this discussion was started with a simple directional coupler, it is possible

to replaced it by more complex arrangements of waveguides, offering a richer dynamics and more intricate quantum interferences. In a multi-port system, the average photon number for a two-photon input state is just the incoherent sum of the average photon number for single photon inputs in channels  $m$  and  $n$ :

$$n_i(z) = |U_{i,m}(z)|^2 + |U_{i,n}(z)|^2 \quad . \quad (2.24)$$

Fig. 2.2 a) depicts the average photon number when a single photon is launched in the middle of the array. It is characterized by having ballistic lobes, which is a characteristic feature of discrete system, known as discrete diffraction [22]. Interestingly this evolution of a single particle can be seen as a implementation of a continuous quantum walk [25].

The correlation function  $\Gamma$  in Eq. (2.17) for a separable two photon state can be written as the coherent sum:

$$\Gamma_{p,q}(z) = |U_{p,m}(z)U_{q,n}(z) + U_{p,n}(z)U_{q,m}(z)|^2 \quad , \quad (2.25)$$

where  $U_{p,m}$  is the probability to find a photon at channel  $p$  when it was launched in channel  $m$ . Fig. 2.2 c) shows the correlation matrix for the separable case when indistinguishable photons are launched in two adjacent waveguides,  $m = 11$  and  $n = 12$  in an array of 21 waveguides, and  $\Gamma(z)$  is calculated at  $z = 1.25\pi/C$ . The plot exhibits higher values of coincidences in equal sites (diagonal) close to either the beginning or end of the array. Conversely the probability to detect photons in separated waveguides (anti-diagonal) is close to zero.

Another interesting input is when two photons are launched either in waveguide  $m$  or  $n$  (with  $m \neq n$ ), that is, the path-entangled state  $\frac{1}{2}[(\hat{a}_m^\dagger)^2 + (\hat{a}_n^\dagger)^2]$ . In this case the correlation function is:

$$\Gamma_{p,q}(z) = |U_{p,m}(z)U_{q,m} + U_{p,n}U_{q,n}|^2 \quad . \quad (2.26)$$

A plot of  $\Gamma$  for the path-entangled case is shown in Fig. 2.2 d). Interestingly the photons are found in separate channels, showing an anti-bunching behavior. The case when  $m = n$ , corresponding to both photons launched in a single waveguide, will lead to no quantum interference because both photons have the same dynamics and they propagate independently from each other. In contrast, considering two distinguishable photons, where the correlation function is the incoherent sum:

$$\Gamma_{p,q}(z) = |U_{p,m}(z)U_{q,n}(z)|^2 + |U_{p,n}(z)U_{q,m}(z)|^2 \quad , \quad (2.27)$$

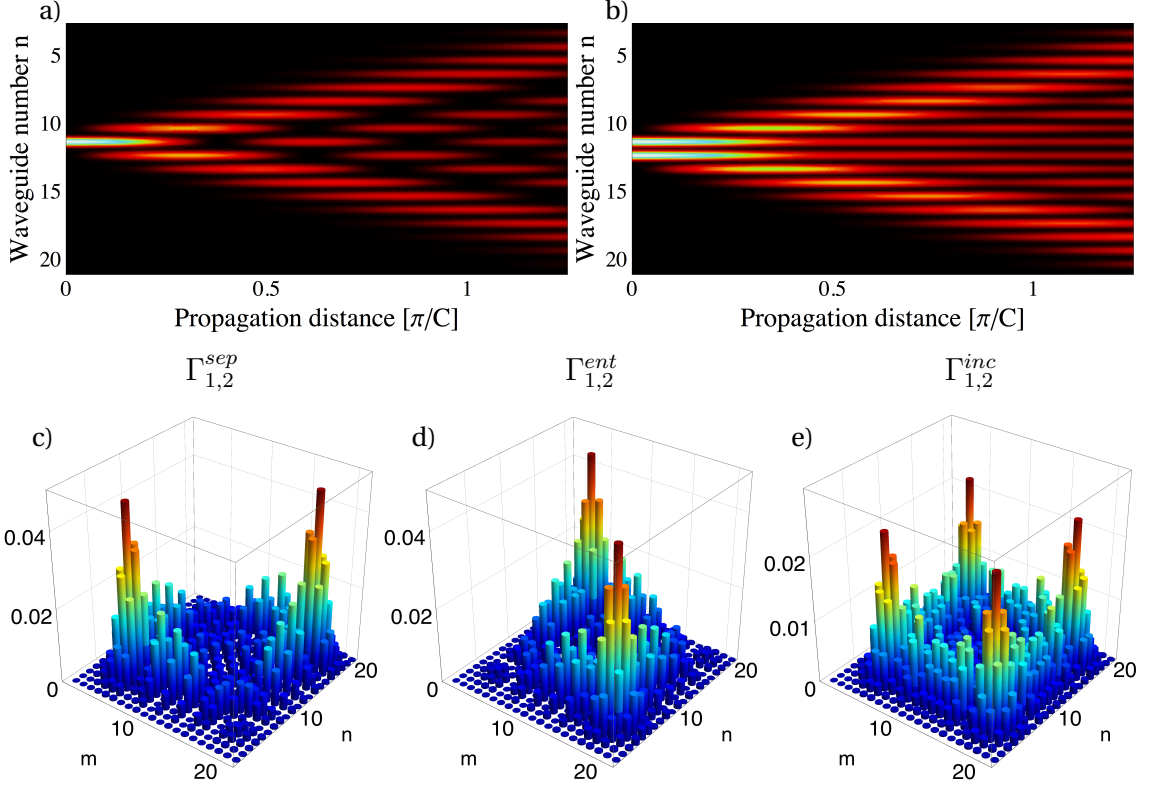


Figure 2.2: Evolution of a single and two-photon state in an array of 21 waveguides. (top) Plots of the average photon number for a single a) and two-photon input b). (bottom) Correlations matrices at  $z = 1.25\pi/C$  for initial conditions c) separable, d) path-entangled and e) distinguishable photons.

will cause occurrence of four characteristic peaks in Fig. 2.2 e). Notice that the average photon number is the same for all the three different inputs  $n_i(z) = |U_{i,m}(z)|^2 + |U_{i,n}(z)|^2$  (Fig. 2.2 b)) so calculating the probability distribution does not reveal quantum properties of light, but using the correlation function the nonclassical features of light are revealed.

## 2.3 Direct laser inscription

As it was discussed in the previous section, propagation of photons in waveguide arrays offers a big potential to see and study quantum properties of light. So the necessity to have a good experimental platform is huge. In that way, several different techniques used to fabricate waveguides for classical light experiments found a good opportunity to be also used for propagation of photons. Silicon-on-silica [27], Ti in-diffusion and proton exchange in lithium niobate [40] and femtosecond laser writing techniques [41, 42] are some of the most commonly used techniques

for fabrication of integrated chips. The latter has been used to realize setups for the photon propagation problems discussed in this thesis, and will therefore be described in more detail in the following.

Femtosecond laser writing technique is a fabrication process in which the laser beam is used to induce structural modifications in various materials. Initially used in [43] to fabricate waveguides in transparent materials, now is also used in several other areas like optofluidics [44] and quantum optics [45]. During the inscription process, ultra short pulses (generated by a femtosecond laser) are focused in a bulk material, whereas the nonlinear absorption and field ionization take place. In the case of fused silica as bulk material, these processes lead to a recombination of the molecular structures of the material, yielding a permanent change of the refractive index [46]. Then, by moving the sample, a continuous region with a higher refractive index is formed, thus creating the waveguides (see Fig. 2.3). It should be noted that there are different regimes of energy which stimulate these processes to happen. In the case of waveguide formation, low energy regimes are shown to be appropriate choice, whereas regimes with intermediate or high power create asymmetric structures and inclusive void zones [46], which can be used in other fields like material processing [47].

As the change of refractive index occurs in the focal volume only, the waveguides are not forced to stay in the same plane and 3D structures can be created by moving the sample on 3D trajectories. This is one of the main advantages of the femtosecond writing technique compared to other methods. Another advantage is that the light intensity dynamics can be directly observed using a fluorescence microscopy technique [48, 49].

It should be mentioned that the resulting waveguides have elliptical shape as well as the modes propagating inside (see Fig. 2.3). Due to ellipticity, the waveguides support two modes with linear orthogonal polarizations, which have different propagation constants. Although this could be seen as a problem if polarization needs to be maintained, it is an advantage in devices where changes in birefringence are needed [50]. So, in order to prevent changes in polarization during dynamics, only one vertical or horizontal polarization has to be chosen during experiments.

Key parameters, such as the coupling  $C$ , which is related to the overlap of the

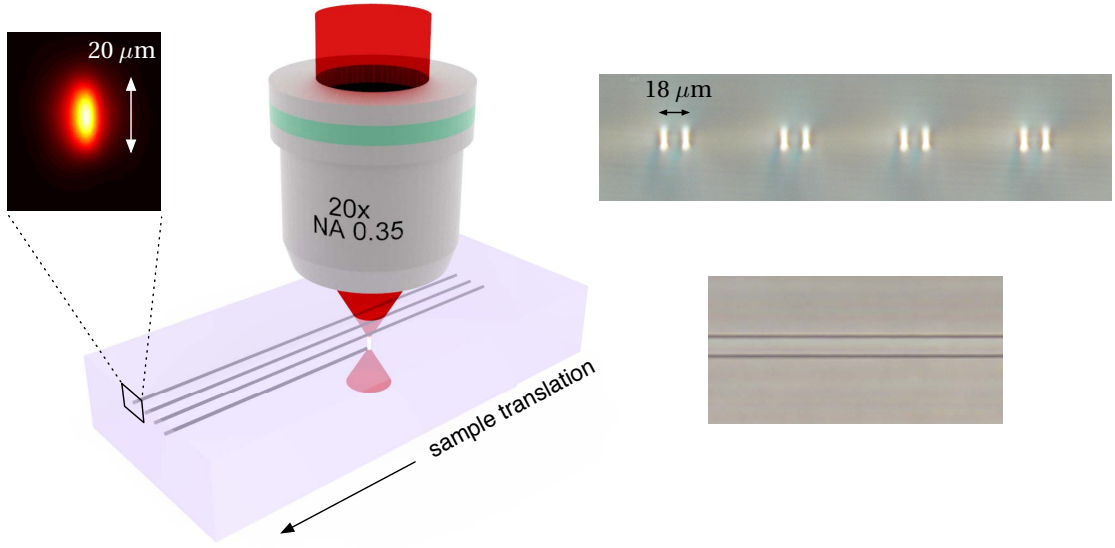


Figure 2.3: Waveguides created by direct laser inscription. To the left, a schematic image of the writing process, where the inset shows a typical elliptical mode field at 800 nm. To the right, microscope images of the cross section of several couplers (top) and a top view of the same coupler (bottom).

evanescent fields of adjacent waveguide modes, can be controlled by changing the spatial separation between waveguides: as the separation between neighboring waveguides increases, in fact, the corresponding coupling decreases. This dependence of the coupling with the separation between waveguides follows an exponential relation [51] (see Fig. 2.4 b)). Another important parameter is the propagation constant  $\beta$  (directly proportional to the change of refractive index), which can be experimentally modified by controlling both the inscription power and writing velocity. Values of the increase of the refractive index are in the order of  $10^{-3}$  to  $10^{-4}$ , while losses are in the range of 0.4 dB/cm [52]. All these values which characterize an array of waveguides are subject to change, since they depend strongly enough on the writing parameters, like pulse duration, pulse energy, polarization, writing velocity, etc. Optimal experimental values used during this work can be found in the following.

The process to create a specific circuit, starts with a previous characterization (calibration), where one knows what value of coupling represent a certain distance between waveguides or how big is the detuning  $\Delta\beta$  for a certain value of writing velocity. This analysis is valid for both classical and quantum light. In order to know the coupling, a coupling vs distance scan is done using couplers with the same

length of propagation  $z_l$  but different coupling distance  $d$  between them. Then, using the coupled mode theory, theoretical solution for a coupler can be derived:

$$\begin{aligned} |a_1(z_l, d)|^2 &= I_1(d) = \cos^2(C(d)z_l) \\ |a_2(z_l, d)|^2 &= I_2(d) = \sin^2(C(d)z_l) \end{aligned} \quad , \quad (2.28)$$

where  $I_n$  is the intensity measured at the output of the sample when a single input in waveguide 1 is used. From here,  $C$  is derived as:

$$C(d) = \frac{\tan^{-1} \left( \sqrt{I_2(d)/I_1(d)} \right)}{z_l} . \quad (2.29)$$

Conducting the same procedure for different distances  $d$  allows to obtain a curve of coupling (see Fig. 2.4 b)). For detuning  $\Delta\beta$ , couplers with same coupling distance and propagation length are used, but with the difference that now one of them was inscribed with a different writing velocity. Assuming theoretical solution for a detuned coupler:

$$\begin{aligned} |a_1(z)|^2 &= \frac{1}{1 + \Delta\beta^2/4C^2} \left[ \frac{\Delta\beta^2}{4C^2} + \cos^2 \left( zC \sqrt{1 + \frac{\Delta\beta^2}{4C^2}} \right) \right] \\ |a_2(z)|^2 &= \frac{1}{1 + \Delta\beta^2/4C^2} \sin^2 \left( zC \sqrt{1 + \frac{\Delta\beta^2}{4C^2}} \right) \end{aligned} \quad , \quad (2.30)$$

it is possible to find the detuning  $\Delta\beta$  and  $C$  (notice that for  $\Delta\beta = 0$ , Eq. (2.28) is obtained) by tracing the entire dynamics through the fluorescence technique. This is possible due to the formation of color centers during the inscription process, which exhibits high absorption at 620 nm. Therefore, when launching light beam at  $\lambda = 633$  nm, these color centers are excited and the emitted fluorescence can be recorded with a camera [41] (see Fig. 2.4 a)). Once the image is obtained, the experimental data are fitted using the analytical solutions so the values of detuning are found for different values of writing velocities.

The laser system used in this work is from *Coherent*, consisting of a pump *Verdi V18*, oscillator *Mira 900* and amplifier *RegA 9000*. It produces ultrashort pulses at 800 nm center wavelength with a repetition rate of 100 kHz, pulse length of approximately 150 fs at full width half maximum (FWHM) and pulse energy of 500 nJ. The pulses are focused into the sample by a 20 $\times$ -objective (numerical aperture of 0.35). The samples used to fabricate waveguides are polished fused silica *Corning®HPFS®7980 Standard Grade* and *Corning®HPFS®7980 ArF Grade*. The

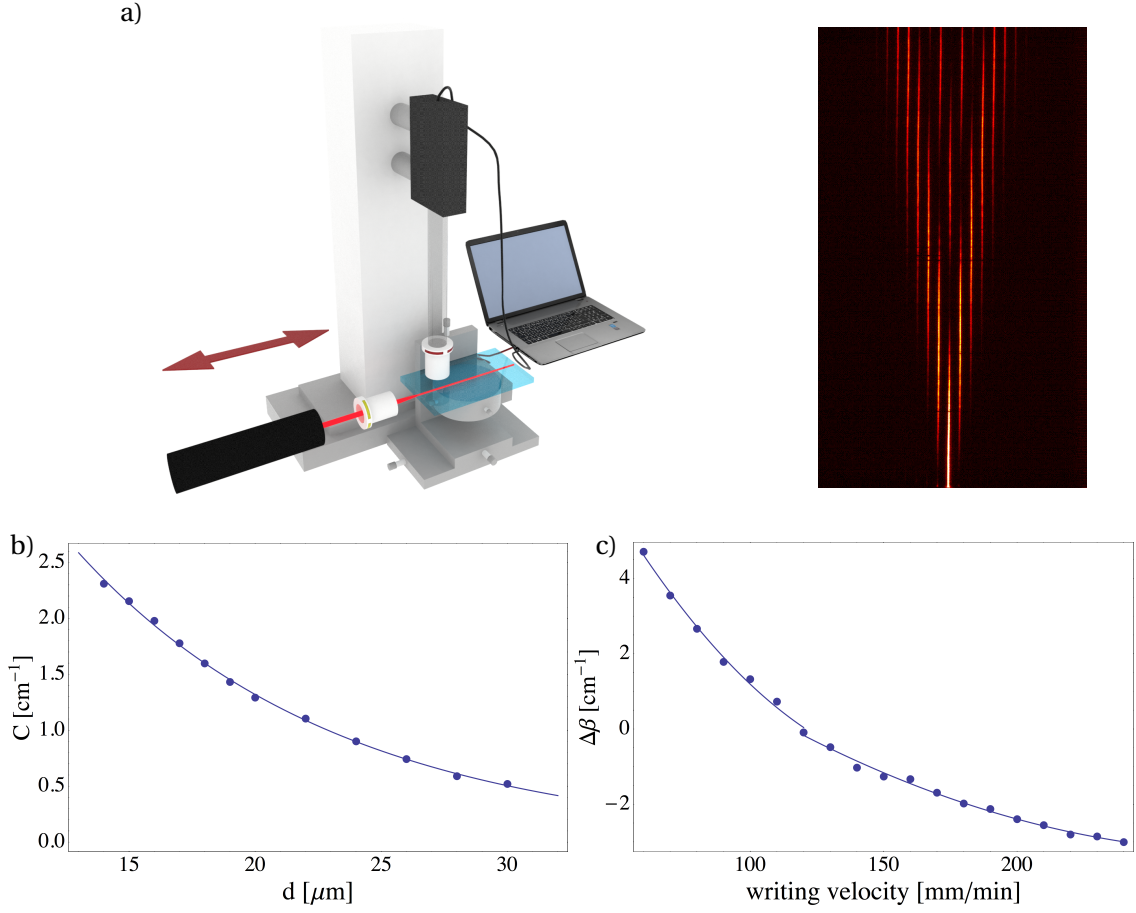


Figure 2.4: Calibration of coupling and detuning. a) Fluorescence setup: red light from a HeNe laser at 633 nm illuminates the sample and sections of the fluorescence pattern are recorded by a CCD camera from the top, which is translated along the sample until the entire pattern is saved. To the right an experimental fluorescence pattern for a homogenous array (from [41]). b) Characteristic curve of coupling  $C$  vs coupling distance  $d$ , where a exponential function is used to fit experimental data. c) Relation between detuning  $\Delta\beta$  and writing velocity. Blue lines correspond to a fit, where slightly different fits were used for positive and negative detuning.

translational movement of the samples is done by a three-axis translation stage *Aerotech ANT130* with typical inscription velocities between 60 mm/min and 200 mm/min. The created waveguides have an elliptical cross section of around  $2 \times 10 \mu\text{m}^2$ . The shape of waveguide mode is elliptical too, as shown in Fig. 2.3, with typical size between  $10 \times 15 \mu\text{m}^2$  to  $15 \times 20 \mu\text{m}$  (FWHM) at 815 nm. Since the connection between the sample with the photons source and detectors is done using commercial fiber-arrays, with a separation of  $127 \mu\text{m}$  between them, a fan-in and fan-out in the sample is required in order to match the position of the fibers. This is done by curved segments at the beginning and at the end of the sample (see Fig. 3.3) where the bending radii is limited to the centimeter regime to avoid extra

losses [53].

In conclusion, the femtosecond laser writing technique has proved to have a huge potential in the area of discrete systems, propagation of light and quantum optics. The 3D capability and fast process of creation (around one minute per waveguide) are the big advantages of this technique. The circuits exhibit high stability, they are permanent and have reduced size (in the order of microns (width) and few millimeters up to centimeters (length)), which is the reason why one speaks about integrated chip. Since photons can be also used in these structures [27], the term quantum integrated optics is referred to those circuits where photons and an integrated chip is used. Therefore, this technique is used in all the experiments throughout this thesis.

## 2.4 Generation and detection of indistinguishable photon pairs

One of the most common sources of indistinguishable photon pairs is based on spontaneous parametric down conversion (SPDC) [54, 55]. This is a nonlinear process, where two photons (called idler with frequency  $\omega_i$  and signal with frequency  $\omega_s$ ) are created from an initial pump photon with frequency  $\omega_p$ . This is a spontaneous process, meaning that not always photon pairs will be created, where the state of the nonlinear crystal is unchanged (parametric process) and the energy and momentum are conserved, with a lower energy of the idler and signal compared to the pump (down conversion). Specifically, the energy conservation is  $\hbar\omega_p = \hbar\omega_i + \hbar\omega_s$  and momentum conservation is  $\vec{k}_p = \vec{k}_i + \vec{k}_s$  which allows only certain directions in  $\vec{k}_j$ , depending on frequencies, orientation of the crystal (optical axis), refractive index and polarization. One can distinguish two types of nonlinear crystal for SPDC, one named type I, where the photon pair have the same polarization (and orthogonal to the polarization of the photon pump) and the second named the type II, where signal and idler have orthogonal polarization. In this work the type I is used, so photon pairs with equal polarization are generated. Consider signal and idler have a certain angle  $\theta_s$  and  $\theta_i$  with respect to the pump direction (see Fig. 2.5), then depending of the angle  $\Theta$  between the photons of the pump and the optical axis of the crystal, it is possible to have the degenerate case  $\omega_s = \omega_i = \omega_p/2$  and  $\theta_s = \theta_i$  (this is why they are also called “twin photons”), where the photons have the same frequency and polarization and are emitted in opposite

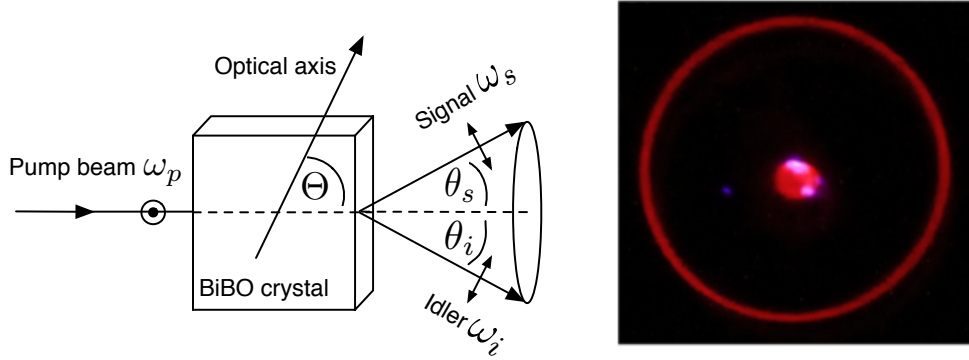


Figure 2.5: Photon pair generated by spontaneous parametric down conversion. a) A pump beam is launched to a nonlinear BiBO crystal where two photons, signal and idler, are generated with some certain angles  $\theta_i$  and  $\theta_s$ . b) Experimental image at the output for the degenerate case  $\theta_i = \theta_s$ , where a ring is formed. The spot at the middle correspond to the pump beam. Image from [56].

sides of a cone of opening angle  $2\theta_s$ , as indicated in Fig. 2.5.

The detection of photons after the sample was done using avalanche photo diodes. Inside these detectors a large voltage is applied against the current transmitting direction of their pn-junction. Once an incoming photon is absorbed, an electron-hole pair is generated, and then both charge carriers are separated and accelerated strongly, so that they generate more carriers by impact ionization. This process repeats leading to avalanche of carriers which can be detected as a macroscopic current [57]. As a single photon suffices to start an avalanche, also it could be two or three photons having the same result, so these detector cannot distinguish the real photon number. So, cases where two photons are populating one waveguide were detected using probabilistic photon number resolving detection using a 50:50 fiber splitter [29].

In Fig. 2.6 the setup for performing quantum experiments used during this work is shown. A continuous wave diode laser *Coherent OBIS 405* at 407.5 nm and 70 mW of optical power illuminates a type I phase-matched 1 mm-thick bismuth borate  $\text{BiB}_3\text{O}_6$  (BiBO) crystal and orientated in such manner that the signal and idler photons at 815 nm (double wavelength of the pump) emerge in an opening angle of 14.4 degrees. Then the photons are passed through a 3 nm band-pass filter *Semrock 830 nm MaxLine®* in order to improve indistinguishability. These photons are coupled to two polarization maintaining single mode optical fibers. The time delay (or equivalent the path length difference) of the incoming photons

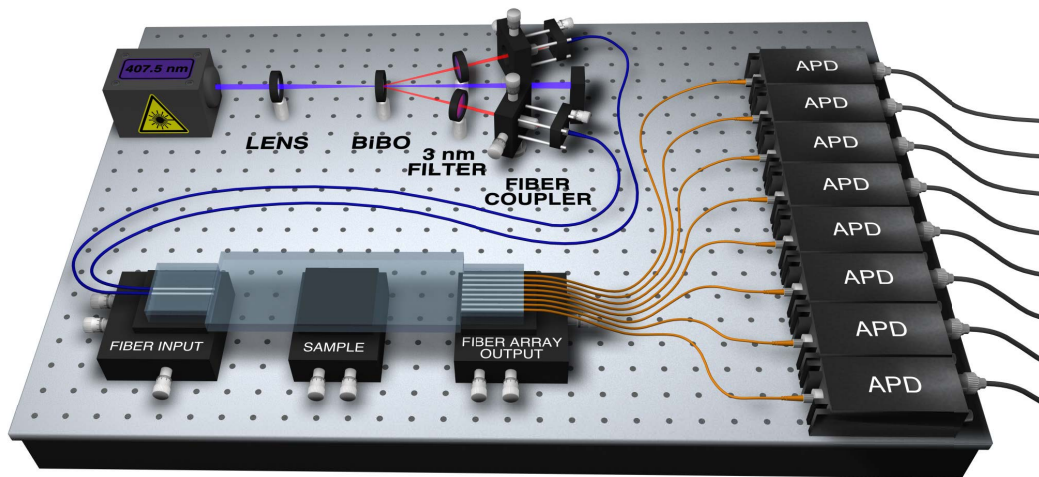


Figure 2.6: Scheme of the experimental quantum setup used in this work. It contains the generation of photon pairs by SPDC (BiBO crystal). Manipulation of the photons is done in an integrated chip (sample) fabricated with the femtosecond writing technique. Detection of the photons is realized with avalanche photo diode detectors (APD).

to the sample are controlled by a  $\mu\text{m}$  actuator connected to one of the fibers. These fibers can be connected to any of the eight polarization maintaining single mode fibers of the input fiber array. As it was mentioned before, the fibers in this input fiber array are separated by  $127\ \mu\text{m}$  so a fan-in and fan-out has to be done in the sample in order to couple it to the fiber array. A second fiber array is used to lead the photons toward the avalanche photo diode detectors which are connected to a computer where photon counting and coincidences are recorded (by a correlation card *Beck & Hickel DPC 230*).

To summarize, this chapter gave brief overview of the three important parts of any quantum integrated photonics circuit: photon source, circuit (or manipulation) and detection. Although here presented as different parts, the state of art is rapidly moving to a fully integrated chip, where the generation of photons, their manipulation and detection is done in a single integrated chip. In the next chapters the focus is put on the circuit itself, where the manipulation of photons through different operations reveals interesting properties in the dynamics of photons.

---

## Prevalence of quantum coherence in open quantum systems

Optical coherence, a property of waves that it can be seen as the relation between the phases of a single or several waves has been greatly studied in classical realm but in the context of a quantum realm it has a deeper meaning. The term coherence, now quantum coherence, is related to the relation between phases of quantum states, and they are described for correlations functions of higher orders which differs with the classical case [58]. Of particular interest is how the quantum coherence is affected or modified during a dynamical process since it has deeper implications in the system itself. That is how the study of loss of coherence could be explained due to the interaction between the system and an environment and this loss of coherence has been postulated as the quantum origin of the classical one [59]. One example where changes in coherence affect the system itself is in the energy transport in the Fenna-Matthews-Olson protein complex [60]. This is a photosynthetic complex where the efficiency of the transport of energy from one site to another is very high. Simulations, however, show an efficiency very smaller with respect to the experimental data, where only coherent transport is assumed. That is how, contrary to what someone could think, the action of decoherence (loss of coherence) is what describes well this high value of transport efficiency, which can be explained due to the interaction between the system and environment [61, 62].

The effects of the decoherence in a system and how affect the coherence is studied in this chapter, considering not only single photons but also two-photon input states. Making a connection between open quantum systems (OQS) and arrays of waveguides with dynamical disorder, an experiment in an integrated chip is performed.

### 3.1 Closed and open quantum systems

Dynamical systems which do not exchange energy (or information, matter, etc) with another system are named closed quantum systems. In these systems the time evolution of a pure state  $|\psi(t)\rangle$  is:

$$\frac{d}{dt} |\psi(t)\rangle = -\frac{i}{\hbar} H(t) |\psi(t)\rangle \quad , \quad (3.1)$$

where  $H$  is the Hamiltonian of the system. Typically  $H$  is hermitian and the evolution of the state can be expressed by an unitary time-evolution operator  $U(t, t_0)$  which transform the initial state  $|\psi(t_0)\rangle$  to  $|\psi(t)\rangle$

$$|\psi(t)\rangle = U(t, t_0) |\psi(t_0)\rangle \quad ,$$

and substituting in Eq. (3.1):

$$\frac{\partial}{\partial t} U(t, t_0) = -\frac{i}{\hbar} H(t) U(t, t_0) \quad . \quad (3.2)$$

Now, if instead of a pure state there is a mixed state, it is used the density matrix:

$$\rho(t_0) = \sum_{\alpha} \omega_{\alpha} |\psi_{\alpha}(t_0)\rangle \langle \psi_{\alpha}(t_0)| \quad , \quad (3.3)$$

then for a time  $t$

$$\begin{aligned} \rho(t) &= \sum_{\alpha} \omega_{\alpha} U(t, t_0) |\psi_{\alpha}(t_0)\rangle \langle \psi_{\alpha}(t_0)| U^{\dagger}(t, t_0) \\ \rho(t) &= U(t, t_0) \rho(t_0) U^{\dagger}(t, t_0) \quad . \end{aligned}$$

Taking the time derivative of equation above

$$\frac{d\rho}{dt} = \frac{\partial}{\partial t} U(t, t_0) \rho(t_0) U^{\dagger}(t, t_0) + U(t, t_0) \rho(t_0) \frac{\partial}{\partial t} U^{\dagger}(t, t_0) \quad ,$$

and using Eq. (3.2)

$$\frac{d\rho}{dt} = -\frac{i}{\hbar} H(t) U(t, t_0) \rho(t_0) U^{\dagger}(t, t_0) + \frac{i}{\hbar} U(t, t_0) \rho(t_0) U^{\dagger}(t, t_0) H(t) \quad ,$$

but  $U(t, t_0) \rho(t_0) U^{\dagger}(t, t_0) = \rho(t)$ , so:

$$\frac{d\rho}{dt} = -\frac{i}{\hbar} [H, \rho] \quad . \quad (3.4)$$

This equation is known as Liouville-von Neumann equation and it is the quantum version of the the classical Liouville equation

$$\frac{\partial \rho}{\partial t} = -\{\rho, H\} \quad ,$$

where  $\rho$  now is the phase space distribution and  $\{ , \}$  are the Poisson brackets.

Now for the case of open quantum systems, consider a system  $S$  which is coupled to another quantum system, the environment  $E$  (which represents a reservoir or a heat bath). Although the combined system is closed, the time evolution of the open system  $S$  is not in general unitary. This is due to the interaction between the environment, consisting of an infinite number of degrees of freedom, and the system. The total Hamiltonian  $H$  can be written as

$$H(t) = H_S \otimes \mathbb{I} + \mathbb{I} \otimes H_E + H_I(t) \quad ,$$

where  $H_S$  and  $H_E$  are the Hamiltonian of the system  $S$  and  $E$  respectively and the interaction is described by  $H_I$ . Because the interest is in the dynamics of the system  $S$  itself and not together to the environment  $E$ , the focus is put in the subset of observables related to the open system  $S$  which leave unaltered the system  $E$  by taking the reduced density matrix:

$$\rho_S = \text{Tr}_E\{\rho\} \quad , \quad (3.5)$$

where  $\text{Tr}$  is the trace. Since the total density matrix evolves unitarily in time

$$\rho_S = \text{Tr}_E\{U(t, t_0)\rho(t_0)U^\dagger(t, t_0)\} \quad .$$

Then

$$\begin{aligned} \frac{d\rho_S}{dt} &= \frac{d}{dt}\text{Tr}_E\{\rho(t)\} \\ &= \text{Tr}_E\left\{\frac{d\rho}{dt}\right\} \end{aligned}$$

but  $d\rho/dt$  can be written as Eq. (3.4), so:

$$\frac{d\rho_S}{dt} = -\frac{i}{\hbar}\text{Tr}_E[H, \rho] \quad . \quad (3.6)$$

From this equation and using dynamical maps and Kraus operators plus Born and Markov approximations it is possible to derive an new equation for the reduced density matrix  $\rho_S$  (the theoretical description of this calculation is beyond the scope of this work, detailed information can be found in [63, 64]), known as master equation:

$$\frac{d\rho_S}{dt} = -\frac{i}{\hbar}[H, \rho_S] + \frac{1}{\hbar} \sum_k (V_k \rho_S V_k^\dagger - \frac{1}{2} V_k^\dagger V_k \rho_S - \frac{1}{2} \rho_S V_k^\dagger V_k) \quad , \quad (3.7)$$

where  $V_k$  are the Lindblad operators and the sum is until  $d^2 - 1$  with  $d$  the dimension of the Hamiltonian  $H$ . This equation also can be found in the so-called Lindblad form [65]:

$$\frac{d\rho_S}{dt} = -\frac{i}{\hbar}[H, \rho_S] + \mathcal{L}[\rho_S] \quad , \quad (3.8)$$

where  $\mathcal{L}$  is the Lindblad operator  $\mathcal{L} = \frac{1}{\hbar} \sum_k (V_k \rho V_k^\dagger - \frac{1}{2} V_k^\dagger V_k \rho - \frac{1}{2} \rho V_k^\dagger V_k)$ .

## 3.2 Master equation for single photon states

As it was established in the previous section, the interaction between a quantum system and a fluctuating environment is called open quantum system, and how the action of the environment affect the dynamics of the system it has been a subject of intensive research in science [66–68]. One way to study the evolution of these open quantum systems is using the Born-Markov approximation [69]. In this approximation the quantum system is weakly coupled to a large environment system (reservoir) where the environment is virtually unaffected by coupling to the quantum system under analysis and also that memory time of the environment is extremely short in comparison to the timescale of the quantum system evolution so memory effects are neglected, that means the future of the dynamics only depends of the present. This action of the environment to the system can be modeled in different ways including dissipation, dephasing, Markovian or non-Markovian fluctuations [62, 70]. In the present work, it will be considered pure dephasing and Markovian fluctuations [71] and the relevance of such dephasing model can be found in several interdisciplinary framework of studies including quantum chemistry [72, 73], biology [61, 62] and ultra-cold atoms [74].

In a quantum system of  $N$  sites (or network) under dephasing, the phase properties of the associated quantum mechanical waves are randomly distorted by the environment. The equation representing that situation and the dynamics of this system, can be written as:

$$i \frac{d}{dt} \varphi_n(t) + \epsilon_n(t) \varphi_n(t) + \sum_{m \neq n}^N \kappa_{m,n} \varphi_m(t) = 0 \quad , \quad (3.9)$$

where  $\varphi_n$  represents the single particle wavefunction at site  $n$ ,  $\kappa_{m,n}$  is the hopping rate between sites  $m$  and  $n$ ,  $\epsilon_n$  stands for the energy at site  $n$  and  $\hbar = 1$ . Notice that this equation is for the system represented by  $\varphi$  and is not for the total system (system + environment), and it will be referred as reduced OQS. Although the

equation above is for the reduced OQS, the action of the environment is indeed present, represented by the fluctuating on-site energy  $\epsilon_n$ . Moreover,  $\epsilon_n$  depends of  $t$ , satisfying the conditions of a Gauss-Markov processes,

$$\langle \epsilon_n(t) \rangle = 0 \quad \text{and} \quad \langle \epsilon_n(t) \epsilon_m(t') \rangle = \mu_n \delta_{m,n} \delta(t - t') \quad ,$$

with  $\langle \dots \rangle$  denoting stochastic average and  $\mu_n$  being the dephasing rates [71]. As it was already seen in Chapter 2, the Schrödinger equation is completely analogous to the paraxial wave equation, and because the experiments done during this work are in the context of photonics, from now the following equation will be used instead of Eq. (3.9):

$$i \frac{d}{dz} \psi_n(z) + \beta_n(z) \psi_n(z) + \sum_{m \neq n}^N C_{m,n} \psi_m(z) = 0 \quad , \quad (3.10)$$

where now  $\psi_n$  represents the amplitude of the mode in site  $n$ ,  $\beta_n$  stands for the propagation constant in site  $n$  and  $C_{m,n}$  is the coupling between sites  $m$  and  $n$ . As before for  $\epsilon_n$ , it is the propagation constant  $\beta_n(z)$  who is changing in  $z$  in this case, according to the function  $\beta_n(z) = \beta_n + \phi_n(z)$ , where  $\phi_n$  satisfies the condition of a Gauss-Markov process  $\langle \phi_n(z) \rangle = 0$  and  $\langle \phi_n(z) \phi_m(z') \rangle = \gamma_n \delta_{m,n} \delta(z - z')$ . The dephasing rate  $\gamma_n$  corresponds to  $\gamma_n = \sigma_n^2 \Delta z$  [75], where  $\sigma$  is the standard deviation of the gaussian distribution and  $\Delta z$  corresponds to the correlation length.

Although Eq. (3.10) is useful to determine the dynamics of the amplitude  $\psi$ , it does not give (explicitly) information about quantum coherence terms. For that it is necessary to write an equation for the density matrix  $\rho$ . Because this can be seen as a stochastic problem, due to the random fluctuations in  $\beta_n(z)$ , work done in the area of stochastic methods will be used, including Wiener processes and Itô's calculus [76]. Writing (3.10) in differential form

$$d\psi_n = i\beta_n \psi_n dz + i \sum_r C_{n,r} \psi_r(z) dz + i\psi_n \phi_n dz \quad .$$

Then introducing the Wiener increments

$$dW_n = \frac{\phi_n(z)}{\sqrt{\gamma_n}} dz \quad \rightarrow \quad \langle dW_n dW_m \rangle = \delta_{n,m} dz \quad ,$$

it produces:

$$d\psi_n = i\beta_n \psi_n dz + i \sum_r C_{n,r} \psi_r dz + i\psi_n \sqrt{\gamma_n} dW_n \quad . \quad (3.11)$$

Then using the Itô's product rule [77]:

$$d(\psi_m \psi_n^*) = d(\psi_n) \psi_m^* + \psi_n d(\psi_m^*) + d(\psi_n) d(\psi_m^*) \quad , \quad (3.12)$$

in which  $d\psi_n$  has to be written in Itô's form [71]:

$$d\psi_n = \left( i\beta_n\psi_n + i \sum_r C_{n,r}\psi_r - \frac{1}{2}\gamma_n\psi_n \right) dz + i\psi_n\sqrt{\gamma_n}dW_n \quad . \quad (3.13)$$

Calculating the right hand side of Eq. (3.12) using Eq. (3.13):

$$\begin{aligned} d(\psi_n\psi_m^*) &= \left[ i(\beta_n - \beta_m) - \frac{1}{2}(\gamma_n + \gamma_m) \right] \psi_n\psi_m^* dz + i \sum_r C_{n,r}\psi_r\psi_m^* dz \\ &- i \sum_r C_{m,r}\psi_n\psi_r^* dz + i\sqrt{\gamma_n}\psi_n\psi_m^* dW_n - i\sqrt{\gamma_m}\psi_n\psi_m^* dW_m + \sqrt{\gamma_n}\sqrt{\gamma_m}\psi_n\psi_m^* dW_n dW_m \quad , \end{aligned} \quad (3.14)$$

where it has been considered terms up to first order in  $dz$ . Finally, by taking the stochastic average of Eq. (3.14), it follows a dynamics equation for the system in term of  $\rho$ :

$$\begin{aligned} \frac{d}{dz}\rho_{n,m}(z) &= \left[ i(\beta_n - \beta_m) - \frac{1}{2}(\gamma_n + \gamma_m) \right] \rho_{n,m}(z) + \sqrt{\gamma_n}\sqrt{\gamma_m}\delta_{n,m}\rho_{n,m}(z) \\ &+ i \sum_r C_{n,r}\rho_{r,m}(z) - i \sum_r C_{m,r}\rho_{n,r}(z) \quad , \end{aligned} \quad (3.15)$$

where it was used the relation  $\rho_{n,m} = \langle \psi_n\psi_m^* \rangle$ . It should be noticed that Eq. (3.10) was used for the reduced OQS, so this density matrix  $\rho$  corresponds to the reduced density matrix. Therefore, this equation is the master equation (Eq. (3.8)), where the coupling terms  $C$  and propagation constant terms  $\beta$  are associated to the Hamiltonian  $H$  and dephasing terms  $\gamma$  are associated to the Lindblad operator (see Appendix A).

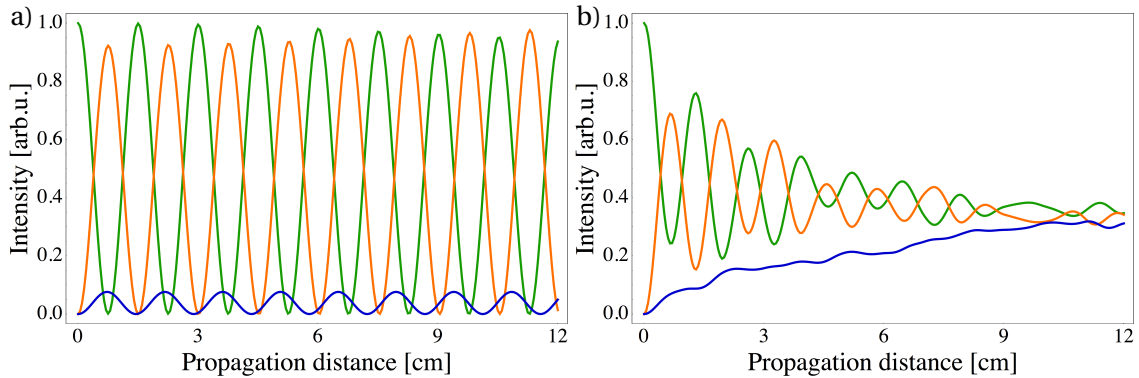


Figure 3.1: Theoretical intensity distribution of the system of three waveguides. a) Case without noise and b) case with a dynamical noise and correspond to the average of 100 simulations. Upper waveguides (green and orange lines) have a stronger coupling compare to the lower waveguide (blue line) due to their proximity.

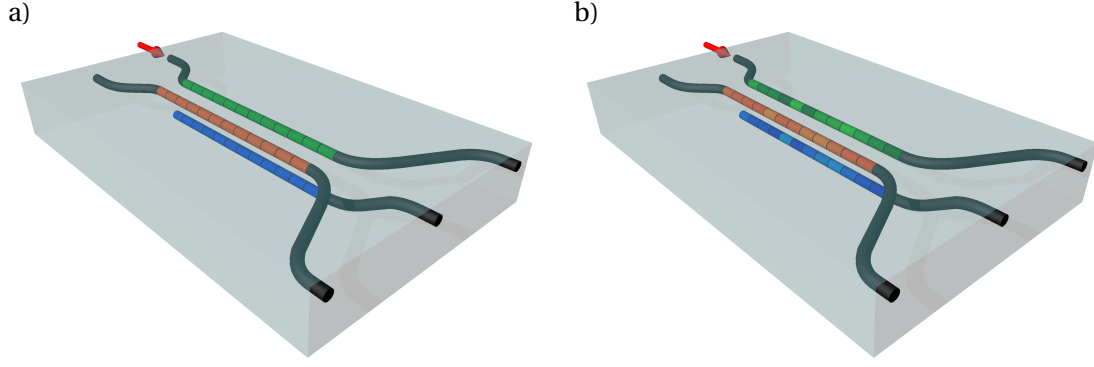


Figure 3.2: Schematic setup of an integrated array of three waveguides used to represent a reduced open quantum system. In (a) the waveguides keep their propagation constant (no dephasing) meanwhile in (b) the waveguides have different propagation constants given by the different color shades. The arrow represents the initial input in only one waveguide. Green waveguide represents waveguide 1, orange is waveguide 2 and blue is waveguide 3.

In order to see how the dephasing affect the dynamics, a simulation of a system with noise and another without disorder is done, where the system consists of three waveguides with fluctuating propagation constants (see Fig. 3.2). In order to be concise, during this work the terms dephasing, noise and disorder means the same, although dephasing will be used in the quantum context and noise in the experimental context. A plot for the theoretical intensity of every waveguide along the propagation distance is shown in Fig. 3.1, which also it corresponds to the diagonal elements of  $\rho$  ( $\rho_{n,n} = \langle \psi_n \psi_n^* \rangle = |\psi_n|^2$  which are the intensities in Fig. 3.1). It is clear that in the order system the evolution is mainly in the upper waveguides and in a coherent fashion where only a small amount of light is going to the lower site. In contrast, the same system but with a fluctuating noise, the average evolution is quite different and now it is observed that in average the wave-packet evolves into an incoherent superposition of delocalized light states, where after 12 cm there is a homogeneous energy distribution in all sites.

### 3.3 Experiment and results

In order to show these results experimentally, it will be used as model an array of three waveguide also called trimer (see Fig. 3.2), which was fabricated using the femtosecond laser writing technique. In this system the two upper waveguides (labeled as waveguide 1 and 2) are closer and they interact weakly with a third waveguide (labeled as waveguide 3). Specifically the values used for the

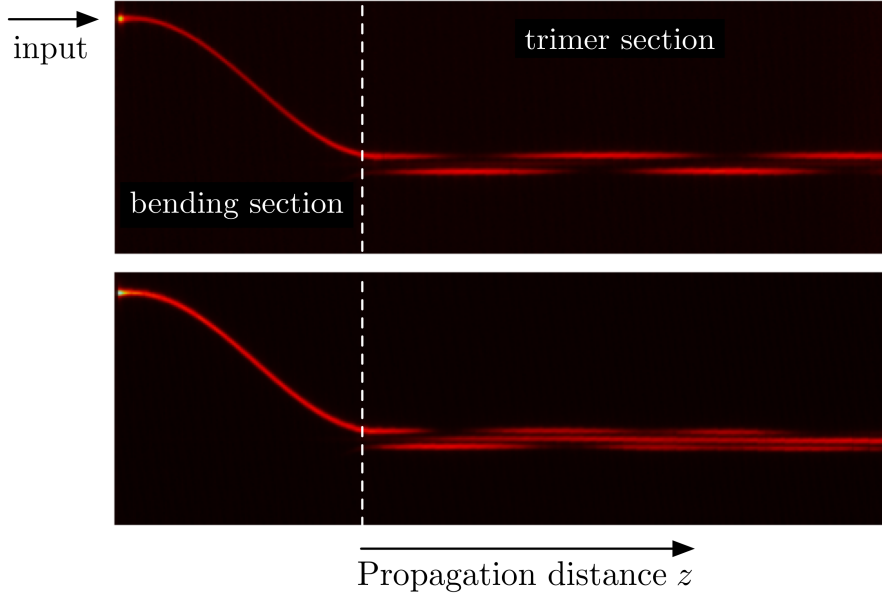


Figure 3.3: Fluorescence images of the system of three waveguides for the first centimeters. (top) order case (bottom) noisy case for a single measurement. Indicated are the input position, the bending and trimer section separated by a dashed white line.

coupling coefficients between upper waveguides were  $C_{1,2} = C_{2,1} = 2 \text{ cm}^{-1}$  and  $C_{1,3} = C_{2,3} = 0.6 \text{ cm}^{-1}$  was the coupling with the lower waveguide. The propagation constants  $\beta_n$  were chosen randomly from a Gaussian distribution with a variance of  $\sigma = 3 \text{ cm}^{-1}$  and mean values of  $\beta_1 = \beta_2 = 1 \text{ cm}^{-1}$  and  $\beta_3 = -1 \text{ cm}^{-1}$ . This was experimentally done changing the writing velocity of the laser inscription. The length used in all experiments was 12 cm and the length of every section  $\beta_n$  was  $\Delta z = 1 \text{ cm}$ . Then, light from a HeNe laser at 632 nm was used to illuminate one of the upper sites of the trimer and images from the top were taken. This allows

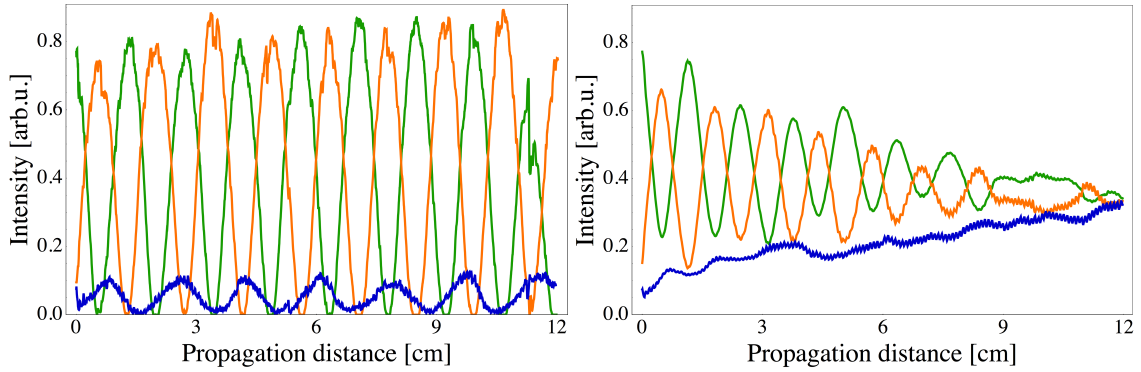


Figure 3.4: Experimental intensity distribution along the propagation distance, where a) corresponds to the order case and b) to the average of the noisy cases. Line colors are the same as in Fig. 3.1.

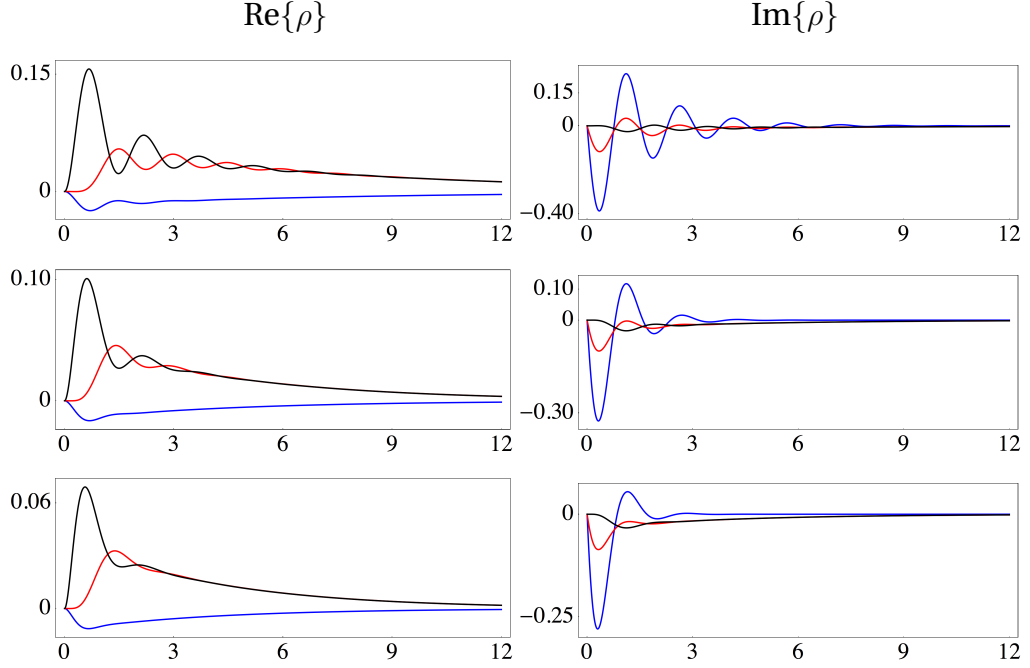


Figure 3.5: Real and imaginary part of the off diagonal elements of  $\rho$  versus propagation distance for different values of dephasing  $\gamma$ . (top)  $\gamma = 0.3\gamma_{exp}$ , (center)  $\gamma = 0.6\gamma_{exp}$  and (bottom)  $\gamma = \gamma_{exp}$  where  $\gamma_{exp} = (1.7275, 1.7435, 1.7645)$ . Blue line corresponds to  $\rho_{1,2}$ , red line to  $\rho_{1,3}$  and black line to  $\rho_{2,3}$ .

to see all propagation along the propagation distance. As example, in Fig. 3.3 is possible to see the experimental pictures for the noiseless case and noisy case. The intensity profiles along the propagation distance are extracted from those pictures and for the noisy case the final intensity profile corresponds to the average over 21 different samples. The results are shown in Fig. 3.4. Comparing the experimental intensity distribution to the theoretical one in Fig. 3.1, the results show that the experimental data is in a very good agreement with the theory. Specially in Fig. 3.4 b), it is evidently how the intensity distribution in the third site (blue line) is growing up, and at 12 cm the three waveguides have almost the same amount of intensity. These results are also a good experimental evidence about how the action of the environment over a system (in this case through dephasing), assists and increments the transport efficiency, given by the increment of intensity in the third waveguide [61]. Apart from this experimental result, the off diagonal components (the coherence terms) of the density matrix  $\rho$  using Eq. (3.15) was calculated. In Fig. 3.5 are plotted the real and imaginary part of the off diagonal components of  $\rho$  for different values of dephasing  $\gamma$ . Those simulations reveal that independently of the value of dephasing  $\gamma$ , the real and imaginary part of  $\rho_{p,q}$   $p \neq q$  tends to zero, meaning that the coherence of the system decay. This results can be explained

watching equation (3.15) where the off diagonal elements  $\rho_{p,q}$  exhibit a complex term  $(\beta_p - \beta_q) - i(\gamma_p + \gamma_q)/2$ , where the negative imaginary part implies attenuation. On the contrary, for the diagonal elements  $\rho_{p,p}$  this term is zero.

This theoretical result along with the experimental observation suggest that Eq. (3.15) can be assumed valid. For single-excitations (in the reduced OQS) the evolution is coherent during certain time and then the system reaches a steady state constituted of an uniform incoherent mixture of states [61, 62, 72], where the coherence of the system has decayed.

### 3.4 Master equation for two-photon states

In the previous section the dynamics for single particle was calculated and one of the result was the quantum coherence decays (see Fig. 3.5), so one natural question is if for two-photon state will happen the same or not. To answer that, a theoretical and experimental study will be developed in this section. In order to obtain the master equation for a two-photon state, a similar approach for single photon case is used. The framework used here is based on the concept of two-photon probability amplitude  $\Psi_{p,q}$ , which describes jointly two photons in sites  $(p, q)$  [78].

By adding the information about what site is initially occupied by the single photon, Eq. (3.10) can be written as follows:

$$i \frac{d}{dz} U_{p,n}(z) + \beta_n(z) U_{p,n}(z) + \sum_r C_{p,r} U_{r,n}(z) = 0 \quad , \quad (3.16)$$

where  $U_{p,n}$  is the probability amplitude in site  $p$  and initially excited in site  $n$ . One can do the same for another photon and calculate  $U_{q,m}$  and in terms of these two amplitudes is defined the two-photon probability at sites  $p$  and  $q$  [79]:

$$\Psi_{p,q}(z) = \sum_{m,n}^{N,N} \alpha_{m,n} [U_{p,n}(z) U_{q,m}(z) + U_{p,m}(z) U_{q,n}(z)] \quad , \quad (3.17)$$

where  $\alpha_{m,n}$  is the initial normalized probability amplitude profile  $(\sum_{m,n} |\alpha_{m,n}|^2 = 1)$ . It worth to mention that in the expression (3.17) the  $+$  sign also can be  $-$  where plus or minus sign are used for boson or fermion statistics respectively [80]. Similar to previous section, Eq. (3.16) is written in differential form:

$$dU_{q,n} = i\beta_q U_{q,n} dz + i \sum_r C_{r,q} U_{r,n} + i\phi_q(z) U_{q,n} dz \quad , \quad (3.18)$$

and also:

$$dU_{p,m} = i\beta_p U_{p,m} dz + i \sum_r C_{r,p} U_{r,m} dz + i\phi_p(z) U_{p,m} dz \quad . \quad (3.19)$$

Introducing the Wiener increments  $dW_p = \frac{\phi_p(z)}{\sqrt{\gamma_p}} dz$  and  $dW_q = \frac{\phi_q(z)}{\sqrt{\gamma_q}} dz$  and replacing them in the equations above:

$$dU_{q,n} = i\beta_q U_{q,n} dz + i \sum_r C_{r,q} U_{r,n} dz + i\sqrt{\gamma_q} U_{q,n} dW_q \quad (3.20)$$

$$dU_{p,m} = i\beta_p U_{p,m} dz + i \sum_r C_{r,p} U_{r,m} dz + i\sqrt{\gamma_p} U_{p,m} dW_p \quad . \quad (3.21)$$

But these equations have to be written in the Itô's form:

$$dU_{q,n} = \left( i\beta_q U_{q,n} + i \sum_r C_{r,q} U_{r,n} - \frac{1}{2} \gamma_q U_{q,n} \right) dz + i\sqrt{\gamma_q} U_{q,n} dW_q \quad (3.22)$$

$$dU_{p,m} = \left( i\beta_p U_{p,m} + i \sum_r C_{r,p} U_{r,m} - \frac{1}{2} \gamma_p U_{p,m} \right) dz + i\sqrt{\gamma_p} U_{p,m} dW_p \quad . \quad (3.23)$$

Then using the Itô's product rule given in Eq. (3.12), the product  $d(U_{q,n} U_{p,m})$  can be obtained

$$\begin{aligned} d(U_{q,n} U_{p,m}) = & \left[ i(\beta_p + \beta_q) U_{q,n} U_{p,m} + i \sum_r C_{r,p} U_{q,n} U_{r,m} \right. \\ & + i \sum_r C_{r,q} U_{r,n} U_{p,m} - \frac{1}{2} (\gamma_p + \gamma_q) U_{q,n} U_{p,m} \Big] dz \\ & + i(\sqrt{\gamma_p} dW_p + \sqrt{\gamma_q} dW_q) U_{q,n} U_{p,m} - \sqrt{\gamma_p \gamma_q} U_{q,n} U_{p,m} dW_p dW_q \quad . \end{aligned}$$

Doing the same for  $d(U_{p,n} U_{q,m})$  and adding those two equations, it is found

$$\begin{aligned} d(U_{p,n} U_{q,m} + U_{q,n} U_{p,m}) = & i(\beta_p + \beta_q) (U_{p,n} U_{q,m} + U_{q,n} U_{p,m}) dz \\ & + i \sum_r C_{r,q} (U_{p,n} U_{r,m} + U_{p,m} U_{r,n}) dz + i \sum_r C_{r,p} (U_{r,n} U_{q,m} + U_{r,m} U_{q,n}) dz \\ & - \frac{1}{2} (\gamma_p + \gamma_q) (U_{p,n} U_{q,m} + U_{q,n} U_{p,m}) dz + i(\sqrt{\gamma_p} dW_p + \sqrt{\gamma_q} dW_q) (U_{p,n} U_{q,m} + U_{q,n} U_{p,m}) \\ & - \sqrt{\gamma_p \gamma_q} (U_{p,n} U_{q,m} + U_{q,n} U_{p,m}) dW_p dW_q \quad , \end{aligned}$$

but by using the definition of  $\Psi_{p,q}$  in Eq. (3.17):

$$\begin{aligned} d\Psi_{p,q} = & i(\beta_p + \beta_q) dz \Psi_{p,q} + i \sum_r (C_{r,p} \Psi_{r,q} + C_{r,q} \Psi_{p,r}) dz - \frac{1}{2} (\gamma_p + \gamma_q) \Psi_{p,q} dz \\ & + i(\sqrt{\gamma_p} dW_p + \sqrt{\gamma_q} dW_q) \Psi_{p,q} - \sqrt{\gamma_p \gamma_q} \Psi_{p,q} dW_p dW_q \quad . \quad (3.24) \end{aligned}$$

Doing the same, but now for the complex conjugate of  $\Psi_{p',q'}$ , it is found the expression:  $d(\Psi_{p,q}\Psi_{p',q'}^*)$

$$\begin{aligned}
d(\Psi_{p,q}\Psi_{p',q'}^*) &= \left[ i(\beta_p + \beta_q - \beta_{p'} - \beta_{q'}) - \frac{1}{2}(\gamma_p + \gamma_q + \gamma_{p'} + \gamma_{q'}) \right] \Psi_{p,q}\Psi_{p',q'}^* dz \\
&+ i \sum_r [C_{r,q}\Psi_{p,r}\Psi_{p',q'}^* + C_{r,p}\Psi_{r,q}\Psi_{r,q'}\Psi_{p',q'}^* - C_{r,q'}\Psi_{p,q}\Psi_{p',r}^* - C_{r,p'}\Psi_{p,q}\Psi_{r,q'}^*] dz \\
&- \sqrt{\gamma_p\gamma_q}\Psi_{p,q}\Psi_{p',q'}^* dW_{p'}dW_{q'} - \sqrt{\gamma_p\gamma_q}\Psi_{p,q}\Psi_{p',q'}^* dW_p dW_q + \sqrt{\gamma_p\gamma_{p'}}\Psi_{p,q}\Psi_{p',q'}^* dW_p dW_{p'} \\
&+ \sqrt{\gamma_q\gamma_{q'}}\Psi_{p,q}\Psi_{p',q'}^* dW_q dW_{q'} + \sqrt{\gamma_p\gamma_{q'}}\Psi_{p,q}\Psi_{p',q'}^* dW_p dW_{q'} + \sqrt{\gamma_q\gamma_{p'}}\Psi_{p,q}\Psi_{p',q'}^* dW_q dW_{p'}.
\end{aligned} \tag{3.25}$$

And finally taking the average:

$$\begin{aligned}
\frac{d}{dz}\rho_{(p,q),(p',q')}(z) &= \left[ i(\beta_p + \beta_q - \beta_{p'} - \beta_{q'}) - \frac{1}{2}(\gamma_p + \gamma_q + \gamma_{p'} + \gamma_{q'}) \right] \rho_{(p,q),(p',q')}(z) \\
&+ [\sqrt{\gamma_p\gamma_{p'}}\delta_{p,p'} + \sqrt{\gamma_p\gamma_{q'}}\delta_{p,q'} + \sqrt{\gamma_q\gamma_{p'}}\delta_{q,p'} + \sqrt{\gamma_q\gamma_{q'}}\delta_{q,q'} - \sqrt{\gamma_p\gamma_q}\delta_{p,q} \\
&- \sqrt{\gamma_{p'}\gamma_{q'}}\delta_{p',q'}] \rho_{(p,q),(p',q')}(z) + i \sum_r [C_{r,p}\rho_{(r,q),(p',q')}(z) + C_{r,q}\rho_{(p,r),(p',q')}(z)] \\
&- i \sum_r [C_{r,p'}\rho_{(p,q),(r,q')}(z) + C_{r,q'}\rho_{(p,q),(p',r)}(z)] \quad , \tag{3.26}
\end{aligned}$$

where it was used the relation  $\rho_{(p,q),(p',q')} = \langle \Psi_{p,q}\Psi_{p',q'}^* \rangle$ . Therefore, Eq. (3.26) corresponds to the master equation for two-photon states. Notice that the diagonal elements of the two-photon density matrix  $\rho$ , which are  $\rho_{(p,q),(p,q)} = \Psi_{p,q}\Psi_{p,q}^* = |\Psi_{p,q}|^2$  are related to Eq. (3.17) by the absolute square value, and correspond to the two-photon correlation function  $\Gamma_{p,q}$  seen in Chapter 2. So by integrating Eq. (3.26) and analyzing the diagonal elements, it is possible to check when there is bunching (elements  $(i,i)$ ,  $(i,i)$  where  $i = 1, 2, 3$ , which are the diagonal elements of  $\Gamma$ ) or antibunching (elements  $(i,j)$ ,  $(i,j)$  where  $i, j = 1, 2, 3$ , which are the off diagonal elements of  $\Gamma$ ).

### 3.5 Experiment and results

In the following, it will be considered the situations when the trimer system is excited by two indistinguishable photons in a separable state  $|\Psi_{sep}\rangle = \frac{1}{\sqrt{2}}(|1_1, 1_2\rangle + |1_2, 1_1\rangle)$  and in an entangled state  $|\Psi_{ent}\rangle = \frac{1}{\sqrt{2}}(|1_1, 1_1\rangle + |1_2, 1_2\rangle)$ , where the subindices represent in which site is the photon. Integration of Eq. (3.26) gives the dynamics of the system and is shown in Fig. 3.6. The results show that density matrix for both separable and entangled photons becomes identical after 12 cm and after 20 cm the

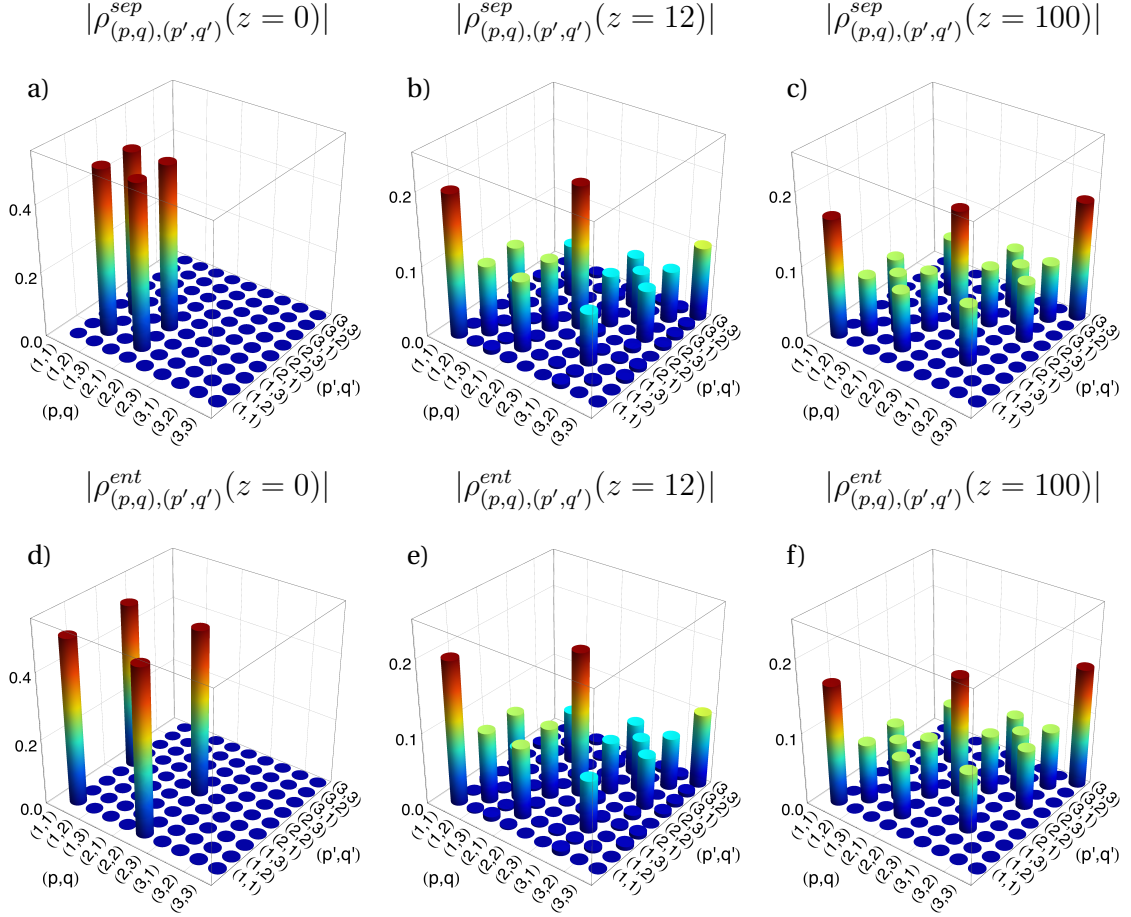


Figure 3.6: Absolute value of  $\rho_{(p,q),(p',q')}(z)$ . At top the separable case  $\rho^{sep}$  for a)  $z = 0$  cm, b)  $z = 12$  cm and c)  $z = 100$  cm. At bottom the path entangled case  $\rho^{ent}$  for d)  $z = 0$  cm, e)  $z = 12$  cm and f)  $z = 100$  cm. The values used for dephasing are equal to the experiment  $\gamma_{exp} = (1.3012, 1.2365, 1.293)$ .

system reaches the steady state. As a steady state, it prevails along the propagation distance for any distance as is shown for  $z = 100$  cm in Fig. 3.6 c) and f). An inspection of this steady state reveals the in the diagonal elements of  $\rho$  both photons bunch into the same site with probability  $\rho_{(1,1),(1,1)} = \rho_{(2,2),(2,2)} = \rho_{(3,3),(3,3)} = 0.15$  while the other terms in the diagonal, which quantify particle anti-bunching, exhibit a lower probability equal to 0.09.

Quite interestingly, there are some off-diagonal terms of the two-photon density matrix which are not zero, meaning that some coherence prevails. To explain this, an analysis of the two-photon master equation is done. Notice that for diagonal elements, the first two elements on the right-hand of Eq. (3.26) (elements factorized by  $\rho_{(p,q),(p',q')}$ ) gives zero. Moreover, the same occurs for the off-diagonal elements accounting for particle indistinguishability, in the form  $\rho_{(p,q),(q,p)}$ . So because these

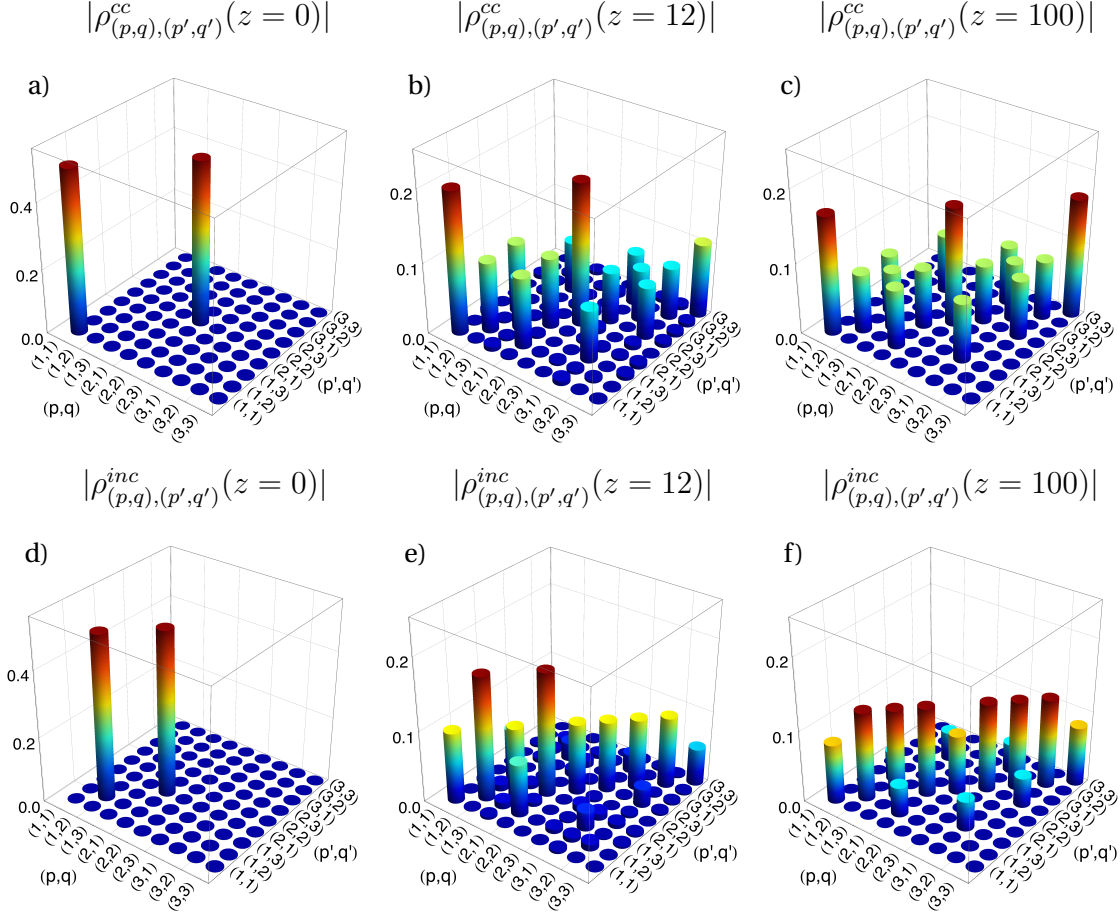


Figure 3.7: Absolute value of  $\rho_{(p,q),(p',q')}(z)$ . (top) Classically correlated state  $\rho_{cc}$  for a)  $z = 0$ , b)  $z = 12$  and c)  $z = 100$  cm, (bottom) incoherent state  $\rho_{inc}$  for d)  $z = 0$  cm, e)  $z = 12$  cm and f)  $z = 100$  cm. The values used for dephasing are equal to the experiment  $\gamma_{exp} = (1.3012, 1.2365, 1.293)$ .

elements are zero, the diagonal and the indistinguishable off-diagonal will remain immune to the dephasing. On the other side, the remaining off-diagonal elements  $\rho_{(p,q),(p',q')}$  will have the element  $i(\beta_p + \beta_q - \beta_{p'} - \beta_{q'}) - (\gamma_p + \gamma_q + \gamma_{p'} + \gamma_{q'})/2$  and the imaginary part will affect these off-diagonal elements, producing finally a decay.

After this analysis one question appearing is, what role does the indistinguishability perform?. Until now, it has been observed that when the input is indistinguishable, the off diagonal indistinguishable elements and diagonal elements prevail after decoherence. So in order to have the complete picture, a similar analysis is done launching two-photon states exhibiting classical probabilities. For that, consider the case of a two-photon state presenting classical correlation  $\rho_{(1,1),(2,2)}^{cc} = (|1_1, 1_1\rangle \langle 1_1, 1_1| + |1_2, 1_2\rangle \langle 1_2, 1_2|)/2$ , where this state involves two indistinguishable photons entering together into anyone of the upper waveguides

with exactly the same classical probability. Also consider the case of an incoherent state  $\rho_{(1,2),(2,1)}^{inc} = (|1_1, 1_2\rangle \langle 1_1, 1_2| + |1_2, 1_1\rangle \langle 1_2, 1_1|)/2$ , where this state represents two distinguishable photons entering separately into the upper waveguides of the system. The dynamics of these two different inputs are shown in Fig. 3.7. Remarkably, for the  $\rho_{(1,1),(2,2)}^{cc}$  case, the dynamics is identical to the cases separable and entangled. In contrast, for the case of  $\rho_{(1,2),(2,1)}^{inc}$  the density matrix looks completely different, where the anti-bunching elements  $\rho_{(1,2),(1,2)} = \rho_{(1,3),(1,3)} = \rho_{(2,1),(2,1)} = \rho_{(2,3),(2,3)} = \rho_{(3,1),(3,1)} = \rho_{(3,2),(3,2)} = 0.15$  are larger than the bunching ones  $\rho_{(1,1),(1,1)} = \rho_{(2,2),(2,2)} = \rho_{(3,3),(3,3)} = 0.09$  at  $z = 100$  cm. It should be mentioned that although they are two distinguishable photons, there are also some small elements outside the diagonal (see Fig. 3.7 f). A possible explanation it could be that due to the phase changes induced by dephasing, at some point, the coherences acquire the proper phase characteristic of indistinguishable particles and allowing it to exist. And once they get excited in a steady state they will remain immune to dephasing.

In order to quantify the difference between all steady states analyzed, it will be used the trace-distance criterion  $D(\rho_m, \rho_n) = \frac{1}{2} \text{Tr}|\rho_m - \rho_n|$ , which yields zero if and only if  $\rho_m = \rho_n$  [81]. For the case under observation  $\rho_n$  represents any combination of steady states using the cases  $\rho_{(1,2),(2,1)}^{sep}, \rho_{(1,1),(2,2)}^{ent}, \rho_{(1,1),(2,2)}^{cc}, \rho_{(1,2),(1,2)}^{inc}$  and it was found that  $D(\rho_m, \rho_n) = 0$  for all cases involving only indistinguishable particles, while for the cases having steady states of indistinguishable and distinguishable particles it was found  $D(\rho_m, \rho_n) = 0.25$ . This reaffirms that is the indistinguishability who becomes one the main factor to decide if the coherence prevails or not under dephasing.

In order to prove experimentally the validity of Eq. (3.26), the two-photon correlation function  $\Gamma$  was measured, which as it was stated before, it corresponds to the diagonal of  $\rho_{(p,q),(p,q)}$ . It was used a separable, entangled, classically correlated and incoherent two-photon states using an ensemble of 37 waveguide arrays (see Fig. 3.2). Indistinguishable separable pair of photons were generated by SPDC using the scheme explained in Chapter 2. Path-entangled two-photon states were generated at the output of a 50:50 coupler when simultaneously exciting the two input modes with the indistinguishable photons generated by the photons source [82]. For classically correlated two-photon states the same approach was used as above, but with the difference that now it was introduced a delay of  $\approx 2$  ps in

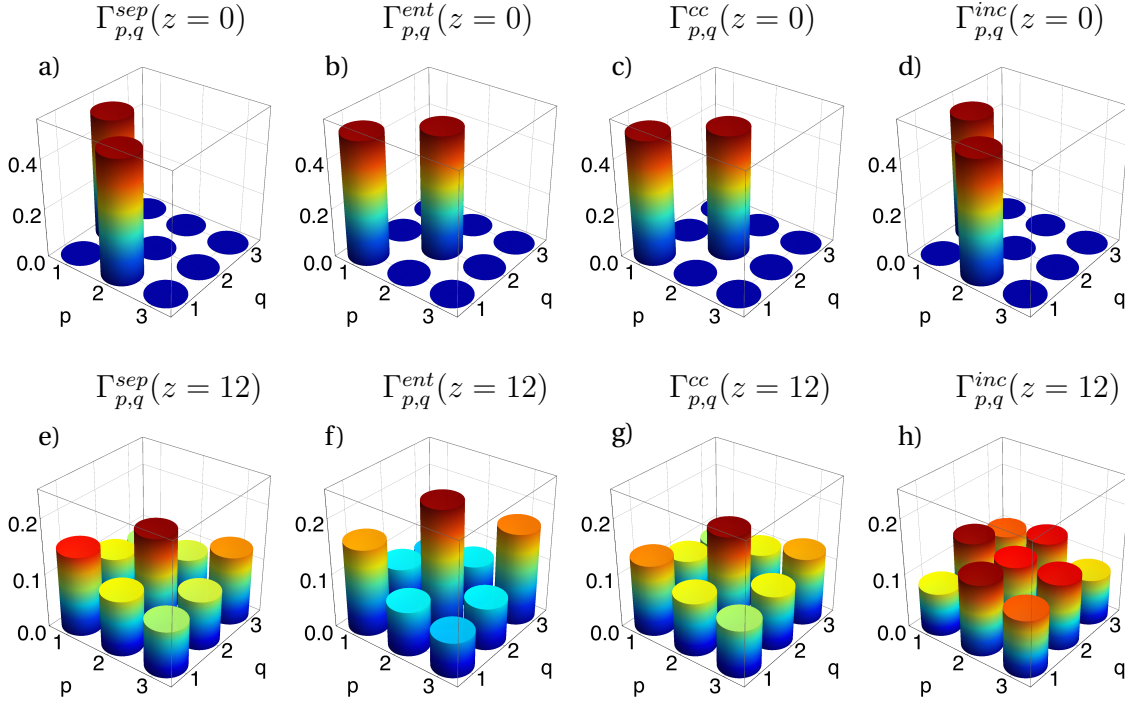


Figure 3.8: Experimental intensity correlation function  $\Gamma_{p,q}(z)$ . The initial inputs for the cases separable, entangled, classically correlated and incoherent are shown in a), b), c) and d) respectively. The respective correlation patterns after 12 cm are shown in e), f), g) and h).

one of the output ports of the 50:50 coupler. Incoherent (distinguishable) two-photon states were produced delaying one of the photons  $\approx 2$  ps with respect to the other before entering in the trimers. Results are plotted in Fig. 3.8 and correspond to the average of 37 different samples. Notice that in all indistinguishable two-particles states, there is a tendency of the photons to bunch into the same waveguide (given by the diagonal) meanwhile off-diagonal elements (anti-bunching events) are smaller. But for the distinguishable case Fig. 3.8 h), the higher coincidences are in the off-diagonal, indicating that the state remains incoherent along evolution. In order to quantify how was the performance of the samples with respect to the theory, it was calculated the average fidelity  $S$  [29] between the experimental  $\Gamma^{exp}$  and theoretical  $\Gamma^{theo}$ , getting  $S = 0.99$  for all cases, where  $S$  is defined by  $S = (\sum_{i,j} \sqrt{\Gamma_{i,j}^{theo} \Gamma_{i,j}^{exp}})^2 / (\sum_{i,j} \Gamma_{i,j}^{theo} \sum_{i,j} \Gamma_{i,j}^{exp})$ . This result indicates that the performance of the samples was good.

### 3.6 Conclusions

With all these results, one can conclude that unlike single photons were the coherence terms are not preserved in the presence of noise, indistinguishable two-

photon states preserve on average quantum coherence, and that happened despite the rate of the dephasing. Moreover, this prevalence of quantum coherence is independently of the actual two-photon state launched into the system provided they are indistinguishable.



---

## Quantum suppression law in $J_x$ lattices

A way to present some of the problems studied in quantum simulation and quantum computation is the following: given an input of single or multi-particles, calculate the output after propagation in some system, characterized by the matrix  $U$ . A possible solution it will depend of several factor, like if the particles are fermions or bosons or if the system described by  $U$  is hermitian or not. In general, the answer is very hard to deal with, and it will depend on the properties of the system itself. One example of this problem is the boson sampling [83, 84], where the output distribution of bosons is sampled. And it has caught a lot of attention because it would be one example of the quantum computational supremacy over classical computers. Now, know if certain output is completely suppressed, only knowing the nature of the input and  $U$ , prior to do the experiment, it is very advantageous. Indeed one very famous example is the HOM effect, where one state is suppressed, the one when the two photons takes different paths. This effect is explained due to the bosonic nature of the photons and today it is used as a way to characterize the quality of the photon sources (how indistinguishable are the generated photons) [85]. The next step is to extend the HOM effect to a setup with more photons and more ports where one would expect also some outputs suppressed like in the original HOM setup. Studies in this area [86] introduce the idea of suppression law, where are described some rules which predict which outputs are suppressed.

Following those studies, here the focus is put in to describe a quantum suppression law having in consideration some symmetries in the input and in the system, specifically in the  $J_x$  lattice.

## 4.1 Multi-photon interference

Consider a system characterized by a unitary matrix  $U$  of dimension  $n \times n$ , where there exist  $n$  input modes. For a single particle input the answer to the question how it will be every mode at the output, can be computed by calculating the average photon number:

$$P_{j,k} = |U_{j,k}|^2 \quad , \quad (4.1)$$

where  $j$  is the input mode and  $k$  the output mode. In Chapter 2 a system of  $n = 2$  is studied, the directional coupler, where the probability to exit every channel at the output is equal, when one photon is launched, but when the number of photons was increased to two, the output is changed, and inclusive there is one output case, the one with the photons going out at different channels, being completely suppressed. If now the number of photons and channels is increased the difficult to know the output distribution is very hard due to the increasing number of path interference. In that context, know a priori if some output state is suppressed can be good deal.

To study this problem consider the case of  $N$  indistinguishable photon entering a lattice represented by a unitary  $U$  with  $n$  ports. Using the notation described in [87], one can define the initial state by a unique mode occupation list:

$$\vec{r} = (r_1, r_2, \dots, r_n) \quad , \quad (4.2)$$

where  $r_1$  is the number of photons in the mode 1,  $r_2$  in mode 2 and so on with  $\sum_j r_j = N$ . The initial state is

$$|\psi\rangle_{in} = \prod_{j=1}^n \frac{(\hat{a}_j^\dagger)^{r_j}}{\sqrt{r_j!}} |0\rangle \quad ,$$

where  $\hat{a}_j^\dagger$  is the creation operator of the mode  $j$  and  $|0\rangle$  is the vacuum state. After propagation, one can define  $\vec{s}$  as the mode occupation list at the output  $\vec{s} = (s_1, \dots, s_n)$ , having an output state

$$|\psi\rangle_{out} = \prod_{j=1}^n \frac{(\hat{b}_j^\dagger)^{s_j}}{\sqrt{s_j!}} |0\rangle \quad ,$$

with  $\hat{b}_i^\dagger = \sum_k U_{i,k} \hat{a}_k^\dagger$ . It is useful to define the mode assignment list  $\vec{d}(\vec{r})$ , in which the entries give the origin of each particle, that is, which modes the  $N$  photons occupy

$$\vec{d}(\vec{r}) = (d_1(\vec{r}), \dots, d_N(\vec{r})) \quad ,$$

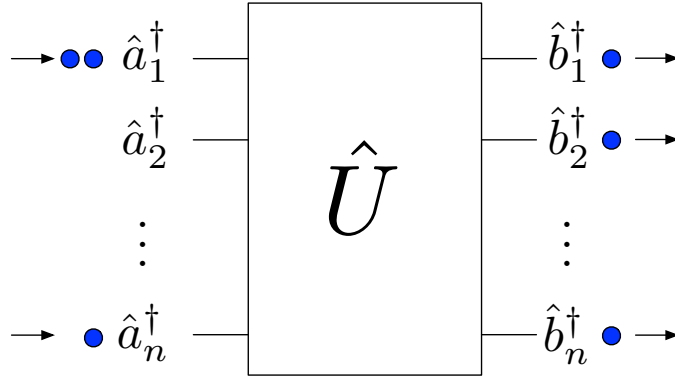


Figure 4.1: Scheme for a multi-photon interference in a array. The transmission of single photons is characterized by the unitary matrix  $\hat{U}$ , where there are  $n$  possible modes at input and output. Each waveguide can be excited by any number of photons represented by the creation operator  $\hat{a}_i^\dagger$  and the output, after transmission in system  $\hat{U}$ , is represented by  $\hat{b}_i^\dagger$ . As an example, two photons (blue circles) are entering in mode 1 and one photon in mode  $n$ . Then the initial occupation list is  $\vec{r} = (2, 0, \dots, 0, 1)$  and the corresponding mode assignment list is  $\vec{d}(\vec{r}) = (1, 1, n)$  and at the output the final occupation list is  $\vec{s} = (1, 1, 0, \dots, 0, 1)$  and the mode assignment list is  $\vec{d}(\vec{s}) = (1, 2, n)$ .

with  $d_i(\vec{r})$  being the mode number occupied by the  $i$ -th photon. For example consider the input state defined as  $\vec{r} = (2, 0, 1, 1)$  then the mode assignment list is  $\vec{d}(\vec{r}) = (1, 1, 3, 4)$ , the number one is repeated two times because there are two photons in mode one, then one photon in mode 3 and one photon in mode 4 (another example is given in the caption of Fig. 4.1). The same analysis for the final state  $\vec{s}$  can be done, where a new mode assignment list  $\vec{d}(\vec{s})$  is obtained. Now the transition probability  $P$  to find a specific state  $\vec{s}$  given an initial state  $\vec{r}$  is obtained via a coherent sum over all possible combinations to distribute the photons at the output [87]:

$$P(\vec{r}, \vec{s}) = \frac{\prod_{j=1}^n s_j!}{\prod_{j=1}^n r_j!} \left| \sum_{\sigma \in S_{\vec{d}(\vec{s})}} \prod_{j=1}^N U_{d_j(\vec{r}), \sigma(j)} \right|^2, \quad (4.3)$$

where  $\sigma$  runs over all permutations  $S_{\vec{d}(\vec{s})}$  of the mode assignment list  $\vec{d}(\vec{s})$ . Notice that for distinguishable photons, the transition probability is just the sum of the single photon probabilities:

$$P_d(\vec{r}, \vec{s}) = \sum_{\sigma \in S_{\vec{d}(\vec{s})}} \prod_{j=1}^N |U_{d_j(\vec{r}), \sigma(j)}|^2. \quad (4.4)$$

In order to see the use of Eq. (4.3) and as example consider the directional coupler ( $n = 2$ ) with an initial input of two photons  $\vec{r} = (1, 1)$  and the output state  $\vec{s} = (1, 1)$

so the mode assignment lists are  $\vec{d}(\vec{r}) = (1, 2)$  and  $\vec{d}(\vec{s}) = (1, 2)$  respectively. Then there are two permutations  $\sigma$ , one is  $\sigma = (1, 2)$  and  $\sigma = (2, 1)$  so writing explicitly Eq. (4.3):

$$\begin{aligned}
P((1, 1), (1, 1)) &= \frac{\prod_{j=1}^2 s_j!}{\prod_{j=1}^2 r_j!} \left| \sum_{\sigma \in S_{\vec{d}(\vec{s})}} \prod_{j=1}^2 U_{d_j(\vec{r}), \sigma(j)} \right|^2 \\
&= \frac{1!1!}{1!1!} \left| \prod_{j=1}^2 U_{d_j((1,2)), (1,2)_j} + \prod_{j=1}^2 U_{d_j((1,2), (2,1)_j)} \right|^2 \\
&= |U_{1,1}U_{2,2} + U_{1,2}U_{2,1}|^2 \\
P((1, 1), (1, 1)) &= \cos^2(2Cz) \quad , \tag{4.5}
\end{aligned}$$

where the values of  $U_{i,j}$  in Eq. (2.18) have been used. If the distance is  $z = \pi/4C$  the probability is  $P = \cos^2(\pi/2) = 0$  (the same as in Chapter 2, where there are not coincident measurement). On the other hand, keeping the same initial state  $\vec{r}$  but looking for output state  $\vec{s} = (2, 0)$  (or  $(0,2)$ ), it is found that

$$P((1, 1), (2, 0)) = P((1, 1), (0, 2)) = 2|U_{1,1}U_{2,1}|^2 = 2\sin^2(2Cz) \quad .$$

At  $z = \pi/4C$  the probability is 1/2, that is one half of the times the two photons exit at the mode 1 (first waveguide) and the other half in mode 2 (waveguide 2), in agreement to Chapter 2.

Notice that the expression in Eq. (4.3) can be written as:

$$P(\vec{r}, \vec{s}) = \frac{1}{\prod_j r_j! s_j!} |\text{perm}(M)|^2 \quad , \tag{4.6}$$

where  $M_{j,k} = U_{d_j(\vec{r}), \sigma(j)}$  and perm is the permanent of a matrix

$$\text{perm}(M) = \sum_{\sigma \in S_n} \prod_i^n a_{i, \sigma(i)} \quad .$$

If instead of photons (bosons) one is working with fermions, the probability from input  $\vec{r}$  to output  $\vec{s}$  is [88]:

$$P_f(\vec{r}, \vec{s}) = \left| \sum_{\sigma \in S_{\vec{d}(\vec{s})}} \text{sgn}(\sigma) \prod_{j=1}^N U_{d_j(\vec{r}), \sigma(j)} \right|^2 = |\det(M)|^2 \quad , \tag{4.7}$$

where det is the determinant of a matrix. Although the expressions for these two functions, the permanent and the determinant, are very similar, the calculations

required to get their evaluations are very different. Although there exist several techniques to obtain the determinant, the calculations of the permanent is exponentially hard in the context of computation (in time/resources) and is considered a #P-complete problem [89]. This problem has become an example of the called “quantum supremacy” (the solutions to a problems which cannot be solved efficiently by classical computers) after the proposal of Aaronson and Arkhipov [83], where the computation of the permanent can be obtained efficiently through the sampling of the output distribution of bosons, named as boson sampling [90–93].

## 4.2 Suppression law for Bell multiport beam splitter

As it was seen, the probability to get some certain output can be hardly and complex to calculate since up to  $N!$  amplitudes has to be summed in Eq. (4.3), so to derive an expression which predicts whether some output events are suppressed it would be very useful. One representative work in this area can be found in [87] and a brief summary is presented here. Others similar works can be found in [94, 95].

Starting from the HOM effect, a general case is a system of  $n$  beam-splitters or multiport beam-splitters. If these beam-splitters are all equal, called Bell multiport [96], all single-particle probabilities are equal  $|U_{j,k}|^2 = 1/n$  with  $n$  the number of photons and the unitary transformation describing this process, is the Fourier matrix

$$U_{j,k}^{\text{Fou}} = \frac{1}{\sqrt{n}} e^{i \frac{2\pi}{n} (j-1)(k-1)} \quad .$$

Due to a property of the Fourier transformation  $(U^{\text{Fou}})^{-1} = (U^{\text{Fou}})^*$ , it is found the input-output symmetry

$$P(\vec{r}, \vec{s}) = P(\vec{s}, \vec{r}) \quad .$$

In this way, using these symmetry relations, given by the Fourier matrix, it is possible to find a criterion for the fully destructive interference. This suppression law says: output states  $\vec{s}$  are suppressed if the sum of the elements of the mode assignment list  $\vec{d}(\vec{s})$  is not divided by  $n$ :

$$\text{mod} \left( \sum_{j=1}^n d_j(\vec{s}), n \right) \neq 0 \quad \Rightarrow \quad P(\vec{r}, \vec{s}) = 0 \quad . \quad (4.8)$$

It is possible to use the same idea of suppressed states for other  $U$ , which is studied in the next section.

### 4.3 Suppression law for parity-symmetric input states in a $J_x$ lattice

In this section, it is considered the case when there is the following symmetry relation in  $U$ :

$$U_{n+1-k,l} = c(n)(-1)^{l-k}U_{k,l} \quad , \quad (4.9)$$

with  $c(n)$  a phase factor depending only on  $n$ . The symmetry involved here relates the transmission amplitude from input site  $k$  to output site  $l$  with the amplitude from the opposite input channel  $n + 1 - k$  to the same output site  $l$  by a phase factor  $c(n)$ . One array that follows this symmetry is the  $J_x$  lattice [97].

The particular  $J_x$  name of this special lattice comes from the area of quantum spin networks, where in order to have a perfect state transfer from one site to another, the coupling in the system has to follow a certain order, which it can be represented by the angular momentum operator  $J_x$  [98]. In order to map the matrix elements of the  $J_x$  operator to the context of waveguides, the coupling  $C$  between waveguides  $k$  and  $k + 1$  will be:

$$C_{k,k+1} = \frac{\kappa_0}{2} \sqrt{k(n-k)} \quad , \quad (4.10)$$

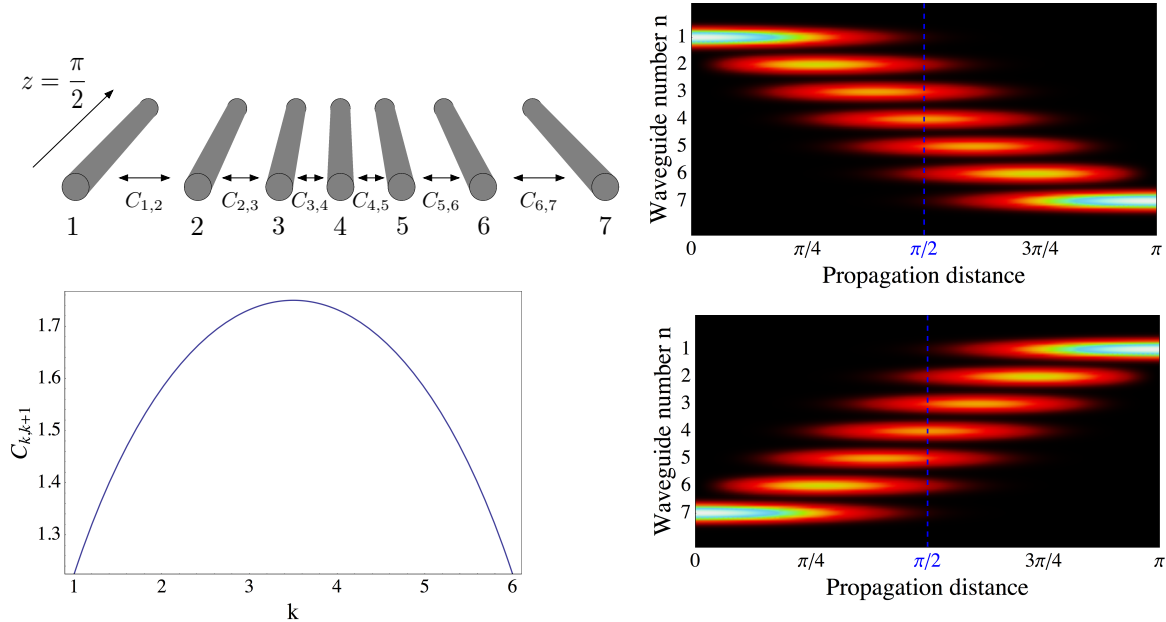


Figure 4.2: Scheme of a  $J_x$  lattice. (left) There is in total  $n = 7$  modes (waveguides) with different couplings between them, following a parabolic rule. (right) Dynamics from 0 to  $\pi$  when the input is in waveguide 1 (top) and when the input is in waveguide 7 (bottom). Notice that in  $z = \pi/2$  the transmission amplitude  $U$  is equal for symmetric inputs with respect to the center,  $U_{1,l} = c(n)(-1)^{l-7}U_{7,l}$ .

with  $\kappa_0$  a scaling factor, which, in the following analysis, is assumed to be 1. This relation is plotted in Fig. 4.2. The equation of motion in the  $J_x$  lattice for the mode  $k$  is

$$i \frac{d\hat{a}_k^\dagger}{dz} = \frac{1}{2} \sqrt{(n-k)k} \hat{a}_{k+1}^\dagger + \frac{1}{2} \sqrt{(n-k+1)(k-1)} \hat{a}_{k-1}^\dagger \quad .$$

Looking for the eigenvectors  $u_l^{(k)}$  of this equation with eigenvalues  $\beta_k$ , one arrives to the solution [97]:

$$u_l^{(k)} = 2^{-\frac{1}{2}(n+1)+l} \sqrt{\frac{(l-1)!(n-l)!}{(k-1)!(n-k)!}} P_{l-1}^{(k-l, n-k-l+1)}(0) \quad , \quad (4.11)$$

where  $P_{l-1}^{(k-l, n-k-l+1)}(0)$  are the Jacobi polynomials of order  $l-1$  evaluated at the origin. As it was seen in Chapter 2, the creator operator can be written as a sum of the elements of the unitary matrix multiplied by the initial condition

$$\hat{a}_p^\dagger(0) = \sum_m^n U_{p,m}^*(z) \hat{a}_m^\dagger(z) \quad ,$$

where

$$U_{p,q}(z) = \sum_{r=1}^n u_q^{(r)} u_p^{(r)} e^{i\lambda_r z} \quad . \quad (4.12)$$

Using properties and an alternative form of the Jacobi polynomials, Eq. (4.12) can be written as [99]

$$U_{p,q}(z) = (-i)^{q-p} \sqrt{\frac{(j+p)!(j-p)!}{(j+q)!(j-q)!}} \left[ \sin\left(\frac{z}{2}\right) \right]^{q-p} \left[ \cos\left(\frac{z}{2}\right) \right]^{-q-p} P_{j+p}^{q-p, -q-p}(\cos(z)) \quad .$$

And evaluating in  $z = \pi/2$ , one arrives to the result:

$$U_{p,q}\left(\frac{\pi}{2}\right) = (-i)^{q-p} 2^p \sqrt{\frac{(j+p)!(j-p)!}{(j+q)!(j-q)!}} P_{j+p}^{q-p, -q-p}(0) = e^{i\frac{\pi}{2}(q-p)} u_p^{(q)} \quad . \quad (4.13)$$

Using the symmetry of the Jacobi-polynomials  $P_m^{(\alpha, \beta)}(0) = (-1)^m P_m^{(\beta, \alpha)}(0)$ , the following relation for the eigenmodes is obtained

$$u_l^{(n+1-k)} = (-1)^{l-1} u_l^{(k)} \quad .$$

Combining Eq. (4.13) and the above equation and after some algebra one can arrives to the final result:

$$U_{n+1-k, l} = e^{i\pi \frac{n-1}{2}} (-1)^{l-k} U_{k, l} \quad , \quad (4.14)$$

where the phase  $e^{i\pi \frac{n-1}{2}}$  only depends in  $n$ . This equation follows the rule said in Eq. (4.9) so the transmission amplitude from site  $k$  to site  $l$  is the same to the

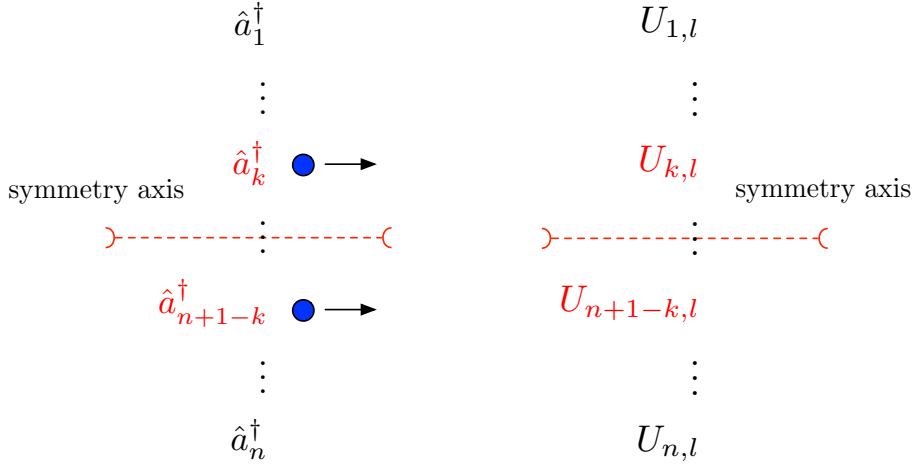


Figure 4.3: Symmetries for suppression law. (left) Scheme for the parity-symmetry input state, (right) mirror symmetry in the transmission matrix  $U$  to the site  $l$ .

transmission amplitude from opposite site  $n + 1 - k$  to site  $l$  (multiplied by a phase factor, see Fig. 4.2). It is said that this system possess a mirror symmetry in  $U$  (see Fig. 4.3). The other condition for the suppression law considered here is related to the input state. The input state has to be symmetric with respect to the centre of the lattice  $r_j = r_{n+1-j}$  so that means:

$$d_j(\vec{r}) = n + 1 - d_{N+1-j}(\vec{r}) \quad . \quad (4.15)$$

This implies that in every factor  $U_{d_j(\vec{r}), \sigma(j)}$  in Eq. (4.3) can be written as

$$U_{d_{N+1-j}(\vec{r}), \sigma(N+1-j)} = U_{n+1-d_j(\vec{r}), \sigma(N+1-j)} = c(n)(-1)^{\sigma(N+1-j)-d_j(\vec{r})} U_{d_j(\vec{r}), \sigma(N+1-j)} \quad ,$$

where the symmetry of  $U$  has been used. Notice that every element has its pair due to the mirror symmetry, but the middle term  $U_{d_{\frac{N+1}{2}}(\vec{r}), \sigma(\frac{N+1}{2})}$  has no a pair if  $N$  is odd. Therefore, the cases for even and odd  $N$  will be treat separately.

### 4.3.1 Even photon number states

In this case, all factors can be grouped in pairs of equal  $d_j(\vec{r})$ , then Eq. (4.3)

$$P(\vec{r}, \vec{s}) = \frac{\prod_{j=1}^n s_j!}{\prod_{j=1}^n r_j!} \left| \sum_{\sigma \in S_{\vec{d}(\vec{s})}} \prod_{j=1}^{N/2} c(n)(-1)^{\sigma(N+1-j)-d_j(\vec{r})} U_{d_j(\vec{r}), \sigma(j)} U_{d_j(\vec{r}), \sigma(N+1-j)} \right|^2 .$$

This expression can be simplified noting that the phase factor  $c(n)$  as well as  $(-1)^{d_j(\vec{r})}$  do not depend on  $\sigma$  so they can factored out from the sum over all permutations. Then:

$$P(\vec{r}, \vec{s}) \propto \left| \sum_{\sigma \in S_{\vec{d}(\vec{s})}} \prod_{j=1}^{N/2} (-1)^{\sigma(N+1-j)} U_{d_j(\vec{r}), \sigma(j)} U_{d_j(\vec{r}), \sigma(N+1-j)} \right|^2 . \quad (4.16)$$

The sum over all permutations  $\sigma$  can be divided in two kinds: they can be symmetric with respect to a reversal of their order,  $\sigma(j) = \sigma(N + 1 - j)$ , or not, which is called non-symmetric. Starting the discussion with the non-symmetric permutations, for every non-symmetric permutation  $\sigma$  there is always a reversed-order permutation  $\sigma' \in S_{\vec{d}(\vec{s})}$  with  $\sigma'(j) = \sigma(N + 1 - j)$ . This means that every summand in Eq. (4.16) can be grouped in pairs of  $\sigma$  and  $\sigma'$ :

$$\begin{aligned}
& \left| \prod_{j=1}^{N/2} (-1)^{\sigma(N+1-j)} U_{d_j(\vec{r}), \sigma(j)} U_{d_j(\vec{r}), \sigma(N+1-j)} + \prod_{k=1}^{N/2} (-1)^{\sigma'(N+1-j)} U_{d_k(\vec{r}), \sigma'(k)} U_{d_k(\vec{r}), \sigma'(N+1-k)} \right|^2 \\
&= \left| \prod_{j=1}^{N/2} (-1)^{\sigma(N+1-j)} U_{d_j(\vec{r}), \sigma(j)} U_{d_j(\vec{r}), \sigma(N+1-j)} + \prod_{k=1}^{N/2} (-1)^{\sigma(k)} U_{d_k(\vec{r}), \sigma(k)} U_{d_k(\vec{r}), \sigma(N+1-k)} \right|^2 \\
&= \left| \left[ \prod_{j=1}^{N/2} (-1)^{\sigma(N+1-j)} + \prod_{k=1}^{N/2} (-1)^{\sigma(k)} \right] \prod_{l=1}^{N/2} U_{d_l(\vec{r}), \sigma(l)} U_{d_l(\vec{r}), \sigma(N+1-l)} \right|^2 \\
P(\vec{r}, \vec{s}) &\propto \prod_{k=1}^{N/2} (-1)^{\sigma(k)} \left[ \prod_{j=1}^{N/2} (-1)^{\sigma(N+1-j)-\sigma(j)} + 1 \right] \prod_{l=1}^{N/2} U_{d_l(\vec{r}), \sigma(l)} U_{d_l(\vec{r}), \sigma(N+1-l)} \Big|^2. \tag{4.17}
\end{aligned}$$

Noticing that there is a sum of -1 and 1 in the term with angular brackets, this term could be zero, if the exponent of (-1) is odd, that is

$$\sum_{j=1}^{N/2} \sigma(N + 1 - j) - \sigma(j) = \sigma(N) + \dots + \sigma(N/2 + 1) - \sigma(N/2) - \dots - \sigma(1)$$

is an odd number. This is also true if the sum of all  $\sigma(j)$  is odd. Hence this condition is equivalent to say that the sum over all entries of the mode assignment list  $\vec{d}$  is odd, which can be written as

$$\text{mod} \left( \sum_{j=1}^N \sigma(j), 2 \right) = \text{mod} \left( \sum_{j=1}^N d_j(\vec{s}), 2 \right) = 1.$$

This condition is fulfilled if and only if there is an odd number of odd entries in  $\vec{d}(\vec{s})$  or equally to say (because  $N$  is even) that there is an odd number of even entries. In resume, in the cases of non-symmetric permutation, the probability goes to zero if there is an odd number of even entries in  $\vec{d}(\vec{s})$ .

To finish the case with an even photon number, the case for symmetric permutations has to be considered. In the symmetric case every element must occur twice

(because  $N$  is even) so there must be an even number of even entries, but for the case of an odd number of even entries there is no symmetric permutation, so the transition probability is zero. Therefore, for the case  $N$  even, all output events with an odd number of photons in even output modes are suppressed.

### 4.3.2 Odd photon number states

The same method of pair terms can be used as before, but taking care that now there is one element, which has no partner  $U_{d_{\frac{N+1}{2}}(\vec{r}), \sigma(\frac{N+1}{2})}$ . However, because the symmetry of the input state, an odd number of waveguides is needed and in the middle of the array has to be the middle photon so  $d_{\frac{N+1}{2}}(\vec{r}) = \frac{n+1}{2}$ . The transmission amplitude can be written as:

$$P(\vec{r}, \vec{s}) \propto \left| \sum_{\sigma \in S_{\vec{d}(\vec{s})}} U_{\frac{n+1}{2}, \sigma(\frac{N+1}{2})} \prod_{j=1}^{\frac{N-1}{2}} (-1)^{\sigma(N+1-j)} U_{d_j(\vec{r}), \sigma(j)} U_{d_j(\vec{r}), \sigma(N+1-j)} \right|^2, \quad (4.18)$$

where again as before the terms  $c(n)$  and  $(-1)^{d_j(\vec{r})}$  have been factored out. Then doing the same as the case of even photon number, it is separated in symmetric and non-symmetric permutations. For the non-symmetric case, doing the same procedure as before one arrives to the same equation in Eq. (4.17) plus the extra factor  $U_{\frac{n+1}{2}, \sigma(\frac{N+1}{2})}$ . So the factor with the sum of -1 and 1 decide if the probability is zero or not:

$$\sum_{j=1}^{\frac{N-1}{2}} \sigma(N+1-j) - \sigma(j) = \sigma(N) + \dots + \sigma\left(\frac{N+3}{2}\right) - \sigma\left(\frac{N-1}{2}\right) - \dots - \sigma(1). \quad (4.19)$$

If this sum is odd the probability vanishes. Then this is true is the sum of the  $\sigma(j)$  is odd or conversely the sum of  $d_j(\vec{s})$  is odd and it happens if and only if there is an odd number of even entries in  $\vec{d}(\vec{s})$ . If there is an odd number of even entries, there must be an even number of odd entries, but for even number of odd entries the probability is zero as it will be seen below: for each permutation  $\sigma$  there are two cases for the factor  $U_{\frac{n+1}{2}, \sigma(\frac{N+1}{2})}$ , either  $\sigma(\frac{N+1}{2})$  is even or odd. If it is even, this implies zero probability due to:

$$U_{\frac{n+1}{2}, \sigma(\frac{N+1}{2})} = e^{i\pi(\frac{n-1}{2} + \sigma(\frac{N+1}{2}) - \frac{n+1}{2})} U_{\frac{n+1}{2}, \sigma(\frac{N+1}{2})} = (-1)^{\sigma(\frac{N+1}{2})-1} U_{\frac{n+1}{2}, \sigma(\frac{N+1}{2})}, \quad (4.20)$$

then, if the factor in the exponent of (-1) is odd, that is if  $\sigma(\frac{N+1}{2})$  is even, then  $U = -U$  which is only true if  $U$  is zero. So  $\sigma(\frac{N+1}{2})$  even, it implies  $U_{\frac{n+1}{2}, \sigma(\frac{N+1}{2})} = 0$ . For the case  $\sigma(\frac{N+1}{2})$  odd, because there is an even number of odd entries, all terms

cancel in Eq. (4.19).

Analyzing now the case for symmetric permutations, they have a structure  $(\sigma(1), \dots, \sigma(\frac{N-1}{2}), \sigma(\frac{N+1}{2}), \sigma(\frac{N-1}{2}), \dots, \sigma(1))$ , so if there is an odd number of even entries, the imposed symmetry can be only achieved by an even central component  $\sigma(\frac{N+1}{2})$ , but it was established by Eq. (4.20) that this case implies zero probability. Hence, an odd number of even entries in  $\vec{d}(\vec{s})$  implies zero transmission probability, as the same rule for the even photon number.

Combining both cases even and odd photon number in one equation, one arrives to the final expression for the suppression law: If the number in even entries at the output mode  $\vec{s}$  is odd, this state is suppressed, and formally written in the following equation:

$$\text{mod} \left( \sum_{j=1}^N d_j(\vec{s}) - N, 2 \right) = 1 \quad \Rightarrow \quad P(\vec{r}, \vec{s}) = 0 \quad . \quad (4.21)$$

## 4.4 Experiment and results

To test the suppression law studied here, an experiment with three photons was performed. The experimental setup is shown in Fig. 4.4. Initially, pulses from a Ti:Sapphire are doubled in frequency going through a non-linear crystal BiBO, and then illuminate a non-linear crystal BBO type II, where events of two pairs of photons by spontaneous parametric down conversion are collected. This is possible to the fact that it is used pulses from a femtosecond laser (200 fs) and high power (400 mW), which makes possible to reach events where not only two photons are generated but also four photons. Those photons are entangled in polarization and they are represented by the state  $\propto |HH\rangle_L |VV\rangle_R + |VV\rangle_L |HH\rangle_R + \sqrt{2} |HV\rangle_L |VH\rangle_R$  where  $H$  and  $V$  are the horizontal and vertical polarization respectively and  $L$  is the left arm and  $R$  is the right arm during collection. By using two polarizing beam-splitters (PBS) it is possible separate the polarization into spatial modes, so in this way for example  $|HH\rangle_L |VV\rangle_R$  goes to  $|2, 0, 0, 2\rangle$  because there are two photons with  $H$  polarization in the spatial mode  $L$  and two photons with  $V$  polarization in the spatial mode  $R$  and zero in the other cases. Doing the same for the rest one arrives to the state  $|2, 0, 0, 2\rangle + |0, 2, 2, 0\rangle + \sqrt{2} |1, 1, 1, 1\rangle$ . The last term is the one needed to perform this experiment because it has only one photon in each mode (although different polarizations). The other two possibilities are eliminated by

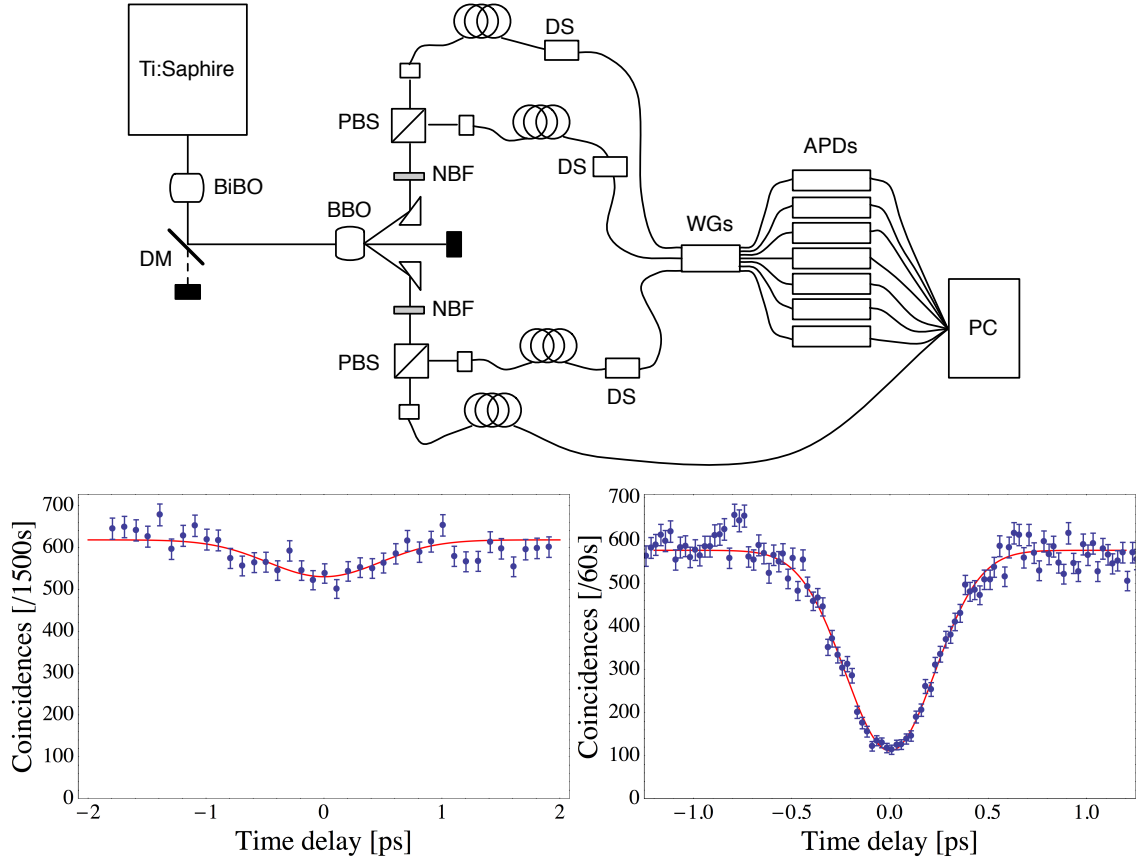


Figure 4.4: Scheme of the experimental setup used for verification of quantum suppression law. (top) The scheme contains: a Ti:Sapphire laser, a non-linear crystal type I BiBO, dichroic mirror DM to separate the original pump from doubled-frequency light, a SPDC source non-linear crystal type II BBO, narrow band filter NBF to get a better indistinguishability, polarizing beam splitter PBS, delay stages DS, integrated chip with waveguides WGs doing a  $J_x$  lattice, avalanche photo diode detectors APD and a computer PC. (bottom) Realization of a HOM-dip experiment for the cases when the photons are distinguishable (left) and when they are indistinguishable (right). Error bars follow a Poissonian distribution of the measured counts.

using one of the photon as herald and taking only four-fold coincidences between this photon and the other three. Then photons with  $V$  polarization are rotated to  $H$  polarization to get equal polarization in all photons entering to the waveguide array. The initial symmetric input state consists of three photons launched in waveguides 1, 4 and 7,  $\vec{r} = (1, 0, 0, 1, 0, 0, 1)$  following the rule in Eq. (4.15) and with the assignment list  $\vec{d}(\vec{r}) = (1, 4, 7)$ . The array of waveguides consist of a  $J_x$  lattice done using the femtosecond laser writing technique and a characterization of the chip using classical light at the same wavelength of generated photons is shown in Fig. 4.5. In this array was used a very recent technique [100], where the final part of every waveguide is written several times, getting an enhancement of the coupling efficiency to the fibers which collect the photons at output. Then these photons

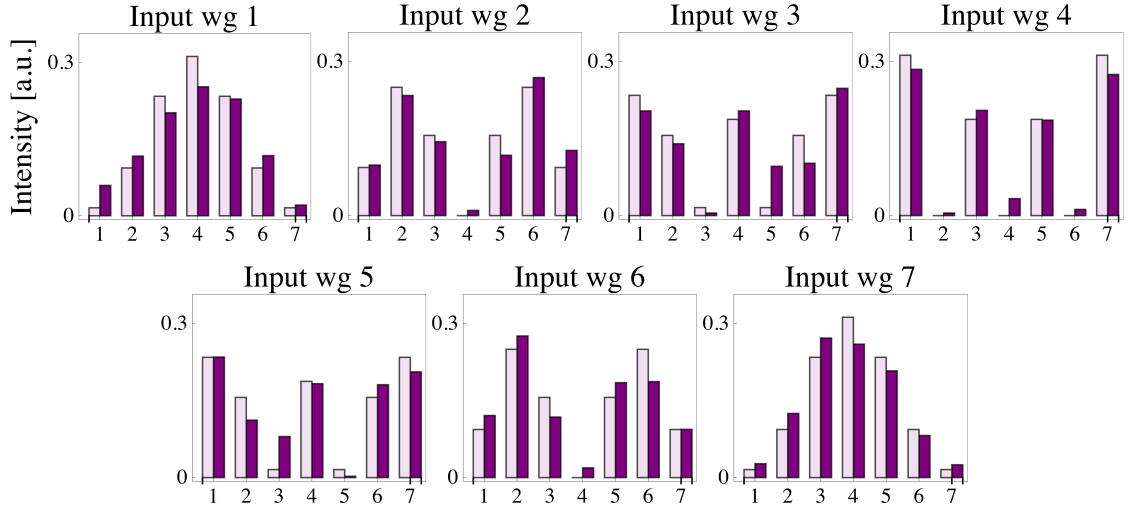


Figure 4.5: Characterization of the  $J_x$  lattice. Intensity values at output for single input in every of the seven waveguides. Purple bar are the experimental value and light purple are the theoretical one

are carried to avalanche photo diodes where the measurements are done.

The output modes  $\vec{s}$  under observation consists of single photons per waveguide, due as it was said before, over all events of four photons created by SPDC, one of them will be used a herald to perform a four-fold coincidence, so cases as  $\vec{d}(\vec{s}) = (1, 1, 2)$  where two photons are in waveguide 1 are not measured. This means there are 35 different  $\vec{d}(\vec{s})$  at output, including cases where the suppression law discussed here can be tested. The results are in Fig. 4.6, where there is a clear difference between the suppressed output states (left side, marked by a dashed line) who have a small probability and the non-suppressed output states (right side) with higher probabilities. The suppressed output states have theoretically a probability equal to zero, but here they are a slightly higher than zero due to small imperfections during the process of fabrication of the  $J_x$  lattice and also that photons are not totally indistinguishable. Taking those elements into account new probabilities were calculated (blue bars) witch match pretty well the experimental data (light blue bars). Just to emphasize, notice that the cases to the right of the dashed line are the non-suppressed states due to they have a even number of even entries (and not a odd number of even entries, which are the suppressed cases to the left). Also it was analyzed the case where the input photons are distinguishable (see Fig. 4.6 bottom), and one can observe that for the same states, the probability to see that output is much higher if the photons are distinguishable (this was done delaying the arrival time of photons using the delay stages in the setup). This

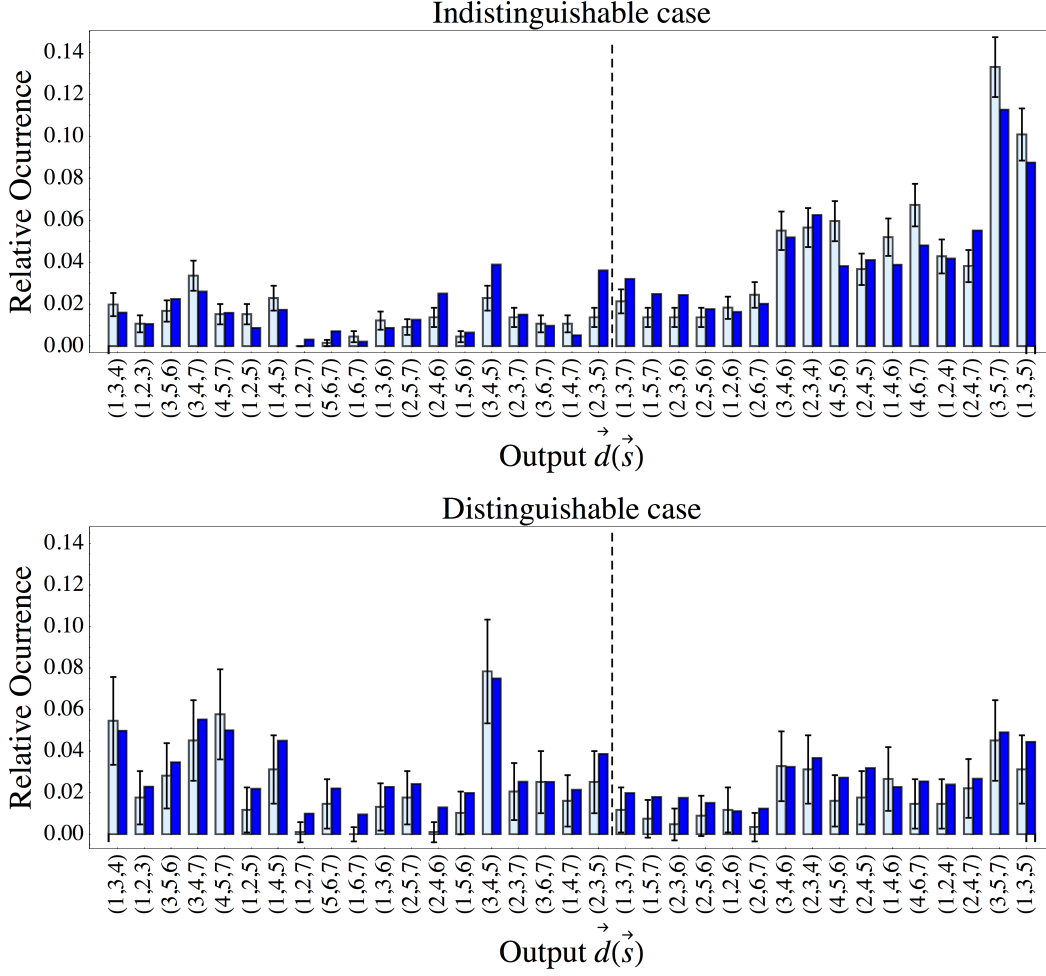


Figure 4.6: Probability at output of the 35 different possibilities of one photon in each waveguide for the initial input  $\vec{d}(\vec{r}) = (1, 4, 7)$ . At top is the indistinguishable case and bottom the distinguishable case. Blue bars are the theoretical values and light blue bars are the experimental values. Dashed line separates the suppressed cases (to the left) from the unsuppressed cases (to the right).

happen because the suppression law is not anymore valid and some output states may be suppressed or not. To quantify the difference between this two cases, the sum of the all probability for the expected suppressed states was calculated, having for the indistinguishable case  $\sum_{s_{supp}} P_{exp}^{indis} = 0.25 \pm 0.02$  ( $\sum_{s_{supp}} P_{theo}^{indis} = 0.29$ ) and for the distinguishable case  $\sum_{s_{supp}} P_{exp}^{dis} = 0.60 \pm 0.03$  ( $\sum_{s_{supp}} P_{theo}^{dis} = 0.59$ ). These values show a closeness with the theoretical value of 0 for an ideal experiment, where the states are completely suppressed.

## 4.5 Conclusions

Here it was studied theoretically a new example of quantum suppressions, specifically for a  $J_x$  lattice and a parity-symmetric input. The result shows if the number

in even entries at the output mode  $\vec{s}$  is odd, this state is suppressed (Eq. (4.21)). This was tested in a experiment using a  $J_x$  integrated photonic lattice of seven sites and launching three single photons, where the results are in agreement with the studied theory.



---

## Experimental realization of a photonic quantum SWAP gate

With the constant progress of quantum information and quantum computation, the experimental realization of the operations related to those fields is the vital importance. In this context, the information can be encoded in quantum bits or qubits, the quantum analog to the classical bits, including a big difference to their classical relative, apart to be in the state  $|0\rangle$  or  $|1\rangle$  (as the classical bit), it can also be in a coherent superposition of  $|0\rangle$  and  $|1\rangle$ . This opens new and interesting possibilities like quantum search algorithm and quantum cryptography [1]. But in order to do experimentally these ideas, the manipulation of single and multiple qubits has to be done carefully. Moreover, the operations carried out in the qubits has to keep their coherence and so do not lose some encoded information. Those operations are known as quantum gates and they are the analog to the classical logic gates. Among the all existing quantum gates, the more commonly used are the Hadamard, phase shift, controlled-not (CNOT) and Toffoli gates among other, where they act over single and multiple qubits. Experimental realizations of these quantum gates have been done in several platforms including superconducting circuits [101, 102], trapped ions [103, 104] and integrated optics [42, 50].

Another common and important operation is the SWAP gate, which is the subject of this chapter. A possible implementation is studied theoretically and later a experimental realization is presented, where one remarkable property is an (theoretical) efficiency of one.

## 5.1 The SWAP operation

The SWAP gate for a two-qubit system swaps an input state  $|\Psi\rangle_{in} = |a, b\rangle$  to the final state  $|\Psi\rangle_{out} = |b, a\rangle$ , that is:

$$|a, b\rangle \xrightarrow{\text{SWAP}} |b, a\rangle \quad . \quad (5.1)$$

The SWAP gate is represented by the following matrix:

$$U_{\text{SWAP}} = \begin{pmatrix} 1 & 0 & 0 & 0 \\ 0 & 0 & 1 & 0 \\ 0 & 1 & 0 & 0 \\ 0 & 0 & 0 & 1 \end{pmatrix} , \quad (5.2)$$

in the computational basis  $|0, 0\rangle, |0, 1\rangle, |1, 0\rangle, |1, 1\rangle$ . It will be used a dual-rail basis to describe qubits, where each qubit is encoded in the spatial modes of two waveguides excited by single photons [1, 105]. So for example an arbitrary qubit  $|\theta\rangle$  can be prepared in the states of the computational basis: zero  $|\theta\rangle = |0\rangle = (1, 0)^T$ , one  $|\theta\rangle = |1\rangle = (0, 1)^T$  or in a coherent superposition  $|\theta\rangle = \alpha|0\rangle + \beta|1\rangle = (\alpha, \beta)^T$  where  $T$  is the transpose of the vector, and  $\alpha$  and  $\beta$  are complex amplitudes satisfying  $|\alpha|^2 + |\beta|^2 = 1$ .

The SWAP operation described by Eq. (5.1) is very useful and an important component for the proper operation of several quantum circuits [106, 107] or in the implementation of some quantum algorithms, for example the Shor's algorithm [108] and a necessary condition for the networkability of quantum computation [109].

One important point is that a SWAP gate can be constructed by the application of three consecutive CNOT gates [1, 110]. And it is known that CNOT gates together to single qubit gates are universal for quantum computation [111, 112], i.e., any unitary operation can be done by using only those gates. Therefore due to the importance of CNOT gates, several studies of SWAP gates based in CNOT operations have been done [110]. But one problem that arises is its possible experimental realization. Up to now the best photonic circuit implementing a CNOT has a probability of success of 1/9 [105], meaning that three of them would work  $(1/9)^3$  of the times, without considerer any extra source of error. This would make any effort unsuccessful by using this approach. So a possible implementation of a SWAP gate with a better probability of success is discussed in the next section.

## 5.2 Implementation of a photonic SWAP gate

In order to make a experimental realization of a SWAP gate, a possible implementation using waveguides is discussed. The system proposed for this task consists of an array of  $N = 2M$  waveguides, with  $M$  the number of qubits and forming a  $J_x$  lattice. This means that the coupling between waveguides is given by  $f(n) = \frac{\kappa_0}{2} \sqrt{n(N-n)}$ , where  $\kappa_0$  is a scaling factor introduced for experimental reasons (a high value of  $\kappa_0$  would imply large values of coupling and a short propagation length but this would produce to be in a regime different to the couple mode theory. A small value of  $\kappa_0$  would not have problem with the couple mode theory but it would produce a very long propagation length and not reachable by the actual experimental settings). The dynamics of single photons in a  $J_x$  lattice is given by the Heisenberg equation for the creator operator  $\hat{a}_n^\dagger$ :

$$\begin{aligned} i \frac{d}{dZ} \hat{a}_1^\dagger(Z) &= f(1) \hat{a}_2^\dagger(Z) \\ i \frac{d}{dZ} \hat{a}_n^\dagger(Z) &= f(n) \hat{a}_{n+1}^\dagger(Z) + f(n-1) \hat{a}_{n-1}^\dagger(Z) \\ i \frac{d}{dZ} \hat{a}_N^\dagger(Z) &= f(N-1) \hat{a}_{N-1}^\dagger(Z) \quad , \end{aligned} \quad (5.3)$$

where  $n$  runs from 2 to  $N-1$ ,  $Z$  is the normalized coordinate given by  $Z = \kappa_0 z$  and  $z$  is the actual propagation distance. As it was seen in Chapter 4, the unitary transformation of a photon launched in site  $q$  and reaching site  $p$  is analytically described by:

$$U_{p,q}(Z) = (-i)^{q-p} \sqrt{\frac{(j+p)!(j-p)!}{(j+q)!(j-q)!}} \left[ \sin\left(\frac{Z}{2}\right) \right]^{q-p} \left[ \cos\left(\frac{Z}{2}\right) \right]^{-q-p} P_{j+p}^{q-p, -q-p}(\cos(Z)). \quad (5.4)$$

A direct evaluation of this equation at  $Z = \pi$  reveals all amplitudes vanish except at particular where  $p = N + 1 - q$ . This means that single photons entering in waveguides located over one side of the array will symmetrically appear from waveguides on the opposite side, as is shown in Fig. 5.1. This is exactly what is needed for a SWAP operation between the spatial modes of the array. Also notice that the array is performing the swapping of the input without any extra measurements or post selection, so it is completely deterministic and due that the input is totally transferred to the output, the efficiency of the operation is 1.

Moreover, the capacity to perform a SWAP operation is not restricted to qubits but also to qudits (name referred to a system with  $d$ -levels, with  $d$  higher than two).

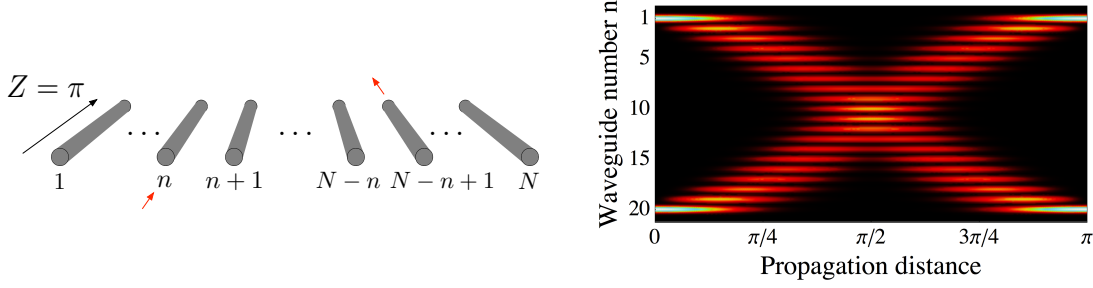


Figure 5.1: Scheme of a  $J_x$  lattice. (left) Perfect transfer from site  $n$  to site  $N - n + 1$  is reached at distance of  $Z = \pi$ . (right) Evolution of the average photon number for two initial inputs in the borders of an array of 20 waveguides. They reach the opposite sites at  $Z = \pi$ , which it could be used as a SWAP operation.

$d = 2$  is for qubits). For that consider an even system of  $N = 2d$  waveguides and two inputs states  $|\theta^L\rangle = (\alpha_1, \alpha_2, \dots, \alpha_d)^T$  and  $|\theta^R\rangle = (\beta_{d+1}, \beta_{d+2}, \dots, \beta_{2d})^T$  entering simultaneously to the array. Here  $L$  and  $R$  denote left and right with respect to the center of the array. Using Eq. (5.4) and after a propagation of  $Z = \pi$  one can notice that the initial two-qudit state  $|\Psi\rangle_{in} = (\alpha_1, \dots, \alpha_d)^T (\beta_{d+1}, \dots, \beta_{2d})^T$  evolves into the output state  $|\Psi\rangle_{out} = (\beta_{2d}, \dots, \beta_{d+1})^T (\alpha_d, \dots, \alpha_1)^T$ , which can be seen as a SWAP operation (the states are symmetrically swapped with respect to the center).

### 5.3 Experiment and results

In order to test experimentally the proposed SWAP operation, an array of  $N = 4$  waveguides was done using the femtosecond laser direct writing technique explained in Chapter 2, to perform operations in a level of two qubit. An scheme of the integrated circuit is shown in Fig. 5.2. The length of the  $J_x$  lattice at the normalized distance  $Z = \pi$  was experimentally equal to 52.3 mm ( $\kappa_0 = 0.06 \text{ mm}^{-1}$ ) and values of coupling between 0.51 and  $0.6 \text{ cm}^{-1}$  were used. According to the dual-rail basis, a single photon exciting the modes of the first (waveguide 1) and second (waveguide 2) waveguides encodes the first input qubit. In the same way, the second qubit is represented by another single photon exciting the modes of the third (waveguide 3) and four (waveguide 4) waveguides. Then the first component of the first qubit is encoded in the mode of waveguide 1, and the second component is encoded in the state of waveguide 2. For the second qubit the first component is encoded in the mode of waveguide 4 and second component is encoded in the state of waveguide 3. Following those definitions, the computational basis  $|0, 0\rangle, |0, 1\rangle, |1, 0\rangle, |1, 1\rangle$  corresponds to the creation operators  $\hat{a}_1^\dagger \hat{a}_4^\dagger |0\rangle, \hat{a}_1^\dagger \hat{a}_3^\dagger |0\rangle, \hat{a}_2^\dagger \hat{a}_4^\dagger |0\rangle, \hat{a}_2^\dagger \hat{a}_3^\dagger |0\rangle$  respectively. After propagation in the array,

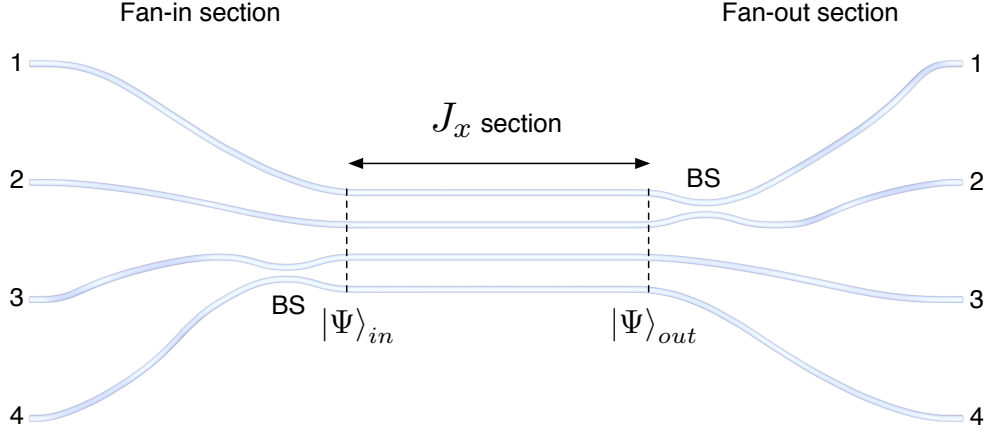


Figure 5.2: Scheme of the integrated chip used for a SWAP gate. Numbers 1,2,3 and 4 are the labels of the four waveguides (modes) used in this experiment. Initially there is a fan-in region in order to match the fiber array used to launch single photons, then the  $J_x$  region, and finally a fan-out section to match the output fiber array which collect the photons and connect them to detectors. BS represents a 50:50 coupler or beam-splitter. The initial state  $|\Psi\rangle_{in}$  and final state  $|\Psi\rangle_{out}$  are located at the start and end of the  $J_x$  section respectively (marked with dashed lines). The first BS is used to create a coherent superposition and second BS is used to test the SWAP operation and it is located after the  $J_x$  section.

the basis is transformed to the states  $|0,0\rangle, |1,0\rangle, |0,1\rangle, |1,1\rangle$ . This evolution is described in matrix notation by:

$$\begin{matrix} & |0,0\rangle & |0,1\rangle & |1,0\rangle & |1,1\rangle \\ \begin{matrix} |0,0\rangle \\ |0,1\rangle \\ |1,0\rangle \\ |1,1\rangle \end{matrix} & \begin{pmatrix} 1 & 0 & 0 & 0 \\ 0 & 0 & 1 & 0 \\ 0 & 1 & 0 & 0 \\ 0 & 0 & 0 & 1 \end{pmatrix} & , & \end{matrix} \quad (5.5)$$

where the basis (dual-rail basis) is putted explicitly. Notice that this matrix (also known as truth table) is equivalent to  $U_{\text{SWAP}}$  in Eq. (5.2).

The  $J_x$  lattice was proved launching classical light from a diode laser at the same wavelength of the photons source used in this work, that is 815 nm. Those results are in Fig. 5.3 a) where single input condition was tested in every waveguide, showing good results compared to the theory. Then, single photons were generated by SPDC, and collected by a fiber array to the chip. Because these fibers form an array with a separation of  $127 \mu\text{m}$  between them, a fan-in (fan-out) structure has to be

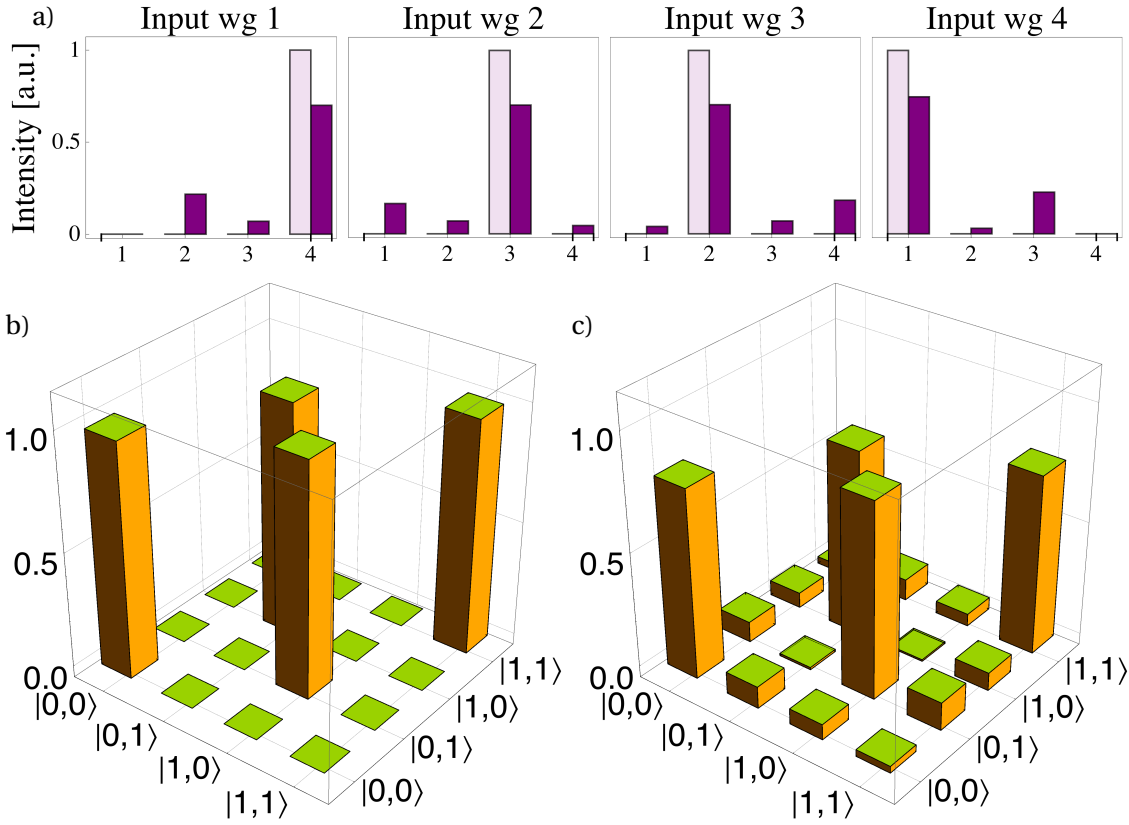


Figure 5.3: Characterization of the integrated SWAP gate. a) Intensity output measurements when input light is launched in every of the four waveguides (wg 1, . . . , wg 4). Purple bar is the experimental value and light purple is the theoretical one. At bottom, the truth table of the SWAP gate for b) theoretical and c) experimental values.

done previous (after) to the place where the dynamics occurs, in this case the  $J_x$  lattice (see Fig. 5.2).

During the theoretical part it was assumed that the photons are indistinguishable, so the experiment has to meet this condition. Experimentally this was checked performing a HOM dip experiment, getting a visibility of 90% on chip. Once the photons are ready to be used in the integrated circuit, the first experiment consisted to test and characterized our device by measuring the truth table of this circuit. For that, the four states of the computational basis were used as input states  $|0,0\rangle$ ,  $|0,1\rangle$ ,  $|1,0\rangle$ ,  $|1,1\rangle$ , this means single photons in waveguide 1 and 4, waveguide 1 and 3, waveguide 2 and 4 and waveguide 2 and 3 respectively and then the output probability is analyzed in the corresponding basis. The theoretical and experimental truth table are showed in Fig. 5.3 b) and c). The result shows a good agreement with the theoretical value, where the calculated similarity of the device was  $S = 0.81 \pm 0.01$ . A possible explanation for this value is, that photons are not

entire indistinguishable but they are partially distinguishable and a non-perfect fabrication of the  $J_x$  lattice. Due the array implements a SWAP operation only at distance  $Z = \pi$  and following a specific values of coupling, small variations and imperfections during the process of fabrication may produce a small detuning in waveguides, therefore having a non-perfect performance of the SWAP gate

Although the truth table is good indicator in how is the performance of the device, experiments with non-trivial input states has to be done in order to clarifier if the circuit is doing a SWAP operation or not. For that, it will be considered the following coherent superposition  $|\Psi\rangle_{cs} = \alpha |0, 0, 1, 0\rangle + \beta |0, 0, 0, 1\rangle$ , this means a single photon entering to the waveguides 3 and 4 with probability  $|\alpha|^2$  and  $|\beta|^2$  respectively. This can be done putting an additional BS before the  $J_x$  section (see Fig. 5.2). Here it was used a 50:50 beam-splitter, so  $\alpha = \beta = 1/\sqrt{2}$ . Also it will be considered a single photon entering into waveguide 1,  $|\Psi\rangle_{sp} = |1, 0, 0, 0\rangle$ .

So, the input state will be

$$|\Psi\rangle_{in} = |\Psi\rangle_{cs} \otimes |\Psi\rangle_{sp} = \alpha |1, 0, 1, 0\rangle + \beta |1, 0, 0, 1\rangle \quad .$$

And after the SWAP operation performed by the integrated circuit one should expect the following state

$$|\Psi\rangle_{out} = |\Psi\rangle_{sp} \otimes |\Psi\rangle_{cs} = \alpha |0, 1, 0, 1\rangle + \beta |1, 0, 0, 1\rangle \quad ,$$

where the coherent superposition initially between channels 3 and 4 is swapped to channels 1 and 2 and the single photon initially in channel 1 is swapped to channel 4. In Fig. 5.4 are the output probabilities in every channel where one can compare the theoretical value Fig. 5.4 a) with the experimental one Fig. 5.4 b). Due it is using a 50:50 coupler to create the coherent superposition, one should observe equal number of counts between channels 1 and 2, nothing in channel 3, and higher counts in waveguide 4. Experimentally the values are close to the theory, where channel 1 and 2 are very similar, although there are a number of counts different to zero in waveguide 3. These measurements give information of the circuit but they have to be complemented with quantum correlations, so in order to have a deeper insight about the quantum properties of the system, the correlation function  $\Gamma_{p,q}$  is calculated [26] (see Fig. 5.4 bottom). The results shows no values on the diagonal, meaning no bunching, and higher values in the expected position (see the theoretical plot to the left), like for example the position (1,4), where the detector in channel 1 receives the single photon from channel 4 and

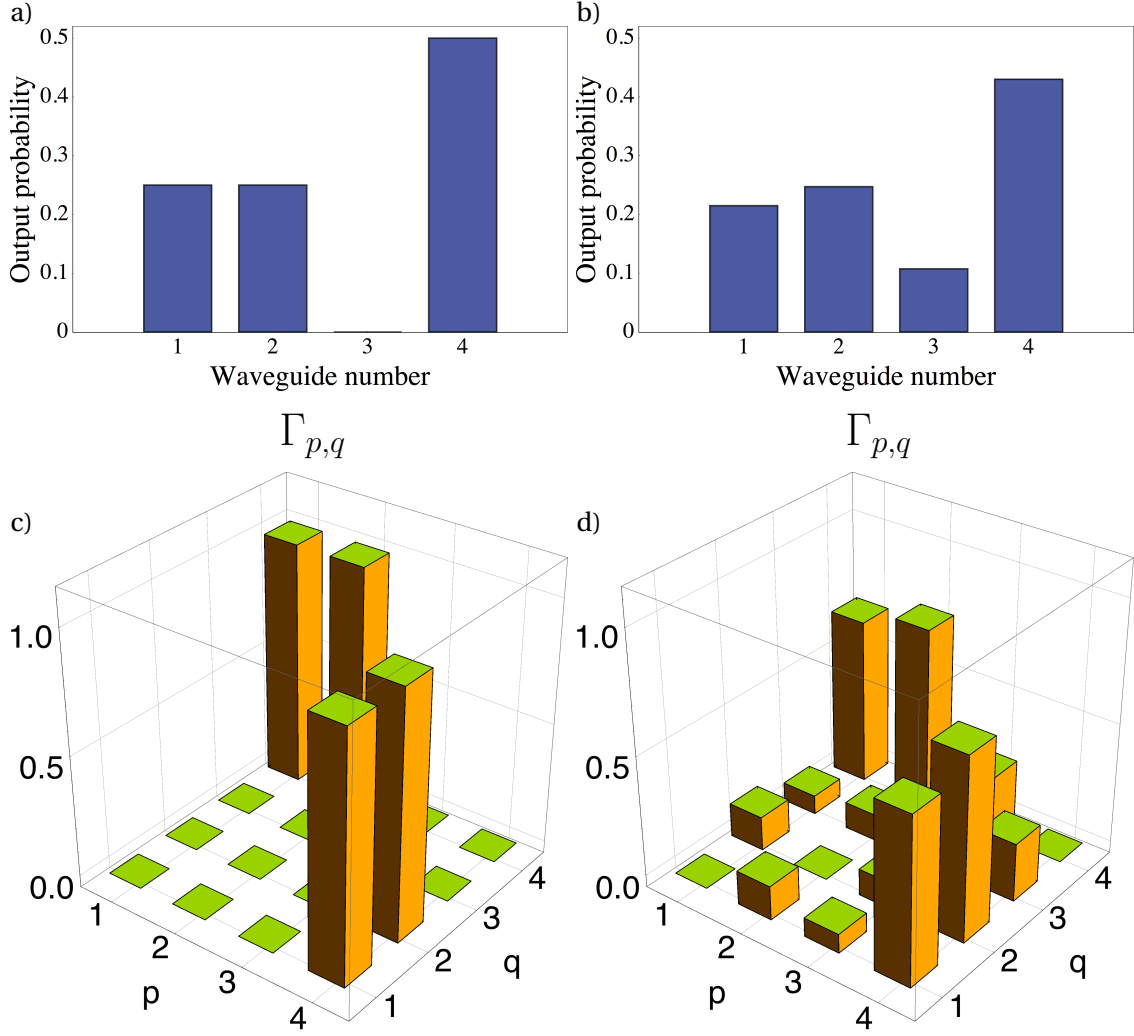


Figure 5.4: Measurements at the output of the  $J_x$  lattice using as input the coherent superposition and a single photon. (top) Output probability in every of the four detectors, where a) is the theoretical value and b) is the experimental one. (bottom) Correlation function  $\Gamma_{p,q}$  (or two-fold coincidence), where two detectors count single photons at the same time. c) is the theoretical value, and d) is the experimental one.

detector in channel 4 receives the one photon of the coherent superposition. The similarity of this measurement was  $0.72 \pm 0.01$ . The same explanation used for the experimental values of the truth table can be used here, where distinguishability of photons and minor imperfections in the  $J_x$  lattice are the main source of errors.

With all this measurements, including the correlation matrix, one can infer that the created device is performing a SWAP operation. An ultimate test would be that indeed the same coherent superposition at input is being swapped to the output. For that an additional BS is added at the output of the  $J_x$  lattice (see Fig. 5.2). This is done because if the initial coherent superposition between waveguides 3 and 4

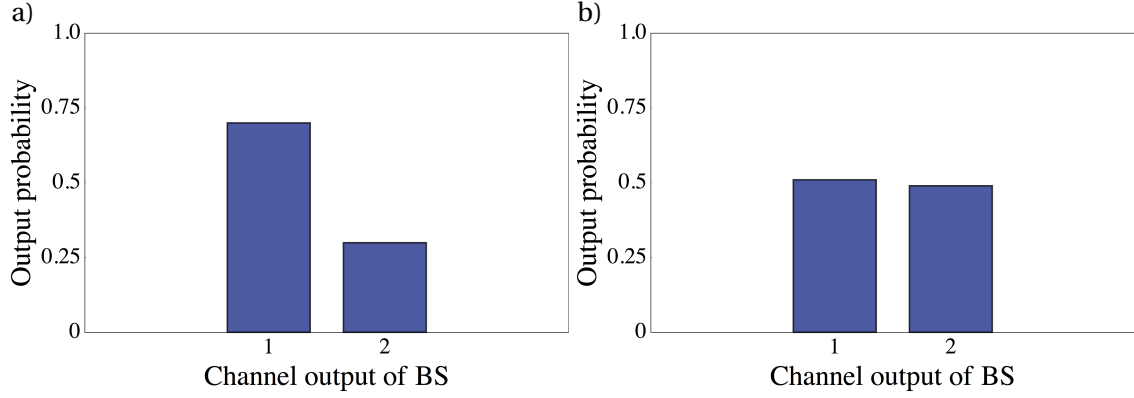


Figure 5.5: Experimental output probability of the BS added at the end of the  $J_x$  lattice. When a coherent superposition is the input, the output shows a tendency to exit in one arm of the BS a). In the other hand, when a single photon is the input, equal probability is measured in both arms b).

is being swapped to waveguides 1 and 2, then the coherent superposition entering to this BS would exit in only one arm of the BS and single photons in this arm should be detected. This was tested and the result of this experiment is shown in Fig. 5.5 where the output probability of the two arms of this BS are plotted, and one can observe a clear tendency of photons to exit in one arm of the BS with a probability of  $0.70 \pm 0.02$ . Moreover when instead of the coherent superposition, a single photon is used as input, it was observed an equal output probability of 0.5 in both arms of the BS (due that a single photon is entering to the BS, equal output probability is expected, see Fig. 5.5 b)). This shows clearly a different behavior of the device depending if either the input is a coherent superposition or a single photon, therefore one can say that the chip is performing a SWAP operation for the coherent superposition.

## 5.4 Conclusions

In this Chapter, a integrated photonic quantum SWAP gate was studied and implemented experimentally using photons. To ensure that the chip was indeed doing a SWAP operation several measurements were taken, including the obtention of the truth table of the device and the use of non trivial input states. One important point is that this operation is completely deterministic, so it has a probability of success of 1. This makes it a good candidate for large and complex networks using SWAP gates.



---

## Conclusions and Outlook

During this work different aspects of the actual quantum technology were studied. All of them characterized by the propagation of single or multi-photon states in complex networks, including certain areas of quantum computation and quantum simulation. They were studied by using dynamical equations, like discrete Schrödinger equation, for classical and quantum light. Interestingly the knowledge about the dynamics of single and multi-photons in guided structures helped to address different works in these areas.

Throughout this thesis, integrated optical circuits fabricated by means of femtosecond writing technology played a crucial role. This technique, in fact, allows to have a access to complex networks, like the  $J_x$  lattice or tuned waveguides and in this way to manipulate the propagation of single and multi-photons states for quantum technologies.

The observation of the very high efficiency quantum transport in photosynthetic complexes due to decoherence, mark the beginning of Chapter 3. By using the formalism of open quantum systems applied to waveguides, a system of three detuned waveguides was used for a quantum simulation. Experimental results in the single photon regime were obtained, where it was observed an increment of the transport efficiency, process known as environment assisted quantum transport [61]. Then the regime of two photons was studied. Unlike single photon regime, results show that indistinguishable two photon states arrives to the same steady state characterized by higher elements in the diagonal of the photon correlation function  $\Gamma$ . Moreover, coherence terms, given by the off-diagonal elements of

the density matrix, survive to the decoherence despite the rate of the dephasing, provided the photons are indistinguishable.

The scattering or propagation of photons in a network it is the special importance in the context of quantum integrated optics. A well known example is the boson sampling problem, indicated as intermediate computation which solve a problem believed to be classically hard to resolve [92]. And this task is related to calculate the permanent of a matrix. In chapter 4, it was discussed cases where, interestingly, this permanent is zero. The suppression of certain output states, given by the permanent, was studied for cases with symmetric conditions for the input and the unitary matrix  $U$ . It was found a condition related to the number of even entries at the output mode: if this number is odd, then that state is suppressed. To test experimentally this condition, an experiment using a  $J_x$  lattice and three photon input states was carried out, where the results have a good agreement with the established suppression law.

Last, but not least, the proposal of a quantum SWAP gate for quantum computation is addressed. The different operations inside a scheme of quantum computation are implemented by quantum gates, where the SWAP operation acts as an intermediate gate swapping states. The SWAP gate can be built by the action of three consecutive CNOT gates, where the CNOT gate is an important operation due to its universality in quantum computation. A big problem to create a SWAP gate using the mentioned approach is that it would have a probability of success of  $(1/9)^3$  [105], making it impracticable experimentally. Here a quantum two qubit SWAP gate was discussed acting in the spatial modes using a  $J_x$  lattice, where the problem of low success is avoid due to its remarkable characteristic of having an efficiency of 1. This means that no post processing is needed, making this implementation a realistic option for future experiments. The gate was characterized and proved using non trivial input states showing good results.

As future work in the area of quantum gates, the proposed SWAP gate in this work could be used to implement a quantum Fredkin gate. The Fredkin gate is a universal classical gate using three inputs which has several applications in quantum computation [113]. This gate is also called controlled-SWAP gate meaning if the control photon is 0, nothing happens to the others two photons (identified by a identity matrix), but if the control photon is 1, the other photons do a SWAP operation (identified by a SWAP matrix). The SWAP operation was already discussed for

two photons, using a  $J_x$  lattice at the distance of  $\pi/2$ . Interestingly, the  $J_x$  lattice at distance of  $\pi$  makes a complete revival of the inputs, which it may be seen as the case when control photon is 0 (because inputs stay equal). Therefore using  $J_x$  lattices at different distances, one could implement a Fredkin gate. It remains to see how control photon does this change, where non-linear operations or the use of ancillary photons may be needed.

Together to the work put in manipulation of photons through quantum gates, work in their detection has to be done also. Click detectors cannot distinguish between events of single photon or many of them, so work in the fabrication of detectors able to make such a distinction is highly desirable. Examples can be found in [114] using superconducting nanowires. Other desirable characteristic of these new detection systems is that they are integrable to the actual integrated circuits, so manipulation and detection would be in the same chip. Example of this, are the the superconducting detectors mounted onto waveguides [115, 116]. One drawback is these devices run only at very low temperature, so operation at room temperature is not yet possible.

The other step in quantum integrated optics is the generation of photons, indispensable for any photonic quantum technology. Although during this work external sources were used, new approaches use sources on chip. One example is photon pairs generated at telecom wavelength through SPDC in periodically-poled lithium niobate waveguides [117]. The work above is interesting, because although the waveguides created during this thesis were in amorphous materials like fused silica, it is also possible to use the same writing technique in crystals [118, 119] like lithium niobate. This opens the possibility to generate non-linear waveguides where the generation of photons pair is possible on chip, by employing the femtosecond laser writing technique [120].

All the obtained results in this thesis shed light upon certain aspects of the propagation of photons in waveguides arrays, where different areas like quantum computation and simulation were studied. They show the study of the dynamics of photons can be used in several areas, and that the use of special arrays, like  $J_x$  lattice have the potential for interesting results in integrated quantum optics, where the femtosecond laser writing technique appears as a good candidate to fabricate such as integrated structures.



# A

## Derivation of the dynamical equation for $\rho$ in OQS

In the following, an analogous way to get Eq. (3.15) in the main text will be developed starting from Eq. (3.7). It is assumed that the system under study corresponds to the array of three waveguide presented in the main text. It is necessary to calculate the component  $n, m$  of  $d\rho/dz$ , where now it will be used  $\rho$  for the reduced density matrix:

$$\frac{d}{dz}\rho_{n,m} = \langle n | \frac{d}{dz}\rho | m \rangle = \langle n | -i[H, \rho] | m \rangle + \langle n | \mathcal{L}[\rho] | m \rangle \quad . \quad (\text{A.1})$$

Analyzing firstly the term  $\langle n | -i[H, \rho] | m \rangle$

$$\langle n | -i[H, \rho] | m \rangle = -i \langle n | H\rho | m \rangle + i \langle n | \rho H | m \rangle \quad ,$$

but the Hamiltonian  $H$  of the trimer system written in a matrix form is  $H = -\sum_p \beta_p |p\rangle \langle p| - \sum_{p,q} C_{p,q} |p\rangle \langle q|$ , then:

$$\begin{aligned} -\langle n | i[H, \rho] | m \rangle &= i \langle n | \sum_p \beta_p |p\rangle \langle p| \rho | m \rangle - i \langle n | \rho \sum_p \beta_p |p\rangle \langle p| m \rangle \\ &\quad + i \langle n | \sum_{p,q} C_{p,q} |p\rangle \langle q| \rho | m \rangle - i \langle n | \rho \sum_{p,q} C_{p,q} |p\rangle \langle q| m \rangle \\ &= i \sum_p \beta_p \delta_{n,p} \rho_{p,m} - i \sum_p \beta_p \rho_{n,p} \delta_{p,m} + i \sum_{p,q} C_{p,q} \delta_{n,p} \rho_{q,m} - i \sum_{p,q} C_{q,p} \rho_{n,p} \delta_{q,m} \\ &= i(\beta_n - \beta_m) \rho_{n,m} + i \sum_q C_{n,q} \rho_{q,m} - i \sum_p C_{p,m} \rho_{n,p} \\ -\langle n | i[H, \rho] | m \rangle &= i(\beta_n - \beta_m) \rho_{n,m} + i \sum_r (C_{n,r} \rho_{r,m} - C_{r,m} \rho_{n,r}) \quad . \end{aligned} \quad (\text{A.2})$$

For the second term

$$\langle n | \mathcal{L}[\rho] | m \rangle = \langle n | \sum_k V_k \rho V_k^\dagger - \frac{1}{2} V_k^\dagger V_k \rho - \frac{1}{2} \rho V_k^\dagger V_k | m \rangle \quad ,$$

but in the main text it is considered only pure dephasing , so  $V_k = \sqrt{\gamma_k} |k\rangle \langle k|$  with  $\gamma_k$  the dephasing rate [61, 121]:

$$\begin{aligned}
\langle n | \mathcal{L}[\rho] | m \rangle &= \langle n | \sum_k \sqrt{\gamma_k} |k\rangle \langle k| \rho \sqrt{\gamma_k} |k\rangle \langle k| m \rangle - \frac{1}{2} \langle n | \sum_k \sqrt{\gamma_k \gamma_k} |k\rangle \langle k| k \rangle \langle k| \rho | m \rangle \\
&\quad - \frac{1}{2} \langle n | \rho \sum_k \sqrt{\gamma_k \gamma_k} |k\rangle \langle k| k \rangle \langle k| m \rangle \\
&= \sum_k \sqrt{\gamma_k} \delta_{n,k} \rho_{k,k} \sqrt{\gamma_k} \delta_{k,m} - \frac{1}{2} \sum_k \gamma_k \delta_{n,k} \rho_{k,m} - \frac{1}{2} \sum_k \gamma_k \rho_{n,k} \delta_{k,m} \\
\langle n | \mathcal{L}[\rho] | m \rangle &= \sqrt{\gamma_n} \sqrt{\gamma_m} \delta_{n,m} \rho_{n,m} - \frac{1}{2} (\gamma_n + \gamma_m) \rho_{n,m}
\end{aligned} \tag{A.3}$$

Then finally:

$$\frac{d}{dz} \rho_{n,m} = i(\beta_n - \beta_m) \rho_{n,m} + i \sum_r (C_{n,r} \rho_{r,m} - C_{r,m} \rho_{n,r}) + \sqrt{\gamma_n} \sqrt{\gamma_m} \delta_{n,m} \rho_{n,m} - \frac{1}{2} (\gamma_n + \gamma_m) \rho_{n,m}, \tag{A.4}$$

which is the result in Eq. (3.15).



---

# Bibliography

- [1] M. A. Nielsen and I. L. Chuang. Quantum Computation and Quantum Information. Cambridge University Press (2010).
- [2] N. Gisin and R. Thew. Quantum communication. *Nat. Photon.* **1**, 165 (2007).
- [3] V. Giovannetti, S. Lloyd and L. Maccone. Quantum-enhanced measurements: Beating the standard quantum limit. *Science* **306**, 1330 (2004).
- [4] I. M. Georgescu, S. Ashhab and F. Nori. Quantum simulation. *Rev. Mod. Phys.* **86**, 153 (2014).
- [5] R. P. Feynman. Simulating physics with computers. *Int. J. Theor. Phys.* **21**, 467 (1982).
- [6] E. Knill, R. Laflamme and G. J. Milburn. A scheme for efficient quantum computation with linear optics. *Nature* **409**, 46 (2001).
- [7] I. Bloch, J. Dalibard and S. Nascimbène. Quantum simulations with ultracold quantum gases. *Nat. Phys.* **8**, 267 (2012).
- [8] J. T. Barreiro, M. Müller, P. Schindler, D. Nigg, T. Monz, M. Chwalla, M. Hennrich, C. F. Roos, P. Zoller and R. Blatt. An open-system quantum simulator with trapped ions. *Nature* **470**, 486 (2011).
- [9] J. Zhang, M.-H. Yung, R. Laflamme, A. Aspuru-Guzik and J. Baugh. Digital quantum simulation of the statistical mechanics of a frustrated magnet. *Nat. Commun.* **3**, 880 (2012).

- [10] J. Du, H. Li, X. Xu, M. Shi, J. Wu, X. Zhou and R. Han. Experimental implementation of the quantum random-walk algorithm. *Phys. Rev. A* **67**, 042316 (2003).
- [11] J. L. O’Brien, A. Furusawa and J. Vučković. Photonic quantum technologies. *Nat. Photon.* **3**, 687 (2009).
- [12] A. Aspuru-Guzik and P. Walther. Photonic quantum simulators. *Nat. Phys.* **8**, 285 (2012).
- [13] K. Park, P. Marek and R. Filip. Qubit-mediated deterministic nonlinear gates for quantum oscillators. *Sci. Rep.* **7**, 11536 (2017).
- [14] X.-C. Yao, T.-X. Wang, P. Xu, H. Lu, G.-S. Pan, X.-H. Bao, C.-Z. Peng, C.-Y. Lu, Y.-A. Chen and J.-W. Pan. Observation of eight-photon entanglement. *Nat. Photon.* **6**, 225 (2012).
- [15] L.-K. Chen, Z.-D. Li, X.-C. Yao, M. Huang, W. Li, H. Lu, X. Yuan, Y.-B. Zhang, X. Jiang, C.-Z. Peng, L. Li, N.-L. Liu, X. Ma, C.-Y. Lu, Y.-A. Chen and J.-W. Pan. Observation of ten-photon entanglement using thin  $\text{BiB}_3\text{O}_6$  crystals. *Optica* **4**, 77 (2017).
- [16] F. Bloch. über die quantenmechanik der elektronen in kristallgittern. *Z. Phys.* **52**, 555 (1928).
- [17] J. Rayleigh. On the maintance of vibrations by forces of double frequency, and on the propagation of waves through a medium endowed with a periodic structure. *Phil. Mag.* **24**, 145 (1887).
- [18] T. Pertsch, P. Dannberg, W. Elflein, A. Bräuer and F. Lederer. Optical Bloch Oscillations in Temperature Tuned Waveguide Arrays. *Phys. Rev. Lett.* **83**, 4752 (1999).
- [19] R. Morandotti, U. Peschel, J. S. Aitchison, H. S. Eisenberg and Y. Silberberg. Experimental Observation of Linear and Nonlinear Optical Bloch Oscillations. *Phys. Rev. Lett.* **83**, 4756 (1999).
- [20] P. Biagioni, G. D. Valle, M. Ornigotti, M. Finazzi, L. Duò, P. Laporta and S. Longhi. Experimental demonstration of the optical Zeno effect by scanning tunneling optical microscopy. *Opt. Express* **16**, 3762 (2008).

- [21] T. Schwartz, G. Bartal, S. Fishman and M. Segev. Transport and Anderson localization in disordered two-dimensional photonic lattices. *Nature* **446**, 52 (2007).
- [22] D. N. Christodoulides, F. Lederer and Y. Silberberg. Discretizing light behaviour in linear and nonlinear waveguide lattices. *Nature* **424**, 817 (2003).
- [23] D. N. Christodoulides and R. I. Joseph. Discrete self-focusing in nonlinear arrays of coupled waveguides. *Opt. Lett.* **13**, 794 (1988).
- [24] Y. Aharonov, L. Davidovich and N. Zagury. Quantum random walks. *Phys. Rev. A* **48**, 1687 (1993).
- [25] H. B. Perets, Y. Lahini, F. Pozzi, M. Sorel, R. Morandotti and Y. Silberberg. Realization of Quantum Walks with Negligible Decoherence in Waveguide Lattices. *Phys. Rev. Lett.* **100**, 170506 (2008).
- [26] Y. Bromberg, Y. Lahini, R. Morandotti and Y. Silberberg. Quantum and Classical Correlations in Waveguide Lattices. *Phys. Rev. Lett.* **102**, 253904 (2009).
- [27] A. Politi, M. J. Cryan, J. G. Rarity, S. Yu and J. L. O'Brien. Silica-on-silicon waveguide quantum circuits. *Science* **320**, 646 (2008).
- [28] A. Crespi, R. Ramponi, R. Osellame, L. Sansoni, I. Bongioanni, F. Sciarrino, G. Vallone and P. Mataloni. Integrated photonic quantum gates for polarization qubits. *Nat. Commun.* **2**, 566 (2011).
- [29] A. Peruzzo, M. Lobino, J. C. F. Matthews, N. Matsuda, A. Politi, K. Poulios, X.-Q. Zhou, Y. Lahini, N. Ismail, K. Wörhoff, Y. Bromberg, Y. Silberberg, M. G. Thompson and J. L. O'Brien. Quantum Walks of Correlated Photons. *Science* **329**, 1500 (2010).
- [30] B. J. Metcalf, J. B. Spring, P. C. Humphreys, N. Thomas-Peter, M. Barbieri, W. S. Kolthammer, X.-M. Jin, N. K. Langford, D. Kundys, J. C. Gates, B. J. Smith, P. G. R. Smith and I. A. Walmsley. Quantum teleportation on a photonic chip. *Nat. Photon.* **8**, 770 (2014).
- [31] J. D. Jackson. Classical electrodynamics. Wiley (1975).
- [32] H. S. Eisenberg, Y. Silberberg, R. Morandotti, A. R. Boyd and J. S. Aitchison. Discrete Spatial Optical Solitons in Waveguide Arrays. *Phys. Rev. Lett.* **81**, 3383 (1998).

- [33] A. Yariv. Coupled-mode theory for guided-wave optics. *IEEE J. Quantum Electron.* **9**, 919 (1973).
- [34] N. W. Ashcroft and N. D. Mermin. Solid State Physics. Holt, Rinehart and Winston (1976).
- [35] P. G. Kevrekidis. Discrete Nonlinear Schrödinger equation: Mathematical Analysis, Numerical Computations and Physical Perspectives. Springer (2009).
- [36] G. S. Agarwal. Quantum optics. Cambridge University Press (2013).
- [37] C. K. Hong, Z. Y. Ou and L. Mandel. Measurement of subpicosecond time intervals between two photons by interference. *Phys. Rev. Lett.* **59**, 2044 (1987).
- [38] Z. Y. Ou, X. Y. Zou, L. J. Wang and L. Mandel. Experiment on nonclassical fourth-order interference. *Phys. Rev. A* **42**, 2957 (1990).
- [39] H. Lee, P. Kok and J. P. Dowling. A quantum rosetta stone for interferometry. *J. Mod. Opt.* **49**, 2325 (2002).
- [40] S. Tanzilli, H. De Riedmatten, W. Tittel, H. Zbinden, P. Baldi, M. De Micheli, D. B. Ostrowsky and N. Gisin. Highly efficient photon-pair source using periodically poled lithium niobate waveguide. *Electron. Lett.* **37**, 26 (2001).
- [41] A. Szameit and S. Nolte. Discrete optics in femtosecond-laser-written photonic structures. *J. Phys. B* **43**, 163001 (2010).
- [42] G. D. Marshall, A. Politi, J. C. F. Matthews, P. Dekker, M. Ams, M. J. Withford and J. L. O'Brien. Laser written waveguide photonic quantum circuits. *Opt. Express* **17**, 12546 (2009).
- [43] K. M. Davis, K. Miura, N. Sugimoto and K. Hirao. Writing waveguides in glass with a femtosecond laser. *Opt. Lett.* **21**, 1729 (1996).
- [44] K. Sugioka, J. Xu, D. Wu, Y. Hanada, Z. Wang, Y. Cheng and K. Midorikawa. Femtosecond laser 3D micromachining: a powerful tool for the fabrication of microfluidic, optofluidic, and electrofluidic devices based on glass. *Lab Chip* **14**, 3447 (2014).

- [45] T. Meany, M. Gräfe, R. Heilmann, A. Perez-Leija, S. Gross, M. J. Steel, M. J. Withford and A. Szameit. Laser written circuits for quantum photonics. *Laser & Photonics Reviews* **9**, 363 (2015).
- [46] K. Itoh, W. Watanabe, S. Nolte and C. B. Schaffer. Ultrafast processes for bulk modification of transparent materials. *MRS Bulletin* **31**, 620 (2006).
- [47] B. N. Chichkov, C. Momma, S. Nolte, F. von Alvensleben and A. Tünnermann. Femtosecond, picosecond and nanosecond laser ablation of solids. *Appl. Phys. A* **63**, 109 (1996).
- [48] A. Szameit, F. Dreisow, H. Hartung, S. Nolte, A. Tünnermann and F. Lederer. Quasi-incoherent propagation in waveguide arrays. *Appl. Phys. Lett.* **90**, 241113 (2007).
- [49] F. Dreisow, M. Heinrich, A. Szameit, S. Döring, S. Nolte, A. Tünnermann, S. Fahr and F. Lederer. Spectral resolved dynamic localization in curved fs laser written waveguide arrays. *Opt. Express* **16**, 3474 (2008).
- [50] R. Heilmann, M. Gräfe, S. Nolte and A. Szameit. Arbitrary photonic wave plate operations on chip: Realizing Hadamard, Pauli-X, and rotation gates for polarisation qubits. *Sci. Rep.* **4**, 4118 (2014).
- [51] A. Szameit, F. Dreisow, T. Pertsch, S. Nolte and A. Tünnermann. Control of directional evanescent coupling in fs laser written waveguides. *Opt. Express* **15**, 1579 (2007).
- [52] D. Blömer, A. Szameit, F. Dreisow, T. Schreiber, S. Nolte and A. Tünnermann. Nonlinear refractive index of fs-laser-written waveguides in fused silica. *Opt. Express* **14**, 2151 (2006).
- [53] E. Marcatili. Bends in optical dielectric guides. *Bell Labs Tech. J.* **48**, 2103 (1969).
- [54] A. Yariv. Quantum electronics. Wiley (1989).
- [55] Y. Shih. Entangled biphoton source - property and preparation. *Rep. Prog. Phys.* **66**, 1009 (2003).
- [56] M. Gräfe. Integrated photonic quantum walks in complex lattice structures. Ph.D. thesis, FSU Jena (2017).

- [57] R. H. Hadfield. Single-photon detectors for optical quantum information applications. *Nat. Photon.* **3**, 696 (2009).
- [58] R. Glauber. The Quantum Theory of Optical Coherence. *Phys. Rev.* **130**, 2529 (1963).
- [59] W. H. Zurek. Decoherence, einselection, and the quantum origins of the classical. *Rev. Mod. Phys.* **75**, 715 (2003).
- [60] J. M. Olson. The FMO Protein. *Photosynth. Res.* **80**, 181 (2004).
- [61] P. Rebentrost, M. Mohseni, I. Kassal, S. Lloyd and A. Aspuru-Guzik. Environment-assisted quantum transport. *New J. Phys.* **11**, 033003 (2009).
- [62] M. B. Plenio and S. F. Huelga. Dephasing-assisted transport: quantum networks and biomolecules. *New J. Phys.* **10**, 113019 (2008).
- [63] A. Rivas and S. F. Huelga. Open Quantum Systems. An Introduction. *arXiv:1104.5242 [quant-ph]* (2012).
- [64] A. Alexander. Master's thesis, University of Vienna (2008).
- [65] G. Lindblad. On the generators of quantum dynamical semigroups. *Comm. Math. Phys.* **48**, 119 (1976).
- [66] R. Brown. XXVII. A brief account of microscopical observations made in the months of June, July and August 1827, on the particles contained in the pollen of plants; and on the general existence of active molecules in organic and inorganic bodies. *Phil. Mag.* **4**, 161 (1828).
- [67] A. Einstein. über die von der molekularkinetischen theorie der wärme geforderte bewegung von in ruhenden flüssigkeiten suspendierten teilchen. *Annalen der Physik* **322**, 549 (1905).
- [68] P. V. E. McClintock. Random fluctuations: Unsolved problems of noise. *Nature* **401**, 23 (1999).
- [69] H. J. Carmichael. Statistical methods in quantum optics. Springer (1998).
- [70] B.-H. Liu, L. Li, Y.-F. Huang, C.-F. Li, G.-C. Guo, E.-M. Laine, H.-P. Breuer and J. Piilo. Experimental control of the transition from markovian to non-markovian dynamics of open quantum systems. *Nat. Phys.* **7**, 931 (2011).

- [71] A. Eisfeld and J. S. Briggs. Classical master equation for excitonic transport under the influence of an environment. *Phys. Rev. E* **85**, 046118 (2012).
- [72] F. Caruso, A. W. Chin, A. Datta, S. F. Huelga and M. B. Plenio. Highly efficient energy excitation transfer in light-harvesting complexes: The fundamental role of noise-assisted transport. *J. Chem. Phys.* **131**, 105106 (2009).
- [73] H. Park, N. Heldman, P. Rebentrost, L. Abbondanza, A. Iagatti, A. Alessi, B. Patrizi, M. Salvalaggio, L. Bussotti, M. Mohseni, F. Caruso, H. C. Johnsen, R. Fusco, P. Foggi, P. F. Scudo, S. Lloyd and A. M. Belcher. Enhanced energy transport in genetically engineered excitonic networks. *Nat. Materials* **15**, 211 (2016).
- [74] D. W. Schönleber, A. Eisfeld, M. Genkin, S. Whitlock and S. Wüster. Quantum Simulation of Energy Transport with Embedded Rydberg Aggregates. *Phys. Rev. Lett.* **114**, 123005 (2015).
- [75] G. J. L. Carlo Laing. Stochastic Methods in Neuroscience. OUP Oxford (2009).
- [76] C. Gardiner. Stochastic Methods: A handbook for the Natural and Social Sciences. Springer Berlin Heidelberg (2010).
- [77] N. G. van Kampen. Itô versus Stratonovich. *J. Stat. Phys.* **24**, 175 (1981).
- [78] A. F. Abouraddy, B. E. A. Saleh, A. V. Sergienko and M. C. Teich. Role of Entanglement in Two-Photon Imaging. *Phys. Rev. Lett.* **87**, 123602 (2001).
- [79] A. Perez-Leija, R. d. J. Leon-Montiel, J. Sperling, H. Moya-Cessa, A. Szameit and K. Busch. Two-particle four-point correlations in dynamically disordered tight-binding networks. arXiv:1706.09289 [quant-ph] (2017).
- [80] J. C. F. Matthews, K. Poullos, J. D. A. Meinecke, A. Politi, A. Peruzzo, N. Ismail, K. Wörhoff, M. G. Thompson and J. L. O'Brien. Observing fermionic statistics with photons in arbitrary processes. *Sci. Rep.* **3**, 1539 EP (2013).
- [81] A. Smirne, S. Cialdi, G. Anelli, M. G. Paris and B. Vacchini. Quantum probes to experimentally assess correlations in a composite system. *Phys. Rev. A* **88**, 012108 (2013).
- [82] M. Lebugle, M. Gräfe, R. Heilmann, A. Perez-Leija, S. Nolte and A. Szameit. Experimental observation of N00N state Bloch oscillations. *Nat. Commun.* **6**, 8273 (2015).

- [83] S. Aaronson and A. Arkhipov. The computational complexity of linear optics. In Proceedings of the 43rd annual ACM symposium on Theory of computing, 333–342. ACM (2011).
- [84] B. T. Gard, K. R. Motes, J. P. Olson, P. P. Rohde and J. P. Dowling. An introduction to boson-sampling. arXiv:1406.6767 [quant-ph] (2014).
- [85] Z. Y. Ou. Temporal distinguishability of an  $n$ -photon state and its characterization by quantum interference. *Phys. Rev. A* **74**, 063808 (2006).
- [86] M. C. Tichy, M. Tiersch, F. de Melo, F. Mintert and A. Buchleitner. Zero-Transmission Law for Multiport Beam Splitters. *Phys. Rev. Lett.* **104**, 220405 (2010).
- [87] M. C. Tichy, M. Tiersch, F. Mintert and A. Buchleitner. Many-particle interference beyond many-boson and many-fermion statistics. *New J. Phys.* **14**, 093015 (2012).
- [88] M. C. Tichy. Interference of identical particles from entanglement to boson-sampling. *J. Phys. B* **47**, 103001 (2014).
- [89] L. Valiant. The complexity of computing the permanent. *Theoret. Comp. Sci.* **8**, 189 (1979).
- [90] J. B. Spring, B. J. Metcalf, P. C. Humphreys, W. S. Kolthammer, X.-M. Jin, M. Barbieri, A. Datta, N. Thomas-Peter, N. K. Langford, D. Kundys, J. C. Gates, B. J. Smith, P. G. R. Smith and I. A. Walmsley. Boson Sampling on a Photonic Chip. *Science* **339**, 798 (2013).
- [91] M. A. Broome, A. Fedrizzi, S. Rahimi-Keshari, J. Dove, S. Aaronson, T. C. Ralph and A. G. White. Photonic Boson Sampling in a Tunable Circuit. *Science* **339**, 794 (2013).
- [92] M. Tillmann, B. Dakić, R. Heilmann, S. Nolte, A. Szameit and P. Walther. Experimental boson sampling. *Nat. Photon.* **7**, 540 (2013).
- [93] A. Crespi, R. Osellame, R. Ramponi, D. J. Brod, E. F. Galvão, N. Spagnolo, C. Vitelli, E. Majorino, P. Mataloni and F. Sciarrino. Integrated multimode interferometers with arbitrary designs for photonic boson sampling. *Nat. Photon.* **7**, 545 (2013).

- [94] A. Crespi. Suppression laws for multiparticle interference in sylvester interferometers. *Phys. Rev. A* **91**, 013811 (2015).
- [95] Y. L. Lim and A. Beige. Generalized Hong–Ou–Mandel experiments with bosons and fermions. *New J. Phys.* **7**, 155 (2005).
- [96] M. Żukowski, A. Zeilinger and M. A. Horne. Realizable higher-dimensional two-particle entanglements via multiport beam splitters. *Phys. Rev. A* **55**, 2564 (1997).
- [97] A. Perez-Leija, R. Keil, H. Moya-Cessa, A. Szameit and D. N. Christodoulides. Perfect transfer of path-entangled photons in  $J_x$  photonic lattices. *Phys. Rev. A* **87**, 022303 (2013).
- [98] M. Christandl, N. Datta, A. Ekert and A. J. Landahl. Perfect state transfer in quantum spin networks. *Phys. Rev. Lett.* **92**, 187902 (2004).
- [99] S. Weimann, A. Perez-Leija, M. Lebugle, R. Keil, M. Tichy, M. Gräfe, R. Heilmann, S. Nolte, H. Moya-Cessa, G. Weihs, D. N. Christodoulides and A. Szameit. Implementation of quantum and classical discrete fractional fourier transforms. *Nat. Commun.* **7**, 11027 (2016).
- [100] R. Heilmann, C. Greganti, M. Gräfe, S. Nolte, P. Walther and A. Szameit. Tapering of femtosecond laser-written waveguides. *Appl. Opt.* **57**, 377 (2018).
- [101] J. H. Plantenberg, P. C. de Groot, C. J. P. M. Harmans and J. E. Mooij. Demonstration of controlled-not quantum gates on a pair of superconducting quantum bits. *Nature* **447**, 836 (2007).
- [102] A. Fedorov, L. Steffen, M. Baur, M. P. da Silva and A. Wallraff. Implementation of a Toffoli gate with superconducting circuits. *Nature* **481**, 170 (2011).
- [103] F. Schmidt-Kaler, H. Häffner, M. Riebe, S. Gulde, G. P. T. Lancaster, T. Deuschle, C. Becher, C. F. Roos, J. Eschner and R. Blatt. Realization of the Cirac–Zoller controlled-NOT quantum gate. *Nature* **422**, 408 (2003).
- [104] C. J. Ballance, T. P. Harty, N. M. Linke, M. A. Sepiol and D. M. Lucas. High-Fidelity Quantum Logic Gates Using Trapped-Ion Hyperfine Qubits. *Phys. Rev. Lett.* **117**, 060504 (2016).
- [105] T. C. Ralph, N. K. Langford, T. B. Bell and A. G. White. Linear optical controlled-not gate in the coincidence basis. *Phys. Rev. A* **65**, 062324 (2002).

- [106] A. Kay. Perfect, efficient, state transfer and its application as a constructive tool. *Int. J. Quantum Inform.* **08**, 641 (2010).
- [107] A. Perez-Leija, R. Keil, A. Kay, H. Moya-Cessa, S. Nolte, L.-C. Kwek, B. M. Rodríguez-Lara, A. Szameit and D. N. Christodoulides. Coherent quantum transport in photonic lattices. *Phys. Rev. A* **87**, 012309 (2013).
- [108] A. G. Fowler, S. J. Devitt and L. C. L. Hollenberg. Implementation of Shor’s Algorithm on a Linear Nearest Neighbour Qubit Array. *Quantum Info. Comput.* **4**, 237 (2004).
- [109] L.-m. Liang and C.-z. Li. Realization of quantum swap gate between flying and stationary qubits. *Phys. Rev. A* **72**, 024303 (2005).
- [110] C. Wilmott. On swapping the states of two qudits. arXiv:1101.4159 [quant-ph] (2011).
- [111] A. Barenco, C. H. Bennett, R. Cleve, D. P. DiVincenzo, N. Margolus, P. Shor, T. Sleator, J. A. Smolin and H. Weinfurter. Elementary gates for quantum computation. *Phys. Rev. A* **52**, 3457 (1995).
- [112] D. P. DiVincenzo. Two-bit gates are universal for quantum computation. *Phys. Rev. A* **51**, 1015 (1995).
- [113] R. B. Patel, J. Ho, F. Ferreyrol, T. C. Ralph and G. J. Pryde. A quantum Fredkin gate. *Sci. Adv.* **2** (2016).
- [114] A. Divochiy, F. Marsili, D. Bitauld, A. Gaggero, R. Leoni, F. Mattioli, A. Korneev, V. Seleznev, N. Kaurova, O. Minaeva, G. Gol’tsman, K. G. Lagoudakis, M. Benkhaoul, F. Lévy and A. Fiore. Superconducting nanowire photon-number-resolving detector at telecommunication wavelengths. *Nat. Photon.* **2**, 302 (2008).
- [115] M. K. Akhlaghi, E. Schelew and J. F. Young. Waveguide integrated superconducting single-photon detectors implemented as near-perfect absorbers of coherent radiation. *Nat. Commun.* **6**, 8233 (2015).
- [116] J. P. Sprengers, A. Gaggero, D. Sahin, S. Jahanmirinejad, G. Frucci, F. Mattioli, R. Leoni, J. Beetz, M. Lerner, M. Kamp, S. Höfling, R. Sanjines and A. Fiore. Waveguide superconducting single-photon detectors for integrated quantum photonic circuits. *Appl. Phys. Lett.* **99**, 181110 (2011).

- [117] H. Jin, F. M. Liu, P. Xu, J. L. Xia, M. L. Zhong, Y. Yuan, J. W. Zhou, Y. X. Gong, W. Wang and S. N. Zhu. On-Chip Generation and Manipulation of Entangled Photons Based on Reconfigurable Lithium-Niobate Waveguide Circuits. *Phys. Rev. Lett.* **113**, 103601 (2014).
- [118] M. Heinrich, A. Szameit, F. Dreisow, S. Döring, J. Thomas, S. Nolte, A. Tünnermann and A. Ancona. Evanescent coupling in arrays of type ii femtosecond laser-written waveguides in bulk x-cut lithium niobate. *Appl. Phys. Lett.* **93**, 101111 (2008).
- [119] R. Osellame, M. Lobino, N. Chiodo, M. Marangoni, G. Cerullo, R. Ramponi, H. T. Bookey, R. R. Thomson, N. D. Psaila and A. K. Kar. Femtosecond laser writing of waveguides in periodically poled lithium niobate preserving the nonlinear coefficient. *Appl. Phys. Lett.* **90**, 241107 (2007).
- [120] S. Atzeni. Master's thesis, Politecnico di Milano (2016).
- [121] D. G. Tempel and A. Aspuru-Guzik. Relaxation and dephasing in open quantum systems time-dependent density functional theory: Properties of exact functionals from an exactly-solvable model system. *Chem. Phys.* **391**, 130 (2011).





---

# List of publications and conference contributions

## Publications

- [I] D. Guzman-Silva, R. Brüning, F. Zimmermann, C. Vetter, M. Gräfe, M. Heinrich, S. Nolte, M. Duparré, A. Aiello, M. Ornigotti and A. Szameit  
Demonstration of local teleportation using classical entanglement  
Laser Photonics Review **10**, 317 (2016)
- [II] M. Gräfe, R. Heilmann, M. Lebugle, D. Guzman-Silva, A. Perez-Leija and A. Szameit  
Integrated photonic quantum walks  
Journal of Optics **18**, 103002 (2016)
- [III] A. Perez-Leija, D. Guzman-Silva, R. de J. Leon-Montiel, M. Gräfe, M. Heinrich, H. Moya-Cessa, K. Busch and A. Szameit  
Endurance of quantum coherence in Born-Markov open quantum systems  
arXiv:1709.04336 (submitted, in review, 2017)

## In preparation

- [IV] D. Guzman-Silva, A. Perez-Leija, E. Meyer and A. Szameit  
Photonic multiqubit SWAP gate
- [V] C. Dittel, R. Keil, M.C. Tichy, D. Guzman-Silva, A. Perez-Leija, T. Kauten, S. Weimann, M. Lebugle, A. Szameit and G. Weihs  
Symmetric suppression in many-body quantum interferences

## Conference contributions

- [•] D. Guzman-Silva, M. Lebugle, A. Perez-Leija, S. Weinmann, S. Nolte and A. Szameit. Poster: Experimental transfer of quantum entangled photons in  $J_x$  photonics lattices. Workshop in integrated quantum photonics 2015, Oxford, UK
- [•] D. Guzman-Silva, R. de J. Leon-Montiel, M. Heinrich, J. P. Torres, H. Moya-Cessa, M. Gräfe, A. Perez-Leija and A. Szameit. Oral talk: Observation of noise-assisted energy transport in dynamically disordered photonic lattices. CLEO 2016, San Jose, California, USA
- [•] D. Guzman-Silva, R. de J. Leon-Montiel, M. Gräfe, M. Heinrich, S. Nolte, K. Busch, H. Moya-Cessa, J. P. Torres, A. Perez-Leija and A. Szameit. Oral talk: Noise-assisted energy transport in dynamically disordered photonic lattices. Control of light and matter waves propagation and localization in photonic lattices 2016, Santiago, Chile
- [•] D. Guzman-Silva, R. de J. Leon-Montiel, M. Gräfe, M. Heinrich, S. Nolte, K. Busch, H. Moya-Cessa, J. P. Torres, A. Perez-Leija and A. Szameit. Oral talk: Noise-assisted energy transport in dynamically disordered photonic lattices. RIAO/OPTILAS 2016, Pucon, Chile
- [•] D. Guzman-Silva, R. Brüning, F. Zimmermann, C. Vetter, M. Gräfe, M. Heinrich, S. Nolte, M. Duparré, A. Aiello, M. Ornigotti and A. Szameit. Oral talk: Demonstration of local teleportation using classical entanglement. CLEO 2017, San Jose, California, USA
- [•] A. Perez-Leija, D. Guzman-Silva, R. de J. Leon-Montiel, M. Gräfe, M. Heinrich, H. Moya-Cessa, K. Busch and A. Szameit. Oral talk: Endurance of quantum coherence in open quantum systems. International conference on integrated quantum photonics 2017, Rome, Italy

## **Selbstständigkeitserklärung**

Hiermit erkläre ich an Eides statt, dass ich die hier vorliegende Dissertation selbstständig und ohne fremde Hilfe verfasst habe, bis auf die in der Bibliographie angegebenen Quellen keine weiteren Quellen benutzt habe und die den Quellen wörtlich oder inhaltlich entnommene Stellen als solche kenntlich gemacht habe.

Beim Anfertigen dieser Arbeit haben mir folgende Personen unentgeltlich geholfen: die Theorie in Kapitel 3 wurde in enger Zusammenarbeit mit Dr. Armando Perez-Leija (Humboldt-Universität zu Berlin) entwickelt. Die Theorie und Experimente aus Kapitel 4 entstanden in Zusammenarbeit mit Dr. Robert Keil und Christoph Dittel (Universität Innsbruck). Die Theorie in Kapitel 5 entstand in Zusammenarbeit mit Dr. Armando Perez Leija.

Diego Guzman Silva

Rostock, den 9. Februar 2018